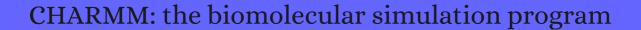
# CITATION REPORT List of articles citing



DOI: 10.1002/jcc.21287 Journal of Computational Chemistry, 2009, 30, 1545-614.

Source: https://exaly.com/paper-pdf/46078446/citation-report.pdf

Version: 2024-04-09

This report has been generated based on the citations recorded by exaly.com for the above article. For the latest version of this publication list, visit the link given above.

The third column is the impact factor (IF) of the journal, and the fourth column is the number of citations of the article.

#	Paper	IF	Citations
2275	7 Log Virus Removal in a Simple Functionalized Sand Filter.		
2274	Conformation and Dynamics of Human Urotensin II and Urotensin Related Peptide in Aqueous Solution.		
2273	Kinematic Flexibility Analysis: Hydrogen Bonding Patterns Impart a Spatial Hierarchy of Protein Motion.		
2272	Cys.sqlite: A Structured-Information Approach to the Comprehensive Analysis of Cysteine Disulfide Bonds in the Protein Databank.		
2271	Interactions between Curcumin Derivatives and Amyloid Fibrils: Insights from Molecular Dynamics Simulations.		
2270	Constant pH Molecular Dynamics Reveals How Proton Release Drives the Conformational Transition of a Transmembrane Efflux Pump.		
2269			
2268	Binding of Divalent Cations to Polygalacturonate: A Mechanism Driven by the Hydration Water.		
2267	Intrinsic Base-Pair Rearrangement in the Hairpin Ribozyme Directs RNA Conformational Sampling and Tertiary Interface Formation.		
2266	Extraction of Protein Conformational Modes from Distance Distributions Using Structurally Imputed Bayesian Data Augmentation.		
2265	Molecular Packing, Hydrogen Bonding, and Fast Dynamics in Lysozyme/Trehalose/Glycerol and Trehalose/Glycerol Glasses at Low Hydration.		
2264	Slow-Down in Diffusion in Crowded Protein Solutions Correlates with Transient Cluster Formation.		
2263	Computational Design of Functional Amyloid Materials with Cesium Binding, Deposition, and Capture Properties.		
2262	Free Energy of Ligand Removal in the MetalOrganic Framework UiO-66.		
2261	Understanding the Nature of Nuclear Magnetic Resonance Relaxation by Means of Fast-Field-Cycling Relaxometry and Molecular Dynamics SimulationsThe Validity of Relaxation Models.		
2260	Molecular Dynamics of Membrane-Spanning DNA Channels: Conductance Mechanism, Electro-Osmotic Transport, and Mechanical Gating.		
2259	Constant pH Molecular Dynamics Reveals pH-Modulated Binding of Two Small-Molecule BACE1 Inhibitors.		

Assembly.

2258 Free Energies of Redox Half-Reactions from First-Principles Calculations. Conformational Activation of a Transmembrane Proton Channel from Constant pH Molecular 2257 Dynamics. 2256 Electrostatic Asymmetry in the Reaction Center of Photosystem II. Simulating the Activation of Voltage Sensing Domain for a Voltage-Gated Sodium Channel Using Polarizable Force Field. Predicting Catalytic Proton Donors and Nucleophiles in Enzymes: How Adding Dynamics Helps Elucidate the StructureFunction Relationships. Merging In-Solution X-ray and Neutron Scattering Data Allows Fine Structural Analysis of MembraneProtein Detergent Complexes. Small-Angle Xray Scattering Curves of Detergent Micelles: Effects of Asymmetry, Shape 2252 Fluctuations, Disorder, and Atomic Details. On the Structural and Dynamical Properties of DOPC Reverse Micelles. Dissolution Processes at Step Edges of Calcite in Water Investigated by High-Speed Frequency 2250 Modulation Atomic Force Microscopy and Simulation. Sequential Bending and Twisting around CC Single Bonds by Mechanical Lifting of a Pre-Adsorbed 2249 Polymer. Chemical Control in the Battle against Fidelity in Promiscuous Natural Product Biosynthesis: The Case of Trichodiene Synthase. High-Efficiency Fluorescence through Bioinspired Supramolecular Self-Assembly. Visualizing Tetrahedral Oxyanion Bound in HIV1 Protease Using Neutrons: Implications for the 2246 Catalytic Mechanism and Drug Design. Plant Polypeptide Hormone Systemin Prefers Polyproline II Conformation in Solution. Calcium Directly Regulates Phosphatidylinositol 4,5-Bisphosphate Headgroup Conformation and 2244 Recognition. Exploring the Role of the Third Active Site Metal Ion in DNA Polymerase with QM/MM Free Energy 2243 Simulations. Glutamine Side Chain 13C18O as a Nonperturbative IR Probe of Amyloid Fibril Hydration and 2242

2241 Dynamic Protonation Dramatically Affects the Membrane Permeability of Drug-like Molecules.

Chemically Controlled Helical Polymorphism in Protein Tubes by Selective Modulation of 2240 Supramolecular Interactions. Critical Role of Confinement in the NMR Surface Relaxation and Diffusion of nHeptane in a Polymer Matrix Revealed by MD Simulations. Role of Dimers in the cAMP-Dependent Activation of Hyperpolarization-Activated 2238 Cyclic-Nucleotide-Modulated (HCN) Ion Channels. Deprotonation of a Single Amino Acid Residue Induces Significant Stability in an Helical Heteropeptide. Dynamical Model for the Counteracting Effects of Trimethylamine NOxide on Urea in Aqueous 2236 Solutions under Pressure. Tunable Energy Barrier for Intercalation of a Carbon Nanotube into Graphene Nanosheets: A Molecular Dynamics Study of a Hybrid Self-Assembly. 2234 Space and Time Evolution of the Electrostatic Potential During the Activation of a Visual Pigment. Molecular Mechanisms Underlying Solute Retention at Heterogeneous Interfaces. Predicting Binding Free Energies in a Large Combinatorial Chemical Space Using Multisite 2232 Dynamics. Overcoming Challenging Substituent Perturbations with Multisite Dynamics: A Case Study 2231 Targeting Secretase 1. Imaging Unstained Synthetic Polymer Crystals and Defects on Atomic Length Scales Using 2230 Cryogenic Electron Microscopy. 2229 Two-Dimensional Band Structure in Honeycomb MetalOrganic Frameworks. Uniform, Polycrystalline, and Thermostable Piperine-Coated Gold Nanoparticles to Target Insulin 2228 Fibril Assembly. Efficient Binding of Flexible and Redox-Active Coenzymes by Oxidoreductases. Semirational Design of Fluoroacetate Dehalogenase RPA1163 for Kinetic Resolution of 2226 -Fluorocarboxylic Acids on a Gram Scale. Molecular Mechanism for Isoform-Selective Inhibition of Acyl Protein Thioesterases 1 and 2 (APT1 2225 and APT2). 2224 Selectively Disrupting m6ADependent ProteinRNA Interactions with Fragments. A Small Molecule Mimetic of the Humanin Peptide as a Candidate for Modulating NMDA-Induced 2223 Neurotoxicity.

2222	Chimeric ProteinProtein Interface Inhibitors Allow Efficient Inhibition of Type III Secretion Machinery and Pseudomonas aeruginosa Virulence.	
2221		
2220	Dynamic Transition from Helices to Sheets in Polypeptide Coiled-Coil Motifs.	
2219		
2218	Dual Role of the Active Site Residues of Thermus thermophilus 3Isopropylmalate Dehydrogenase: Chemical Catalysis and Domain Closure.	
2217	Biocatalytic Routes to Lactone Monomers for Polymer Production.	
2216	Modeling pK Shift in DNA Triplexes Containing Locked Nucleic Acids.	
2215		
2214	Surface Probing by Fragment-Based Screening and Computational Methods Identifies Ligandable Pockets on the von HippelLindau (VHL) E3 Ubiquitin Ligase.	
2213	Molecular modeling of nucleic acid structure: electrostatics and solvation. <b>2001</b> , Chapter 7, Unit 7.9	2
2212	Molecular modeling of nucleic acid structure: energy and sampling. 2001, Chapter 7, Unit 7.8	2
2211	Differential quantum tunneling contributions in nitroalkane oxidase catalyzed and the uncatalyzed proton transfer reaction. <b>2009</b> , 106, 20734-9	63
2210	Inversion of radial distribution functions to pair forces by solving the Yvon-Born-Green equation iteratively. <b>2009</b> , 131, 134107	37
2209	Conformational sampling and energetics of drug-like molecules. <b>2009</b> , 16, 3381-413	56
2208	Analysis of the free-energy surface of proteins from reversible folding simulations. <b>2009</b> , 5, e1000428	21
2207	Isotropic periodic sum of electrostatic interactions for polar systems. <b>2009</b> , 131, 024107	35
2206	On the dielectric conductivity of molecular ionic liquids. <b>2009</b> , 131, 114504	53
2205	Protein-protein docking using region-based 3D Zernike descriptors. <b>2009</b> , 10, 407	116

2204	CHARMM general force field: A force field for drug-like molecules compatible with the CHARMM all-atom additive biological force fields. <i>Journal of Computational Chemistry</i> , <b>2010</b> , 31, 671-90	3.5	2953	
2203	A molecular mechanics model for imatinib and imatinib:kinase binding. <i>Journal of Computational Chemistry</i> , <b>2010</b> , 31, 1550-60	3.5	13	
2202	Coarse-grained model of nucleic acid bases. <i>Journal of Computational Chemistry</i> , <b>2010</b> , 31, 1644-55	3.5	28	
2201	Library screening by fragment-based docking. <b>2010</b> , 23, 183-93		23	
2200	Complex formation between calmodulin and a peptide from the intracellular loop of the gap junction protein connexin43: Molecular conformation and energetics of binding. <b>2009</b> , 144, 130-5		12	
2199	Mechanical signaling on the single protein level studied using steered molecular dynamics. <b>2009</b> , 55, 141-52		26	
2198	Structure and hydration of membranes embedded with voltage-sensing domains. 2009, 462, 473-9		166	
2197	N-acylpolyamine inhibitors of HDM2 and HDMX binding to p53. <b>2009</b> , 17, 7884-93		21	
2196	A fluorescence quenching assay to discriminate between specific and nonspecific inhibitors of dengue virus protease. <b>2009</b> , 395, 195-204		79	
2195	Kinetic characterization of xenobiotic reductase A from Pseudomonas putida 86. <b>2009</b> , 48, 11412-20		13	
2194	Amyloid-like self-assembly of peptide sequences from the adenovirus fiber shaft: insights from molecular dynamics simulations. <b>2009</b> , 113, 15639-47		35	
2193	Free energy and kinetics of conformational transitions from Voronoi tessellated milestoning with restraining potentials. <b>2009</b> , 5, 2589-2594		46	
2192	Flaviviral protease inhibitors identified by fragment-based library docking into a structure generated by molecular dynamics. <b>2009</b> , 52, 4860-8		70	
2191	Direct kinetic evidence that lysine 215 is involved in the phospho-transfer step of human 3-phosphoglycerate kinase. <b>2009</b> , 48, 6998-7008		6	
2190	Liquid-ordered phase formation in cholesterol/sphingomyelin bilayers: all-atom molecular dynamics simulations. <b>2009</b> , 113, 15795-802		40	
2189	NanC crystal structure, a model for outer-membrane channels of the acidic sugar-specific KdgM porin family. <b>2009</b> , 394, 718-31		32	
2188	Predicted structural basis for CD1c presentation of mycobacterial branched polyketides and long lipopeptide antigens. <b>2009</b> , 47, 253-60		11	
2187	Structure-based optimization of potent and selective inhibitors of the tyrosine kinase erythropoietin producing human hepatocellular carcinoma receptor B4 (EphB4). <b>2009</b> , 52, 6433-46		78	

2186	How does a simplified-sequence protein fold?. <b>2009</b> , 97, 1737-46	18
2185	Tetracycline-tet repressor binding specificity: insights from experiments and simulations. <b>2009</b> , 97, 2829-38	13
2184	CHARMM additive all-atom force field for aldopentofuranoses, methyl-aldopentofuranosides, and fructofuranose. <b>2009</b> , 113, 12466-76	107
2183	Boxed molecular dynamics: a simple and general technique for accelerating rare event kinetics and mapping free energy in large molecular systems. <b>2009</b> , 113, 16603-11	65
2182	The basic concepts of molecular modeling. <b>2009</b> , 467, 307-334	13
2181	Preferential interactions of guanidinum ions with aromatic groups over aliphatic groups. <b>2009</b> , 131, 16689-96	66
2180	Structural interactomics: informatics approaches to aid the interpretation of genetic variation and the development of novel therapeutics. <b>2009</b> , 5, 1456-72	8
2179	Fast and accurate predictions of protein NMR chemical shifts from interatomic distances. <b>2009</b> , 131, 13894-5	196
2178	Combinatorial library enumeration and lead hopping using comparative interaction fingerprint analysis and classical 2D QSAR methods for seeking novel GABA(A) alpha(3) modulators. <b>2009</b> , 49, 2498-511	15
2177	CHARMM Additive All-Atom Force Field for Glycosidic Linkages between Hexopyranoses. <b>2009</b> , 5, 2353-2370	473
2176	Predicting pKa values with continuous constant pH molecular dynamics. <b>2009</b> , 466, 455-75	65
2175	Structural and energetic determinants of thermal stability and hierarchical unfolding pathways of hyperthermophilic proteins, Sac7d and Sso7d. <b>2010</b> , 114, 1707-18	23
2174	TAMkin: a versatile package for vibrational analysis and chemical kinetics. <b>2010</b> , 50, 1736-50	127
2173	What is the conformation of physiologically-active dinucleoside polyphosphates in solution? Conformational analysis of free dinucleoside polyphosphates by NMR and molecular dynamics simulations. <b>2010</b> , 8, 4637-52	28
2172	Simulation of Osmotic Pressure in Concentrated Aqueous Salt Solutions. <b>2010</b> , 1, 183-189	208
2171	Update of the CHARMM all-atom additive force field for lipids: validation on six lipid types. <b>2010</b> , 114, 7830-43	2654
2170	Bioinformatics and molecular modeling in glycobiology. <b>2010</b> , 67, 2749-72	73
2169	Forces mediating proteinprotein interactions: a computational study of p53 approaching IMDM2. <b>2010</b> , 125, 621-635	16

2168	Protein isolation through impact desolvation of electrosprayed microdroplets (IDEM): Molecular dynamics simulation. <b>2010</b> , 289, 119-127	7
2167	In silico experiments of single-chain antibody fragment against drugs of abuse. <b>2010</b> , 153, 97-103	5
2166	Simulation studies of the insolubility of cellulose. <b>2010</b> , 345, 2060-6	135
2165	NMR in structural proteomics and beyond. <b>2010</b> , 56, 247-66	29
2164	Conformational sampling of S- and R-warfarin in polar solvents: Implications for stereoselective complex formation. <b>2010</b> , 949, 41-51	
2163	Polarizability rescaling and atom-based Thole scaling in the CHARMM Drude polarizable force field for ethers. <b>2010</b> , 16, 567-76	58
2162	Na(+), K (+) and Tl(+) hydration from QM/MM computations and MD simulations with a polarizable force field. <b>2010</b> , 2, 12-20	4
2161	Interaction of the ⊞2A domain of integrin with small collagen fragments. <b>2010</b> , 1, 393-405	23
2160	T-Analyst: a program for efficient analysis of protein conformational changes by torsion angles. <b>2010</b> , 24, 819-27	24
2159	Targeting biomolecular flexibility with metadynamics. <b>2010</b> , 20, 148-54	113
2158	Evolution: a guide to perturb protein function and networks. <b>2010</b> , 20, 351-9	22
2157	Pi release from myosin: a simulation analysis of possible pathways. <b>2010</b> , 18, 458-70	41
2156	Current trends in antimicrobial agent research: chemo- and bioinformatics approaches. <b>2010</b> , 15, 540-6	58
2155	Comparison of the Ewald and Wolf methods for modeling electrostatic interactions in nanowires. <b>2010</b> , 84, 1541-1551	20
2154	High-throughput virtual screening using quantum mechanical probes: discovery of selective kinase inhibitors. <b>2010</b> , 5, 1007-14	35
2153	Computational analysis of missense mutations causing Snyder-Robinson syndrome. <b>2010</b> , 31, 1043-9	66
2152	Establishing effective simulation protocols for beta- and alpha/beta-peptides. III. Molecular mechanical model for acyclic beta-amino acids. <i>Journal of Computational Chemistry</i> , <b>2010</b> , 31, 2063-77	14

2150	Computational Methods for the Development of Polymeric Biomaterials. <b>2010</b> , 12, B3-B17	15
2149	Structural basis for substrate specificity of alphavirus nsP2 proteases. <b>2010</b> , 29, 46-53	29
2148	Fine grained sampling of residue characteristics using molecular dynamics simulation. <b>2010</b> , 34, 172-83	4
2147	T-cell epitope prediction and immune complex simulation using molecular dynamics: state of the art and persisting challenges. <b>2010</b> , 6 Suppl 2, S4	22
2146	Probing the folding of mini-protein Beta3s by two-dimensional infrared spectroscopy; simulation study. <b>2010</b> , 3, 8	5
2145	RNA polymerase II flexibility during translocation from normal mode analysis. <b>2010</b> , 78, 434-46	22
2144	Versatile substrate protein recognition mechanism of the eukaryotic chaperonin CCT. <b>2010</b> , 78, 1254-65	6
2143	On the orientation of the catalytic dyad in aspartic proteases. <b>2010</b> , 78, 1575-82	11
2142	Thermodynamic resolution: how do errors in modeled protein structures affect binding affinity predictions?. <b>2010</b> , 78, 1613-7	4
2141	Solution structure of the C-terminal DUF1000 domain of the human thioredoxin-like 1 protein. <b>2010</b> , 78, 2176-80	6
2140	FoldGPCR: structure prediction protocol for the transmembrane domain of G protein-coupled receptors from class A. <b>2010</b> , 78, 2189-201	31
2139	Structural characterization of two pore-forming peptides: consequences of introducing a C-terminal tryptophan. <b>2010</b> , 78, 2238-50	7
2138	The flexible C-terminal arm of the Lassa arenavirus Z-protein mediates interactions with multiple binding partners. <b>2010</b> , 78, 2251-64	9
2137	Performance of ZDOCK and ZRANK in CAPRI rounds 13-19. <b>2010</b> , 78, 3104-10	63
2136	Species specificity of the complement inhibitor compstatin investigated by all-atom molecular dynamics simulations. <b>2010</b> , 78, 2655-67	32
2135	Extending the PRIME model for protein aggregation to all 20 amino acids. <b>2010</b> , 78, 2950-60	98
2134	Beta-barrel models of soluble amyloid beta oligomers and annular protofibrils. <b>2010</b> , 78, 3458-72	30
2133	Models of membrane-bound Alzheimer's Abeta peptide assemblies. <b>2010</b> , 78, 3473-87	52

2132	Evaporation of solvent molecules by ultrafast heating: effect on conformation of solvated protein. <b>2010</b> , 24, 349-54	3
2131	The major determinant of exendin-4/glucagon-like peptide 1 differential affinity at the rat glucagon-like peptide 1 receptor N-terminal domain is a hydrogen bond from SER-32 of exendin-4. <b>2010</b> , 160, 1973-84	24
2130	Computational design and biological testing of highly cytotoxic colchicine ring A modifications. <b>2010</b> , 75, 541-50	11
2129	Crystal structure of the halotolerant gamma-glutamyltranspeptidase from Bacillus subtilis in complex with glutamate reveals a unique architecture of the solvent-exposed catalytic pocket. <b>2010</b> , 277, 1000-9	47
2128	Enhanced thermostability of methyl parathion hydrolase from Ochrobactrum sp. M231 by rational engineering of a glycine to proline mutation. <b>2010</b> , 277, 4901-8	82
2127	Structure of a fucose transporter in an outward-open conformation. <b>2010</b> , 467, 734-8	226
2126	GUI-BioPASED: A program for molecular dynamics simulations of biopolymers with a graphical user interface. <b>2010</b> , 44, 648-654	21
2125	APBSmem: a graphical interface for electrostatic calculations at the membrane. <b>2010</b> , 5, e12722	74
2124	Entrapment and structure of an extrahelical guanine attempting to enter the active site of a bacterial DNA glycosylase, MutM. <b>2010</b> , 285, 1468-78	43
2123	Protein dynamics investigated by inherent structure analysis. <b>2010</b> , 107, 9152-7	49
2122	Molecular basis for optical clearing of collagenous tissues. <b>2010</b> , 15, 055002	51
2121	Engineering of substrate selectivity for tissue factor.factor VIIa complex signaling through protease-activated receptor 2. <b>2010</b> , 285, 19959-66	25
2120	The electrostatics of solvent and membrane interfaces and the role of electronic polarizability. <b>2010</b> , 132, 185101	37
2119	PARP1 ADP-ribosylates lysine residues of the core histone tails. <b>2010</b> , 38, 6350-62	192
2118	Two mechanisms of ion selectivity in protein binding sites. <b>2010</b> , 107, 20329-34	69
2117	Assessment of the validity of the double superhelix model for reconstituted high density lipoproteins: a combined computational-experimental approach. <b>2010</b> , 285, 41161-71	50
2116	Water evaporation and conformational changes from partially solvated ubiquitin. 2010, 2010, 213936	6
2115	Structural insights into retinitis pigmentosa from unfolding simulations of rhodopsin mutants. <b>2010</b> , 24, 3196-209	34

2114	experiments. <b>2011</b> , 181-92	17
2113	Coordinate-dependent diffusion in protein folding. <b>2010</b> , 107, 1088-93	221
2112	Human TLRs 10 and 1 share common mechanisms of innate immune sensing but not signaling. <b>2010</b> , 184, 5094-103	175
2111	Understanding Enzyme Catalysis Using Computer Simulation. <b>2010</b> ,	2
2110	Perturbing the folding energy landscape of the bacterial immunity protein Im7 by site-specific N-linked glycosylation. <b>2010</b> , 107, 22528-33	58
2109	Structure of pleiotrophin- and hepatocyte growth factor-binding sulfated hexasaccharide determined by biochemical and computational approaches. <b>2010</b> , 285, 27673-85	27
2108	Molecular dynamics simulations show that conformational selection governs the binding preferences of imatinib for several tyrosine kinases. <b>2010</b> , 285, 13807-15	65
2107	Binding of imidazole to the heme of cytochrome c1 and inhibition of the bc1 complex from Rhodobacter sphaeroides: I. Equilibrium and modeling studies. <b>2010</b> , 285, 22513-21	9
2106	UV Resonance Raman Study of TTR(105🛘15) Structural Evolution as a Function of Temperature. <b>2010</b> ,	
2105	Simulating polarizable molecular ionic liquids with Drude oscillators. <b>2010</b> , 133, 154511	77
2104	A gain-of-function mutation of Arabidopsis cryptochrome1 promotes flowering. <b>2010</b> , 154, 1633-45	37
2103	Interlaced P3M algorithm with analytical and ik-differentiation. <b>2010</b> , 132, 234103	22
2102	Assessing the accuracy of approximate treatments of ion hydration based on primitive quasichemical theory. <b>2010</b> , 132, 234101	24
2101	Free energy surfaces for the interaction of D-glucose with planar aromatic groups in aqueous solution. <b>2010</b> , 133, 155103	22
2100	Relationship between population of the fibril-prone conformation in the monomeric state and oligomer formation times of peptides: insights from all-atom simulations. <b>2010</b> , 132, 165104	38
2099	Nucleotides that are essential but not conserved; a sufficient L-tryptophan site in RNA. <b>2010</b> , 16, 1915-24	8
2098	Refinement of ensembles describing unstructured proteins using NMR residual dipolar couplings. <b>2010</b> , 132, 4626-32	53
2097	A combined experimental and theoretical study of ion solvation in liquid N-methylacetamide. <b>2010</b> , 132, 10847-56	32

2096	Global dynamics of proteins: bridging between structure and function. <b>2010</b> , 39, 23-42	454
2095	Insights into the mechanism of binding of arachidonic acid to mammalian 15-lipoxygenases. <b>2010</b> , 114, 7037-46	30
2094	A repulsive electrostatic mechanism for protein export through the type III secretion apparatus. <b>2010</b> , 98, 452-61	16
2093	Mechanical unfolding of an ankyrin repeat protein. <b>2010</b> , 98, 1294-301	45
2092	The contribution of interchain salt bridges to triple-helical stability in collagen. <b>2010</b> , 98, 2634-43	28
2091	Exploring the ion selectivity properties of a large number of simplified binding site models. <b>2010</b> , 98, 2877-85	29
2090	Revisiting hydrophobic mismatch with free energy simulation studies of transmembrane helix tilt and rotation. <b>2010</b> , 99, 175-83	91
2089	Electron microscopy and persistence length analysis of semi-rigid smooth muscle tropomyosin strands. <b>2010</b> , 99, 862-8	42
2088	Chemomechanical regulation of SNARE proteins studied with molecular dynamics simulations. <b>2010</b> , 99, 1221-30	16
2087	Toward a consensus view of duplex RNA flexibility. <b>2010</b> , 99, 1876-85	46
2086	RNA polymerase II with open and closed trigger loops: active site dynamics and nucleic acid translocation. <b>2010</b> , 99, 2577-86	49
2085	Residue-specific side-chain packing determines the backbone dynamics of transmembrane model helices. <b>2010</b> , 99, 2541-9	25
2084	The O-glycosylated linker from the Trichoderma reesei Family 7 cellulase is a flexible, disordered protein. <b>2010</b> , 99, 3773-81	89
2083	Toward modeling thermoresponsive polymer networks: a molecular dynamics simulation study of N-isopropyl acrylamide co-oligomers. <b>2010</b> , 114, 8301-12	37
2082	Cholesterol flip-flop: insights from free energy simulation studies. <b>2010</b> , 114, 13342-8	97
2081	Development of molecular simulation methods to accurately represent protein-surface interactions: The effect of pressure and its determination for a system with constrained atoms. <b>2010</b> , 5, 85-95	22
2080	Practically Efficient QM/MM Alchemical Free Energy Simulations: The Orthogonal Space Random Walk Strategy. <b>2010</b> , 6, 2253-66	29
	Walk Sciacegy. <b>2010</b> , 0, 2233-00	

## (2010-2010)

2078	A computational study of the mechanism of the selective crystallization of $\oplus$ - and $\oplus$ glycine from water and methanol-water mixture. <b>2010</b> , 114, 13764-72	36
2077	Comparing simulated and experimental translation and rotation constants: range of validity for viscosity scaling. <b>2010</b> , 114, 12501-7	43
2076	Amplitude of pancreatic lipase lid opening in solution and identification of spin label conformational subensembles by combining continuous wave and pulsed EPR spectroscopy and molecular dynamics. <b>2010</b> , 49, 2140-9	23
2075	Slow folding of cross-linked alpha-helical peptides due to steric hindrance. <b>2010</b> , 114, 2023-7	14
2074	Electronic properties and desolvation penalties of metal ions plus protein electrostatics dictate the metal binding affinity and selectivity in the copper efflux regulator. <b>2010</b> , 132, 18092-102	32
2073	Effective Approximation of Molecular Volume Using Atom-Centered Dielectric Functions in Generalized Born Models. <b>2010</b> , 6, 2790-803	22
2072	Absolute binding free energy calculations of sparsomycin analogs to the bacterial ribosome. <b>2010</b> , 114, 9525-39	45
2071	Extracting physically intuitive reaction coordinates from transition networks of a beta-sheet miniprotein. <b>2010</b> , 114, 6979-89	20
2070	Mechanism of the calcium-induced trans-cis isomerization of a non-prolyl peptide bond in Clostridium histolyticum collagenase. <b>2010</b> , 49, 5314-20	10
2069	Merging Implicit with Explicit Solvent Simulations: Polyethylene Glycol. <b>2010</b> , 6, 1871-83	8
2068	Soluble Protofibrils as Metastable Intermediates in Simulations of Amyloid Fibril Degradation Induced by Lipid Vesicles. <b>2010</b> , 1, 471-474	20
2067	Experimentally consistent ion association predicted for metal solutions from free energy simulations. <b>2010</b> , 114, 7286-93	16
2066	Molecular simulations on the thermal stabilization of DNA by hyperthermophilic chromatin protein Sac7d, and associated conformational transitions. <b>2010</b> , 114, 16548-57	12
2065	Atomistic details of the ligand discrimination mechanism of S(MK)/SAM-III riboswitch. <b>2010</b> , 114, 9920-5	8
2064	The 1.4 A crystal structure of the ArsD arsenic metallochaperone provides insights into its interaction with the ArsA ATPase. <b>2010</b> , 49, 5206-12	17
2063	Conformational Free-Energy Difference of a Miniprotein from Nonequilibrium Simulations. <b>2010</b> , 1, 1922-192	.6 <sub>17</sub>
2062	Structural, NMR spectroscopic, and computational investigation of hemin loading in the hemophore HasAp from Pseudomonas aeruginosa. <b>2010</b> , 132, 9857-72	58
	Ion selectivity of alpha-hemolysin with beta-cyclodextrin adapter. II. Multi-ion effects studied with	

2060	Crosstalk along the stalk: dynamics of the interaction of subunits B and F in the A(1)A(O) ATP synthase of Methanosarcina mazei $G\square 1$ . <b>2010</b> , 49, 4181-90	6
2059	Equipartition and the Calculation of Temperature in Biomolecular Simulations. <b>2010</b> , 6, 2045-58	32
2058	Probing the strand orientation and registry alignment in the propagation of amyloid fibrils. <b>2010</b> , 49, 5290-8	26
2057	Conformational dynamics in human purine nucleoside phosphorylase with reactants and transition-state analogues. <b>2010</b> , 114, 16263-72	25
2056	A new coarse-grained model for water: the importance of electrostatic interactions. <b>2010</b> , 114, 10524-9	150
2055	Pyranose ring transition state is derived from cellobiohydrolase I induced conformational stability and glycosidic bond polarization. <b>2010</b> , 132, 12800-3	37
2054	Constraining binding hot spots: NMR and molecular dynamics simulations provide a structural explanation for enthalpy-entropy compensation in SH2-ligand binding. <b>2010</b> , 132, 11058-70	37
2053	Molecular dynamics simulation of bovine pancreatic ribonuclease A-CpA and transition state-like complexes. <b>2010</b> , 114, 7371-82	20
2052	Molecular dynamics simulations and elastic network analysis of protein kinase B (Akt/PKB) inactivation. <b>2010</b> , 50, 1602-10	28
2051	Coarse-grained model for simulation of RNA three-dimensional structures. <b>2010</b> , 114, 13497-506	73
2050	Current status of the AMOEBA polarizable force field. <b>2010</b> , 114, 2549-64	914
2049	Sterol binding and membrane lipid attachment to the Osh4 protein of yeast. <b>2010</b> , 114, 13562-73	4
2048	Amyloid fibril polymorphism is under kinetic control. <b>2010</b> , 132, 14960-70	106
2047	Conformational switching between protein substates studied with 2D IR vibrational echo spectroscopy and molecular dynamics simulations. <b>2010</b> , 114, 17187-93	31
2046	Crowding Effects on Amyloid Aggregation Kinetics. <b>2010</b> , 1, 3027-3032	45
2045	Role of electrostatics in modulating hydrophobic interactions and barriers to hydrophobic assembly. <b>2010</b> , 114, 8107-17	14
2044	Ion selectivity of alpha-hemolysin with a beta-cyclodextrin adapter. I. Single ion potential of mean force and diffusion coefficient. <b>2010</b> , 114, 952-8	34
2043	Helix formation in a pentapeptide: experiment and force-field dependent dynamics. <b>2010</b> , 114, 12391-402	36

## (2010-2010)

2042	Modeling anesthetic binding sites within the glycine alpha one receptor based on prokaryotic ion channel templates: the problem with TM4. <b>2010</b> , 50, 2248-55	22
2041	Ring puckering: a metric for evaluating the accuracy of AM1, PM3, PM3CARB-1, and SCC-DFTB carbohydrate QM/MM simulations. <b>2010</b> , 114, 17142-54	73
2040	Molecular description of flexibility in an antibody combining site. <b>2010</b> , 114, 7359-70	24
2039	Combining metabolic and protein engineering of a terpenoid biosynthetic pathway for overproduction and selectivity control. <b>2010</b> , 107, 13654-9	267
2038	The relationship between curvature, flexibility and persistence length in the tropomyosin coiled-coil. <b>2010</b> , 170, 313-8	68
2037	The shape and flexibility of tropomyosin coiled coils: implications for actin filament assembly and regulation. <b>2010</b> , 395, 327-39	97
2036	Role of the adenine ligand on the stabilization of the secondary and tertiary interactions in the adenine riboswitch. <b>2010</b> , 396, 1422-38	51
2035	A conserved protonation-induced switch can trigger "ionic-lock" formation in adrenergic receptors. <b>2010</b> , 397, 1339-49	30
2034	Many local motions cooperate to produce the adenylate kinase conformational transition. <b>2010</b> , 400, 618-31	78
2033	The impact of viral RNA on the association rates of capsid protein assembly: bacteriophage MS2 as a case study. <b>2010</b> , 400, 935-47	19
2032	Structural and dynamic determinants of ligand binding and regulation of cyclin-dependent kinase 5 by pathological activator p25 and inhibitory peptide CIP. <b>2010</b> , 401, 478-92	15
2031	Ion selectivity of the KcsA channel: a perspective from multi-ion free energy landscapes. <b>2010</b> , 401, 831-42	74
2030	The unique binding mode of cellulosomal CBM4 from Clostridium thermocellum cellobiohydrolase A. <b>2010</b> , 402, 374-87	25
2029	Probing the periplasmic-open state of lactose permease in response to sugar binding and proton translocation. <b>2010</b> , 404, 506-21	28
2028	A novel unstructured scaffold based on 4EBP1 enables the functional display of a wide range of bioactive peptides. <b>2010</b> , 404, 819-31	5
2027	Molecular dynamics simulations of protein dynamics and their relevance to drug discovery. <b>2010</b> , 10, 738-44	109
2026	Conformational coupling, bridge helix dynamics and active site dehydration in catalysis by RNA polymerase. <b>2010</b> , 1799, 575-87	26
2025	Antimicrobial peptides in toroidal and cylindrical pores. <b>2010</b> , 1798, 1485-93	102

2024	Population distribution of flexible molecules from maximum entropy analysis using different priors as background information: application to the III: onformational space of the II-(1>2)-linked mannose disaccharide present in N- and O-linked glycoproteins. <b>2010</b> , 8, 3684-95	43
2023	Predicting solvation energies for kinetic modeling. <b>2010</b> , 106, 211	44
2022	Internal proton transfer in the external pyridoxal 5'-phosphate Schiff base in dopa decarboxylase. <b>2010</b> , 49, 84-94	32
2021	CHARMM additive all-atom force field for glycosidic linkages in carbohydrates involving furanoses. <b>2010</b> , 114, 12981-94	129
2020	Molecular switch controlling the binding of anionic bile acid conjugates to human apical sodium-dependent bile acid transporter. <b>2010</b> , 53, 4749-60	22
2019	A Guide to QM/MM Methodology and Applications. <b>2010</b> , 59, 353-400	24
2018	Free Energy Perturbation Hamiltonian Replica-Exchange Molecular Dynamics (FEP/H-REMD) for Absolute Ligand Binding Free Energy Calculations. <b>2010</b> , 6, 2559-2565	180
2017	Allosteric regulation of glycogen synthase kinase 3🛭 a theoretical study. <b>2010</b> , 49, 10890-901	24
2016	Transmembrane structures for Alzheimer's AI(1-42) oligomers. <b>2010</b> , 132, 13300-12	116
2015	Probing the structural determinants for the function of intracellular loop 2 in structurally cognate G-protein-coupled receptors. <b>2010</b> , 49, 10691-701	16
2014	Comparison of solid-state dipolar couplings and solution relaxation data provides insight into protein backbone dynamics. <b>2010</b> , 132, 5015-7	45
2013	Accurate Calculation of Hydration Free Energies using Pair-Specific Lennard-Jones Parameters in the CHARMM Drude Polarizable Force Field. <b>2010</b> , 6, 1181-1198	116
2012	Maximum Flux Transition Paths of Conformational Change. <b>2010</b> , 6, 2411-2423	25
2011	How does bone sialoprotein promote the nucleation of hydroxyapatite? A molecular dynamics study using model peptides of different conformations. <b>2010</b> , 26, 9848-59	76
2010	Using fit functions in computational dielectric spectroscopy. <b>2010</b> , 132, 244109	45
2009	Free energy surfaces from single-distance information. <b>2010</b> , 114, 15227-35	27
2008	A second generation distributed point polarizable water model. <b>2010</b> , 132, 014309	102
2007	Atomistic simulations of 2D bicomponent self-assembly: from molecular recognition to self-healing. <b>2010</b> , 132, 17880-5	70

2006 Mitosis method for directly calculating	ng the interfacial free energy of nuclei. <b>2010</b> , 36, 498-504	8
lon-size effect within the aqueous so studies. <b>2010</b> , 12, 13566-73	olution interface at the Pt(111) surface: molecular dynamics	2
identification of amino acids respons module from a fungal cellulase. <b>2010</b>	sible for processivity in a Family 1 carbohydrate-binding <b>)</b> , 114, 1447-53	102
Structural determinants for transpor conjugates. <b>2010</b> , 7, 2240-54	t across the intestinal bile acid transporter using C-24 bile acid	20
	onpolarizable inorganic salt solution interfaces: NaCl, NaBr, ar potential 4-point with charge dependent polarizability 13	12
Study on interaction between ampic aided protein-protein docking for bic	illin antibody and detection interfering proteins by computer osensor interesting. <b>2010</b> ,	0
2000 The sodium/galactose symporter cry	rstal structure is a dynamic, not so occluded state. <b>2010</b> , 6, 1040-6	25
1999 coarse-grained molecular models" by	ntegration time step in molecular dynamics simulations of y M. Winger, D. Trzesniak, R. Baron and W. F. van Gunsteren, 934. <b>2010</b> , 12, 2254-6; author reply 2257-8	60
An Artificial Neural Network Based A an Extended Forcefield. <b>2011</b> ,	Approach for Identification of Native Protein Structures Using	1
High performance screening, structu <sup>1997</sup> from TCM Database@Taiwan. <b>2011</b> ,	ıral and molecular dynamics analysis to identify H1 inhibitors 7, 3366-74	34
	d molecular mechanical method using modified generalized electronic excited states. <b>2011</b> , 13, 11731-8	9
On the efficient and accurate short-r 1995 109, 1195-1211	anged simulations of uniform polar molecular liquids. 2011,	22
Bacterial degradation of strobilurin f the subtilisin proteases?. <b>2011</b> , 29, 1	fungicides: a role for a promiscuous methyl esterase activity of 19-129	20
Nucleotide promiscuity of 3-phospho 1993 better anti-HIV analogues. <b>2011</b> , 7, 1	oglycerate kinase is in focus: implications for the design of 863-73	10
1992 Solvation studies of a zinc finger pro	tein in hydrated ionic liquids. <b>2011</b> , 13, 6955-69	43
1991 Traditional Chinese medicine, a solut	cion for reducing dual stroke risk factors at once?. <b>2011</b> , 7, 2711-9	39
	bonding on the stability of Trp-cage miniprotein. A TIP4P-Ew water models. <b>2011</b> , 13, 19840-7	63
1989 Efficient solvent boundary potential	for hybrid potential simulations. <b>2011</b> , 13, 10503-9	16

1988	A Kirkwood-Buff force field for the aromatic amino acids. <b>2011</b> , 13, 18154-67	33
1987	Insertion domain within mammalian mitochondrial translation initiation factor 2 serves the role of eubacterial initiation factor 1. <b>2011</b> , 108, 3918-23	41
1986	Molecular-level origins of biomass recalcitrance: decrystallization free energies for four common cellulose polymorphs. <b>2011</b> , 115, 4118-27	161
1985	The role of local hydration and hydrogen-bonding dynamics in ion and solute release from ion-coupled secondary transporters. <b>2011</b> , 50, 1848-56	47
1984	Direct evidence for methyl group coordination by carbon-oxygen hydrogen bonds in the lysine methyltransferase SET7/9. <b>2011</b> , 286, 18658-63	51
1983	Influence of solvent and intramolecular hydrogen bonding on the conformational properties of o-linked glycopeptides. <b>2011</b> , 115, 11215-29	49
1982	Continuous Constant pH Molecular Dynamics in Explicit Solvent with pH-Based Replica Exchange. <b>2011</b> , 7, 2617-29	134
1981	Molecular mechanism by which palmitate inhibits PKR autophosphorylation. <b>2011</b> , 50, 1110-9	9
1980	Understanding the Mechanisms of Bioprotection: A Comparative Study of Aqueous Solutions of Trehalose and Maltose upon Supercooling. <b>2011</b> , 2, 977-982	42
1979	UV resonance Raman study of TTR(105-115) structural evolution as a function of temperature. <b>2011</b> , 115, 4088-98	6
1978	Delineation of folding pathways of a 🛭 sheet miniprotein. <b>2011</b> , 115, 13065-74	39
1977	Rational and computational design of stabilized variants of cyanovirin-N that retain affinity and specificity for glycan ligands. <b>2011</b> , 50, 10698-712	18
1976	Optimization of a cyclic peptide inhibitor of Ser/Thr phosphatase PPM1D (Wip1). <b>2011</b> , 50, 4537-49	36
1975	Water-exclusion and liquid-structure forces in implicit solvation. <b>2011</b> , 115, 14668-82	26
1974	Calculation of the Vibrational Stark Effect Using a First-Principles QM/MM Approach. 2011, 2011, 553-556	15
1973	Importance of domain closure for the autoactivation of ERK2. <b>2011</b> , 50, 8038-48	21
1972	Enhancing QM/MM molecular dynamics sampling in explicit environments via an orthogonal-space-random-walk-based strategy. <b>2011</b> , 115, 3924-35	20
1971	4-Hydroxynonenal inhibits SIRT3 via thiol-specific modification. <b>2011</b> , 24, 651-62	93

1970	Structural insights into the two sequential folding transition states of the PB1 domain of NBR1 from Palue analysis and biased molecular dynamics simulations. <b>2011</b> , 50, 125-35	3
1969	Dynamics in the active site of 🛭 secretase: a network analysis of atomistic simulations. <b>2011</b> , 50, 9328-39	18
1968	Stabilization of the predominant disease-causing aldolase variant (A149P) with zwitterionic osmolytes. <b>2011</b> , 50, 663-71	6
1967	Accommodating a nonconservative internal mutation by water-mediated hydrogen bonding between I-sheet strands: a comparison of human and rat type B (mitochondrial) cytochrome b5. <b>2011</b> , 50, 5544-54	11
1966	The extent of conformational rigidity determines hydration in nonaromatic hexacyclic systems. <b>2011</b> , 115, 2608-16	9
1965	Dielectric properties of organic solvents from non-polarizable molecular dynamics simulation with electronic continuum model and density functional theory. <b>2011</b> , 115, 12571-6	17
1964	Inhibition of multidrug resistance-linked P-glycoprotein (ABCB1) function by 5'-fluorosulfonylbenzoyl 5'-adenosine: evidence for an ATP analogue that interacts with both drug-substrate-and nucleotide-binding sites. <b>2011</b> , 50, 3724-35	12
1963	L-arginine binding to human inducible nitric oxide synthase: an antisymmetric funnel route toward isoform-specific inhibitors?. <b>2011</b> , 51, 1325-35	2
1962	On the mechanism of crystalline polymorph selection by polymer heteronuclei. <b>2011</b> , 27, 7575-9	61
1961	Molecular Dynamics Simulations of a Binding Intermediate between FKBP12 and a High-Affinity Ligand. <b>2011</b> , 7, 725-41	5
1960	Parallel Generalized Born Implicit Solvent Calculations with NAMD. <b>2011</b> , 7, 3635-3642	111
1959	Conformation and dynamics of poly(N-isopropyl acrylamide) trimers in water: a molecular dynamics and metadynamics simulation study. <b>2011</b> , 115, 5827-39	29
1958	Free energy simulations of a GTPase: GTP and GDP binding to archaeal initiation factor 2. <b>2011</b> , 115, 6749-63	26
1957	Optimizing Nucleus Size Metrics for Liquid-Solid Nucleation from Transition Paths of Near-Nanosecond Duration. <b>2011</b> , 2, 1133-8	48
1956	Exploration of transferability in multiscale coarse-grained peptide models. <b>2011</b> , 115, 11911-26	20
1955	Alpha7 helix plays an important role in the conformational stability of PTP1B. <b>2011</b> , 28, 675-93	20
1954	High-temperature behavior of cellulose I. <b>2011</b> , 115, 2155-66	110
1953	Conformational Dependence of Isotropic Polarizabilities. <b>2011</b> , 7, 1404-14	13

1952	Iterative Optimization of Molecular Mechanics Force Fields from NMR Data of Full-Length Proteins. <b>2011</b> , 7, 1773-82	66
1951	Using solvent binding and dielectric friction to interpret the hydration behavior of complex anions. <b>2011</b> , 115, 1045-55	10
1950	Gramicidin A backbone and side chain dynamics evaluated by molecular dynamics simulations and nuclear magnetic resonance experiments. I: molecular dynamics simulations. <b>2011</b> , 115, 7417-26	31
1949	SwissDock, a protein-small molecule docking web service based on EADock DSS. <b>2011</b> , 39, W270-7	984
1948	Application of the SCC-DFTB method to neutral and protonated water clusters and bulk water. <b>2011</b> , 115, 6790-805	71
1947	Tropomyosin position on F-actin revealed by EM reconstruction and computational chemistry. <b>2011</b> , 100, 1005-13	135
1946	Molecular dynamics studies of ion permeation in VDAC. <b>2011</b> , 100, 602-610	68
1945	Enantiospecificity of chloroperoxidase-catalyzed epoxidation: biased molecular dynamics study of a cis-I-methylstyrene/chloroperoxidase-compound I complex. <b>2011</b> , 100, 1066-75	14
1944	Cy3-DNA stacking interactions strongly depend on the identity of the terminal basepair. <b>2011</b> , 100, 1049-57	62
1943	Solid-state NMR ensemble dynamics as a mediator between experiment and simulation. <b>2011</b> , 100, 2922-8	17
1942	Glu-286 rotation and water wire reorientation are unlikely the gating elements for proton pumping in cytochrome C oxidase. <b>2011</b> , 101, 61-9	31
1941	Transmembrane helix orientation and dynamics: insights from ensemble dynamics with solid-state NMR observables. <b>2011</b> , 100, 2913-21	28
1940	Transmembrane signaling of chemotaxis receptor tar: insights from molecular dynamics simulation studies. <b>2011</b> , 100, 2955-63	32
1939	Protein unfolding under force: crack propagation in a network. <b>2011</b> , 101, 736-44	10
1938	Steric and electronic influences on the torsional energy landscape of retinal. <b>2011</b> , 101, L17-9	16
1937	Membrane tension, lipid adaptation, conformational changes, and energetics in MscL gating. <b>2011</b> , 101, 671-9	14
1936	On the origin of order in the genome organization of ssRNA viruses. <b>2011</b> , 101, 774-80	12
1935	Hysteresis-based mechanism for the directed motility of the Ncd motor. <b>2011</b> , 101, 1105-13	10

1934	The structural pathway for water permeation through sodium-glucose cotransporters. <b>2011</b> , 101, 1887-95	35
1933	A conformational transition in the myosin VI converter contributes to the variable step size. <b>2011</b> , 101, 2436-44	16
1932	Base-flipping mechanism in postmismatch recognition by MutS. <b>2011</b> , 101, 2223-31	21
1931	Atomistic ensemble modeling and small-angle neutron scattering of intrinsically disordered protein complexes: applied to minichromosome maintenance protein. <b>2011</b> , 101, 2999-3007	15
1930	Biocatalytic self-assembly of 2D peptide-based nanostructures. <b>2011</b> , 7, 10032	56
1929	Conformational relaxation and water penetration coupled to ionization of internal groups in proteins. <b>2011</b> , 115, 4042-53	32
1928	Theoretical studies of the base pair fidelity of selenium-modified DNA. <b>2011</b> , 115, 10041-8	7
1927	Reproducing crystal binding modes of ligand functional groups using Site-Identification by Ligand Competitive Saturation (SILCS) simulations. <b>2011</b> , 51, 877-96	85
1926	Molecular modeling and molecular dynamics simulation studies of the GSK3I/ATP/substrate complex: understanding the unique P+4 primed phosphorylation specificity for GSK3II substrates. <b>2011</b> , 51, 1025-36	28
1925	Simulating pH titration of a single surfactant in ionic and nonionic surfactant micelles. <b>2011</b> , 115, 14980-90	21
1924	GRIFFIN: A versatile methodology for optimization of protein-lipid interfaces for membrane protein simulations. <b>2011</b> , 7, 1167-1176	47
1923	Conformational Sampling in Structure Prediction and Refinement with Atomistic and Coarse-Grained Models. <b>2011</b> , 85-109	3
1922	Structure of the chromophore binding pocket in the Pr state of plant phytochrome phyA. <b>2011</b> , 115, 1220-31	33
1921	Consensus 3D model of Eppioid receptor ligand efficacy based on a quantitative Conformationally Sampled Pharmacophore. <b>2011</b> , 115, 7487-96	18
1920	Dynamics on the electronically excited state surface of the bioluminescent firefly luciferase-oxyluciferin system. <b>2011</b> , 133, 12040-9	48
1919	Dynamics, flexibility and ligand-induced conformational changes in biological macromolecules: a computational approach. <b>2011</b> , 3, 2079-100	27
1918	Boxed Molecular Dynamics: Decorrelation Time Scales and the Kinetic Master Equation. <b>2011</b> , 7, 1244-52	41
1917	Motion of a disordered polypeptide chain as studied by paramagnetic relaxation enhancements, 15N relaxation, and molecular dynamics simulations: how fast is segmental diffusion in denatured ubiquitin?. <b>2011</b> , 133, 14614-28	45

1916	Theoretical Investigations on the Conformation of the I-d-Arabinofuranoside Ring. 2011, 7, 420-32	17
1915	Computational ligand-based rational design: Role of conformational sampling and force fields in model development. <b>2011</b> , 2, 356-370	58
1914	Self-templating 2D supramolecular networks: a new avenue to reach control over a bilayer formation. <b>2011</b> , 3, 4125-9	39
1913	Theoretical study of bone sialoprotein in bone biomineralization. <b>2011</b> , 194, 182-7	18
1912	A QM/MM study of the phosphoryl transfer to the Kemptide substrate catalyzed by protein kinase A. The effect of the phosphorylation state of the protein on the mechanism. <b>2011</b> , 13, 530-9	23
1911	Origin of chiral selectivity in gas-phase serine tetramers. <b>2011</b> , 13, 877-85	8
1910	A Generic Force Field Based on Quantum Chemical Topology. <b>2011</b> , 505-526	3
1909	Examination of the ∃-chitin structure and decrystallization thermodynamics at the nanoscale. <b>2011</b> , 115, 4516-22	61
1908	Combination of spectroscopic and computational methods to get an understanding of supramolecular chemistry of drugs: from simple host systems to biomolecules. <b>2011</b> , 13, 20893-905	25
1907	A Grid-enabled web portal for NMR structure refinement with AMBER. <b>2011</b> , 27, 2384-90	51
1906	Solvent effect on the absorption spectra of coumarin 120 in water: A combined quantum mechanical and molecular mechanical study. <b>2011</b> , 134, 014501	16
1905	The high dielectric constant of staphylococcal nuclease is encoded in its structural architecture. <b>2011</b> , 133, 20072-5	13
1904	Free Energy Profiles along Consensus Normal Modes Provide Insight into HIV-1 Protease Flap Opening. <b>2011</b> , 7, 2348-52	25
1903	Fragment-Based Approaches in Virtual Screening. <b>2011</b> , 467-489	2
1902	Dissecting force interactions in cellulose deconstruction reveals the required solvent versatility for overcoming biomass recalcitrance. <b>2011</b> , 133, 14033-41	111
1901	Decrystallization of Oligosaccharides from the Cellulose I $\square$ Surface with Molecular Simulation. <b>2011</b> , 2, 1546-1550	50
1900	Toward canonical ensemble distribution from self-guided Langevin dynamics simulation. <b>2011</b> , 134, 134108	33
1899	Force-momentum-based self-guided Langevin dynamics: a rapid sampling method that approaches the canonical ensemble. <b>2011</b> , 135, 204101	18

1898	Probing pH-dependent dissociation of HdeA dimers. <b>2011</b> , 133, 19393-8	37
1897	Protein allostery at the solid-liquid interface: endoglucanase attachment to cellulose affects glucan clenching in the binding cleft. <b>2011</b> , 133, 16617-24	22
1896	Molecular dynamics simulation and binding energy calculation for estimation of oligonucleotide duplex thermostability in RNA-based therapeutics. <b>2011</b> , 51, 1957-65	14
1895	Network Biology. <b>2011</b> ,	3
1894	The influence of polarizability on the dielectric spectrum of the ionic liquid 1-ethyl-3-methylimidazolium triflate. <b>2011</b> , 13, 12240-8	39
1893	Predicting fragment binding poses using a combined MCSS MM-GBSA approach. <b>2011</b> , 51, 1092-105	35
1892	Preparation and refinement of model protein-ligand complexes. 2012, 857, 351-73	11
1891	Inverse problems in ion channel modelling. <b>2011</b> , 27, 083001	20
1890	Evaluation of spectrophotometric and HPLC methods for shikimic acid determination in plants: models in glyphosate-resistant and -susceptible crops. <b>2011</b> , 59, 2202-12	28
1889	Scoring and lessons learned with the CSAR benchmark using an improved iterative knowledge-based scoring function. <b>2011</b> , 51, 2097-106	25
1888	ROSETTA3: an object-oriented software suite for the simulation and design of macromolecules. <b>2011</b> , 487, 545-74	1216
1887	GROMOS++ Software for the Analysis of Biomolecular Simulation Trajectories. <b>2011</b> , 7, 3379-90	160
1886	Hybrid Quantum and Classical Simulations of the Dihydrofolate Reductase Catalyzed Hydride Transfer Reaction on an Accurate Semi-Empirical Potential Energy Surface. <b>2011</b> , 7, 3420-37	43
1885	Microscopic Symmetry Imposed by Rotational Symmetry Boundary Conditions in Molecular Dynamics Simulation. <b>2011</b> , 7, 3346-3353	5
1884	Multi-Site Edynamics for simulated Structure-Activity Relationship studies. <b>2011</b> , 7, 2728-2739	51
1883	Lipid membranes with a majority of cholesterol: applications to the ocular lens and aquaporin 0. <b>2011</b> , 115, 6455-64	38
1882	Orientation of fluorescent lipid analogue BODIPY-PC to probe lipid membrane properties: insights from molecular dynamics simulations. <b>2011</b> , 115, 6157-65	24
1881	Conformational properties of methyl □-maltoside and methyl □- and □-cellobioside disaccharides. <b>2011</b> , 115, 597-608	42

1880	Specific interactions of sodium salts with alanine dipeptide and tetrapeptide in water: insights from molecular dynamics. <b>2011</b> , 115, 13389-400	18
1879	Lipid chain branching at the iso- and anteiso-positions in complex Chlamydia membranes: a molecular dynamics study. <b>2011</b> , 1808, 323-31	41
1878	On the role of anionic lipids in charged protein interactions with membranes. <b>2011</b> , 1808, 1673-83	34
1877	G117C MelB, a mutant melibiose permease with a changed conformational equilibrium. <b>2011</b> , 1808, 2508-16	13
1876	Weak long-range correlated motions in a surface patch of ubiquitin involved in molecular recognition. <b>2011</b> , 133, 10336-9	138
1875	The effect of mutations on the alloreactive T cell receptor/peptide-MHC interface structure: a molecular dynamics study. <b>2011</b> , 115, 8317-27	13
1874	Simulation of solution phase electron transfer in a compact donor-acceptor dyad. <b>2011</b> , 115, 12135-44	24
1873	Free energy of conformational transition paths in biomolecules: the string method and its application to myosin VI. <b>2011</b> , 134, 085103	97
1872	Amyloid-like self-assembly of a dodecapeptide sequence from the adenovirus fiber shaft: Perspectives from molecular dynamics simulations. <b>2011</b> , 357, 717-722	16
1871	Probing designability via a generalized model of helical bundle geometry. <b>2011</b> , 405, 1079-100	152
1870	Mechanism of binding site conformational switching in the CD44-hyaluronan protein-carbohydrate binding interaction. <b>2011</b> , 406, 631-47	23
1869	Electrostatic interactions mediate binding of obscurin to small ankyrin 1: biochemical and molecular modeling studies. <b>2011</b> , 408, 321-34	14
1868	The evolution of catalytic function in the HIV-1 protease. <b>2011</b> , 408, 792-805	4
1867	Role of <b>2</b> 9 connector channel loops in late-stage DNA packaging. <b>2011</b> , 410, 50-9	43
1866	A concerted mechanism for opening the GDP binding pocket and release of the nucleotide in hetero-trimeric G-proteins. <b>2011</b> , 411, 298-312	26
1865	Surfactant effects on amyloid aggregation kinetics. <b>2011</b> , 414, 303-12	20
1864	Computational studies of protegrin antimicrobial peptides: a review. <b>2011</b> , 32, 188-201	54
1863	Molecular dynamics simulation studies of caffeine aggregation in aqueous solution. <b>2011</b> , 115, 10957-66	58

## (2011-2011)

	High-performance scalable molecular dynamics simulations of a polarizable force field based on classical Drude oscillators in NAMD. <b>2011</b> , 2, 87-92	191
1861	Development of CHARMM polarizable force field for nucleic acid bases based on the classical Drude oscillator model. <b>2011</b> , 115, 580-96	105
1860	A model of calcium activation of the cardiac thin filament. <b>2011</b> , 50, 7405-13	67
1859	Coarse-grained model for PEGylated lipids: effect of PEGylation on the size and shape of self-assembled structures. <b>2011</b> , 115, 7830-7	93
1858	Probing amyloid-beta fibril stability by increasing ionic strengths. <b>2011</b> , 115, 2075-81	16
1857	Thermodynamic coupling between activation and inactivation gating in potassium channels revealed by free energy molecular dynamics simulations. <b>2011</b> , 138, 571-80	47
1856	CHARMM additive all-atom force field for carbohydrate derivatives and its utility in polysaccharide and carbohydrate-protein modeling. <b>2011</b> , 7, 3162-3180	403
1855	Algorithm improvements for molecular dynamics simulations. <b>2011</b> , 1, 93-108	26
1854	Structural basis for inhibiting Pamyloid oligomerization by a non-coded Pbreaker-substituted endomorphin analogue. <b>2011</b> , 6, 1265-76	28
1853	Carbon-nanotube-based artificial peptide channel: Transportation of small peptide under external electric field force. <b>2011</b> , 42, 724-726	2
1852		
1052	. 2011,	26
1851	. 2011,  Neoamphimedine circumvents metnase-enhanced DNA topoisomerase II⊞ activity through ATP-competitive inhibition. 2011, 9, 2397-408	<ul><li>26</li><li>16</li></ul>
	Neoamphimedine circumvents metnase-enhanced DNA topoisomerase II⊞ activity through	
1851	Neoamphimedine circumvents metnase-enhanced DNA topoisomerase IIH activity through ATP-competitive inhibition. <b>2011</b> , 9, 2397-408  Molecular mechanism of a green-shifted, pH-dependent red fluorescent protein mKate variant.	16
1851 1850	Neoamphimedine circumvents metnase-enhanced DNA topoisomerase II⊞ activity through ATP-competitive inhibition. <b>2011</b> , 9, 2397-408  Molecular mechanism of a green-shifted, pH-dependent red fluorescent protein mKate variant. <b>2011</b> , 6, e23513  Crystal structure of the HIV-2 neutralizing Fab fragment 7C8 with high specificity to the V3 region	16
1851 1850 1849	Neoamphimedine circumvents metnase-enhanced DNA topoisomerase IIII activity through ATP-competitive inhibition. 2011, 9, 2397-408  Molecular mechanism of a green-shifted, pH-dependent red fluorescent protein mKate variant. 2011, 6, e23513  Crystal structure of the HIV-2 neutralizing Fab fragment 7C8 with high specificity to the V3 region of gp125. 2011, 6, e18767	16 8 5
1851 1850 1849 1848	Neoamphimedine circumvents metnase-enhanced DNA topoisomerase IIII activity through ATP-competitive inhibition. 2011, 9, 2397-408  Molecular mechanism of a green-shifted, pH-dependent red fluorescent protein mKate variant. 2011, 6, e23513  Crystal structure of the HIV-2 neutralizing Fab fragment 7C8 with high specificity to the V3 region of gp125. 2011, 6, e18767  Multiple pH regime molecular dynamics simulation for pK calculations. 2011, 6, e20116  In silico and in vitro investigations of the mutability of disease-causing missense mutation sites in	<ul><li>16</li><li>8</li><li>5</li><li>9</li></ul>

1844	Symmetry-based self-assembled nanotubes constructed using native protein structures: the key role of flexible linkers. <b>2011</b> , 18, 362-72	1
1843	Development of small-molecule PUMA inhibitors for mitigating radiation-induced cell death. <b>2011</b> , 11, 281-90	49
1842	Structural variants of IFN⊞ preferentially promote antiviral functions. <b>2011</b> , 118, 2567-77	22
1841	Product energy deposition of CN + alkane H abstraction reactions in gas and solution phases. <b>2011</b> , 134, 214508	45
1840	Comparison of two adaptive temperature-based replica exchange methods applied to a sharp phase transition of protein unfolding-folding. <b>2011</b> , 134, 244111	27
1839	Structural modelling of red cell surface proteins. <b>2011</b> , 100, 129-39	7
1838	Insight into the phosphodiesterase mechanism from combined QM/MM free energy simulations. <b>2011</b> , 278, 2579-95	19
1837	Knowledge-based identification of the ERK2/STAT3 signal pathway as a therapeutic target for type 2 diabetes and drug discovery. <b>2011</b> , 78, 471-6	12
1836	Molecular dynamics method for proteins with ionization-conformation coupling and equilibrium titration. <b>2011</b> , 45, 309-317	
1835	The hidden energetics of ligand binding and activation in a glutamate receptor. <b>2011</b> , 18, 283-7	99
1835 1834	The hidden energetics of ligand binding and activation in a glutamate receptor. <b>2011</b> , 18, 283-7  Extracellular complexes of the hematopoietic human and mouse CSF-1 receptor are driven by common assembly principles. <b>2011</b> , 19, 1762-72	99
	Extracellular complexes of the hematopoietic human and mouse CSF-1 receptor are driven by	
1834	Extracellular complexes of the hematopoietic human and mouse CSF-1 receptor are driven by common assembly principles. <b>2011</b> , 19, 1762-72  Computer simulations of water flux and salt permeability of the reverse osmosis FT-30 aromatic	33
1834 1833	Extracellular complexes of the hematopoietic human and mouse CSF-1 receptor are driven by common assembly principles. <b>2011</b> , 19, 1762-72  Computer simulations of water flux and salt permeability of the reverse osmosis FT-30 aromatic polyamide membrane. <b>2011</b> , 384, 1-9  Comparison of implicit solvent models and force fields in molecular dynamics simulations of the	33 69
1834 1833 1832	Extracellular complexes of the hematopoietic human and mouse CSF-1 receptor are driven by common assembly principles. 2011, 19, 1762-72  Computer simulations of water flux and salt permeability of the reverse osmosis FT-30 aromatic polyamide membrane. 2011, 384, 1-9  Comparison of implicit solvent models and force fields in molecular dynamics simulations of the PB1 domain. 2011, 515, 283-289  MEMO associated with an ErbB2 receptor phosphopeptide reveals a new phosphotyrosine motif.	<ul><li>33</li><li>69</li><li>5</li></ul>
1834 1833 1832	Extracellular complexes of the hematopoietic human and mouse CSF-1 receptor are driven by common assembly principles. 2011, 19, 1762-72  Computer simulations of water flux and salt permeability of the reverse osmosis FT-30 aromatic polyamide membrane. 2011, 384, 1-9  Comparison of implicit solvent models and force fields in molecular dynamics simulations of the PB1 domain. 2011, 515, 283-289  MEMO associated with an ErbB2 receptor phosphopeptide reveals a new phosphotyrosine motif. 2011, 585, 2688-92  A computational modeling approach for enhancing self-assembly and biofunctionalisation of	<ul><li>33</li><li>69</li><li>5</li><li>3</li></ul>
1834 1833 1832 1831 1830	Extracellular complexes of the hematopoietic human and mouse CSF-1 receptor are driven by common assembly principles. 2011, 19, 1762-72  Computer simulations of water flux and salt permeability of the reverse osmosis FT-30 aromatic polyamide membrane. 2011, 384, 1-9  Comparison of implicit solvent models and force fields in molecular dynamics simulations of the PB1 domain. 2011, 515, 283-289  MEMO associated with an ErbB2 receptor phosphopeptide reveals a new phosphotyrosine motif. 2011, 585, 2688-92  A computational modeling approach for enhancing self-assembly and biofunctionalisation of collagen biomimetic peptides. 2011, 32, 7275-85  Conformational preferences in diglycosyl disulfides: NMR and molecular modeling studies. 2011,	<ul><li>33</li><li>69</li><li>5</li><li>3</li><li>29</li></ul>

1826	Force fields for homology modeling. <b>2012</b> , 857, 83-106	9
1825	Stable associates of polyether oligomers with chlorine anion as revealed by the data of electrospray mass spectrometry and molecular dynamics. <b>2011</b> , 66, 1341-1347	3
1824	Modeling the mechanism of hydrolysis of cyclic guanosine monophosphates in aqueous solution. <b>2011</b> , 66, 229-231	2
1823	The canonical equilibrium of constrained molecular models. <b>2011</b> , 200, 5-54	8
1822	Efficient Calculation of QM/MM Frequencies with the Mobile Block Hessian. <b>2011</b> , 7, 496-514	29
1821	MSCALE: A General Utility for Multiscale Modeling. <b>2011</b> , 7, 1208-1219	38
1820	Substrate binding to mammalian 15-lipoxygenase. <b>2011</b> , 25, 825-35	15
1819	Computational and experimental studies of the interaction between phospho-peptides and the C-terminal domain of BRCA1. <b>2011</b> , 25, 1071-84	24
1818	Dynamic bond-order force field. <b>2011</b> , 10, 2-20	7
1817	Domain cooperativity in multidomain proteins: what can we learn from molecular alignment in anisotropic media?. <b>2011</b> , 51, 131-50	18
1816	Biochemical and enzymatic study of rice BADH wild-type and mutants: an insight into fragrance in rice. <b>2011</b> , 30, 529-38	11
1815	Identification of a novel prostate cancer susceptibility variant in the KLK3 gene transcript. <b>2011</b> , 129, 687-94	72
1814	RNA and protein 3D structure modeling: similarities and differences. <b>2011</b> , 17, 2325-36	67
1813	A computerized protein-protein interaction modeling study of ampicillin antibody specificity in relation to biosensor development. <b>2011</b> , 17, 2873-82	3
1812	Modeling of ligand binding to G protein coupled receptors: cannabinoid CB1, CB2 and adrenergic © 2 AR. <b>2011</b> , 17, 2353-66	27
1811	Trends in template/fragment-free protein structure prediction. <b>2011</b> , 128, 3-16	41
1810	NaCl interactions with phosphatidylcholine bilayers do not alter membrane structure but induce long-range ordering of ions and water. <b>2011</b> , 244, 35-42	33
1809	Two polymorphic residues account for the differences in DNA binding and transcriptional activation by NF- <b>B</b> proteins encoded by naturally occurring alleles in Nematostella vectensis. <b>2011</b> , 73, 325-36	7

1808	Improving the description of salt bridge strength and geometry in a Generalized Born model. <b>2011</b> , 29, 676-84	15
1807	Intramolecular hydrogen bonding in articaine can be related to superior bone tissue penetration: a molecular dynamics study. <b>2011</b> , 154, 18-25	29
1806	Effect of osteogenesis imperfecta mutations on free energy of collagen model peptides: a molecular dynamics simulation. <b>2011</b> , 156, 146-52	6
1805	Improving the thermostability of a methyl parathion hydrolase by adding the ionic bond on protein surface. <b>2011</b> , 165, 989-97	13
1804	Meet me halfway: when genomics meets structural bioinformatics. <b>2011</b> , 4, 281-303	10
1803	Structure propensities in mutated polyglutamine peptides. <b>2011</b> , 3, 1-16	3
1802	FEARCF a multidimensional free energy method for investigating conformational landscapes and chemical reaction mechanisms. <b>2011</b> , 54, 1962-1973	11
1801	A full-length 3D structure for MAPK/ERK kinase 2 (MEK2). <b>2011</b> , 54, 336-41	8
1800	Molecular dynamics simulations and in silico peptide ligand screening of the Elk-1 ETS domain. <b>2011</b> , 3, 49	4
1799	Computational studies of colicin insertion into membranes: the closed state. <b>2011</b> , 79, 126-41	8
1798	Effect of flanking residues on the conformational sampling of the internal fusion peptide from Ebola virus. <b>2011</b> , 79, 1109-17	11
1797	Topology-based modeling of intrinsically disordered proteins: balancing intrinsic folding and intermolecular interactions. <b>2011</b> , 79, 1251-66	60
1796	Structural mechanism associated with domain opening in gain-of-function mutations in SHP2 phosphatase. <b>2011</b> , 79, 1573-88	27
1795	Computational protein design with a generalized Born solvent model: application to Asparaginyl-tRNA synthetase. <b>2011</b> , 79, 3448-68	19
1794	A missense mutation in CLIC2 associated with intellectual disability is predicted by in silico modeling to affect protein stability and dynamics. <b>2011</b> , 79, 2444-54	50
1793	Toward accurate prediction of pKa values for internal protein residues: the importance of conformational relaxation and desolvation energy. <b>2011</b> , 79, 3364-73	46
1792	Docking and free energy simulations to predict conformational domains involved in hCG-LH receptor interactions using recombinant antibodies. <b>2011</b> , 79, 3108-22	6
1791	Exploring conformational changes coupled to ionization states using a hybrid Rosetta-MCCE protocol. <b>2011</b> , 79, 3356-63	9

1790	Design of a modified mouse protein with ligand binding properties of its human analog by molecular dynamics simulations: the case of C3 inhibition by compstatin. <b>2011</b> , 79, 3166-79	23
1789	pH replica-exchange method based on discrete protonation states. <b>2011</b> , 79, 3420-36	89
1788	A multilayer evaluation approach for protein structure prediction and model quality assessment. <b>2011</b> , 79 Suppl 10, 172-84	8
1787	Progress in the prediction of pKa values in proteins. <b>2011</b> , 79, 3260-75	189
1786	Predicting extreme pKa shifts in staphylococcal nuclease mutants with constant pH molecular dynamics. <b>2011</b> , 79, 3276-86	39
1785	Observation of poly(ethylene glycol) clusters with the chlorine anion in the gas phase under electrospray conditions. <b>2011</b> , 25, 713-8	9
1784	CHARMM force field parameterization of rosiglitazone. <b>2011</b> , 111, 1346-1354	13
1783	CHARMM-based parameterization of neutral articaine widely used local anesthetic. 2011, 111, 1339-1345	7
1782	Molecular Dynamics Simulations Using Graphics Processing Units. <b>2011</b> , 30, 498-504	21
1781	A Mechanism for Evolving Novel Plant Sesquiterpene Synthase Function. <b>2011</b> , 30, 896-906	6
1780	Electrostatic modifications of the human leukocyte antigen-DR P9 peptide-binding pocket and susceptibility to primary sclerosing cholangitis. <b>2011</b> , 53, 1967-76	40
1779	Electrostatic modifications of the human leukocyte antigen DR P9 peptide-binding pocket in primary sclerosing cholangitis: back to the future with human leukocyte antigen DR 2011, 53, 1798-800	4
1778	Small molecule binding to proteins: affinity and binding/unbinding dynamics from atomistic simulations. <b>2011</b> , 6, 1578-80	26
1777	Computing ensembles of transitions from stable states: Dynamic importance sampling. <i>Journal of Computational Chemistry</i> , <b>2011</b> , 32, 196-209	40
1776	A reoptimized GROMOS force field for hexopyranose-based carbohydrates accounting for the relative free energies of ring conformers, anomers, epimers, hydroxymethyl rotamers, and glycosidic linkage conformers. <i>Journal of Computational Chemistry</i> , <b>2011</b> , 32, 998-1032	128
1775	Non-Boltzmann sampling and Bennett's acceptance ratio method: how to profit from bending the rules. <i>Journal of Computational Chemistry</i> , <b>2011</b> , 32, 1082-90	60
1774	Wordom: a user-friendly program for the analysis of molecular structures, trajectories, and free energy surfaces. <i>Journal of Computational Chemistry</i> , <b>2011</b> , 32, 1183-94	187
1773	Efficiency of alchemical free energy simulations. II. Improvements for thermodynamic integration.  Journal of Computational Chemistry, <b>2011</b> , 32, 1320-33	76

1772	Efficiency of alchemical free energy simulations. I. A practical comparison of the exponential formula, thermodynamic integration, and Bennett's acceptance ratio method. <i>Journal of Computational Chemistry</i> , <b>2011</b> , 32, 1303-19	3.5	85
1771	Impact of 2'-hydroxyl sampling on the conformational properties of RNA: update of the CHARMM all-atom additive force field for RNA. <i>Journal of Computational Chemistry</i> , <b>2011</b> , 32, 1929-43	3.5	249
1770	MDAnalysis: a toolkit for the analysis of molecular dynamics simulations. <i>Journal of Computational Chemistry</i> , <b>2011</b> , 32, 2319-27	3.5	1205
1769	Fast docking using the CHARMM force field with EADock DSS. <i>Journal of Computational Chemistry</i> , <b>2011</b> , 32, 2149-59	3.5	269
1768	Acceleration of the GAMESS-UK electronic structure package on graphical processing units. <i>Journal of Computational Chemistry</i> , <b>2011</b> , 32, 2313-8	3.5	37
1767	SwissParam: a fast force field generation tool for small organic molecules. <i>Journal of Computational Chemistry</i> , <b>2011</b> , 32, 2359-68	3.5	1025
1766	A versatile method for systematic conformational searches: application to CheY. <i>Journal of Computational Chemistry</i> , <b>2011</b> , 32, 2369-85	3.5	3
1765	Avoiding the van der Waals endpoint problem using serial atomic insertion. <i>Journal of Computational Chemistry</i> , <b>2011</b> , 32, 2449-58	3.5	14
1764	Solvation properties of N-acetyl-I-glucosamine: molecular dynamics study incorporating electrostatic polarization. <i>Journal of Computational Chemistry</i> , <b>2011</b> , 32, 3339-53	3.5	23
1763	Surveying implicit solvent models for estimating small molecule absolute hydration free energies. Journal of Computational Chemistry, <b>2011</b> , 32, 2909-23	3.5	58
1762	The distributed diagonal force decomposition method for parallelizing molecular dynamics simulations. <i>Journal of Computational Chemistry</i> , <b>2011</b> , 32, 3005-13	3.5	4
1761	Glycan Reader: automated sugar identification and simulation preparation for carbohydrates and glycoproteins. <i>Journal of Computational Chemistry</i> , <b>2011</b> , 32, 3135-41	3.5	118
1760	Zinc-homocysteine binding in cobalamin-dependent methionine synthase and its role in the substrate activation: DFT, ONIOM, and QM/MM molecular dynamics studies. <i>Journal of Computational Chemistry</i> , <b>2011</b> , 32, 3154-67	3.5	13
1759	Fast and accurate computation schemes for evaluating vibrational entropy of proteins. <i>Journal of Computational Chemistry</i> , <b>2011</b> , 32, 3188-93	3.5	65
1758	Applying efficient implicit nongeometric constraints in alchemical free energy simulations. <i>Journal of Computational Chemistry</i> , <b>2011</b> , 32, 3423-32	3.5	32
1757	Life and death with arsenic. Arsenic life: an analysis of the recent report "A bacterium that can grow by using arsenic instead of phosphorus". <b>2011</b> , 33, 350-7		57
1756	Chemical synthesis, crystal structure and enzymatic evaluation of a dinucleotide spore photoproduct analogue containing a formacetal linker. <b>2011</b> , 17, 9658-68		19
1755	Understanding the physical basis of the salt dependence of the electrostatic binding free energy of mutated charged ligand-nucleic acid complexes. <b>2011</b> , 156, 79-87		12

## (2011-2011)

1754	Sugar-binding sites on the surface of the carbohydrate-binding module of CBH I from Trichoderma reesei. <b>2011</b> , 346, 839-46	24
1753	A QM/MM study on the last two steps of the catalytic cycle of acetohydroxyacid synthase. <b>2011</b> , 966, 159-166	8
1752	Applications of computational science for understanding enzymatic deconstruction of cellulose. <b>2011</b> , 22, 231-8	111
1751	Topology and dynamics of the interaction between 5-nitroimidazole radiosensitizers and duplex DNA studied by a combination of docking, molecular dynamic simulations and NMR spectroscopy. <b>2011</b> , 992, 65-71	13
1750	Fast Analysis of Molecular Dynamics Trajectories with Graphics Processing Units-Radial Distribution Function Histogramming. <b>2011</b> , 230, 3556-3569	140
1749	ClickMD: an intuitive web-oriented molecular dynamics platform. <b>2011</b> , 3, 923-31	4
1748	Recent advances in ligand-based drug design: relevance and utility of the conformationally sampled pharmacophore approach. <b>2011</b> , 7, 10-22	149
1747	Lagrangian formulation with dissipation of Born-Oppenheimer molecular dynamics using the density-functional tight-binding method. <b>2011</b> , 135, 044122	58
1746	A conserved asparagine residue in transmembrane segment 1 (TM1) of serotonin transporter dictates chloride-coupled neurotransmitter transport. <b>2011</b> , 286, 30823-30836	31
1745	Structural implications of conserved aspartate residues located in tropomyosin's coiled-coil core. <b>2011</b> , 1, 250-255	16
1744	Chemical states of the N-terminal "lid" of MDM2 regulate p53 binding: simulations reveal complexities of modulation. <b>2011</b> , 10, 82-9	27
1743	Approaching post-Hartreeflock quality potential energy surfaces with simple pair-wise expressions: parameterising point-charge-based force fields for liquid water using the adaptive force matching method. <b>2011</b> , 37, 591-605	39
1742	The effect of thiobarbituric acid on tyrosinase: inhibition kinetics and computational simulation. <b>2011</b> , 29, 463-70	21
1741	Non-Markovian Theory of Vibrational Energy Relaxation and its Applications to Biomolecular Systems. <b>2011</b> , 1-33	6
1740	All-atom modeling of anisotropic atomic fluctuations in protein crystal structures. <b>2011</b> , 135, 144114	9
1739	In vivo patterns of resistance to the HIV attachment inhibitor BMS-488043. <b>2011</b> , 55, 729-37	39
1738	Resistance of Akt kinases to dephosphorylation through ATP-dependent conformational plasticity. <b>2011</b> , 108, E1120-7	62
1737	Unfolding and translocation pathway of substrate protein controlled by structure in repetitive allosteric cycles of the ClpY ATPase. <b>2011</b> , 108, 2234-9	28

1736	Integrating diffusion maps with umbrella sampling: application to alanine dipeptide. <b>2011</b> , 134, 135103	55
1735	Ion access pathway to the transmembrane pore in P2X receptor channels. <b>2011</b> , 137, 579-90	55
1734	MDpocket: open-source cavity detection and characterization on molecular dynamics trajectories. <b>2011</b> , 27, 3276-85	190
1733	Myosin cleft closure determines the energetics of the actomyosin interaction. <b>2011</b> , 25, 111-21	17
1732	Water-assisted proton transfer in ferredoxin I. <b>2011</b> , 286, 23679-87	14
1731	Bimolecular Complementation to Visualize Filovirus VP40-Host Complexes in Live Mammalian Cells: Toward the Identification of Budding Inhibitors. <b>2011</b> , 2011,	23
1730	Understanding the determinants of selectivity in drug metabolism through modeling of dextromethorphan oxidation by cytochrome P450. <b>2011</b> , 108, 6050-5	82
1729	Nucleotide modifications and tRNA anticodon-mRNA codon interactions on the ribosome. <b>2011</b> , 17, 2177-88	40
1728	Simulating Kinetic Processes in Time and Space on a Lattice. <b>2011</b> , 6, 159-197	1
1727	A mechanistic and structural analysis of the inhibition of the 90-kDa heat shock protein by the benzoquinone and hydroquinone ansamycins. <b>2011</b> , 79, 823-32	15
1726	Probing carbohydrate product expulsion from a processive cellulase with multiple absolute binding free energy methods. <b>2011</b> , 286, 18161-9	64
1725	Flexible cullins in cullin-RING E3 ligases allosterically regulate ubiquitination. <b>2011</b> , 286, 40934-42	43
1724	Unsuspected pathway of the allosteric transition in hemoglobin. <b>2011</b> , 108, 5608-13	64
1723	Mammalian testis-determining factor SRY and the enigma of inherited human sex reversal: frustrated induced fit in a bent protein-DNA complex. <b>2011</b> , 286, 36787-807	13
1722	Multiple functions of aromatic-carbohydrate interactions in a processive cellulase examined with molecular simulation. <b>2011</b> , 286, 41028-35	88
1721	Structure of apolipoprotein A-I N terminus on nascent high density lipoproteins. <b>2011</b> , 286, 2966-75	22
1720	Molecular dynamics simulations of the Cx26 hemichannel: evaluation of structural models with Brownian dynamics. <b>2011</b> , 138, 475-93	69
1719	Ion selectivity in channels and transporters. <b>2011</b> , 137, 415-26	127

## (2011-2011)

1718	Mutant alcohol dehydrogenase leads to improved ethanol tolerance in Clostridium thermocellum. <b>2011</b> , 108, 13752-7	147
1717	Protonation of key acidic residues is critical for the K+-selectivity of the Na/K pump. <b>2011</b> , 18, 1159-63	47
1716	Design of a switchable eliminase. <b>2011</b> , 108, 6823-7	102
1715	Molecular Modeling in Nucleic Acid-Targeted Drug Design. <b>2011</b> , 258-271	
1714	Disordered binding of small molecules to AI(12-28). <b>2011</b> , 286, 41578-41588	43
1713	Protein-protein binding affinity prediction on a diverse set of structures. <b>2011</b> , 27, 3002-9	86
1712	An Overview of String-Based Path Sampling Methods. <b>2011</b> , 7, 89-97	3
1711	The role of response elements organization in transcription factor selectivity: the IFN-□ enhanceosome example. <b>2011</b> , 7, e1002077	15
1710	Two birds with one stone? Possible dual-targeting H1N1 inhibitors from traditional Chinese medicine. <b>2011</b> , 7, e1002315	72
1709	Mutation D816V alters the internal structure and dynamics of c-KIT receptor cytoplasmic region: implications for dimerization and activation mechanisms. <b>2011</b> , 7, e1002068	59
1708	The adipophilin C terminus is a self-folding membrane-binding domain that is important for milk lipid secretion. <b>2011</b> , 286, 23254-65	33
1707	On the proper calculation of electrostatic interactions in solid-supported bilayer systems. <b>2011</b> , 134, 055109	21
1706	Redistribution of carbonyl stretch mode energy in isolated and solvated N-methylacetamide: kinetic energy spectral density analyses. <b>2011</b> , 135, 214504	15
1705	Role of histone tails in structural stability of the nucleosome. <b>2011</b> , 7, e1002279	77
1704	Identification of potent EGFR inhibitors from TCM Database@Taiwan. <b>2011</b> , 7, e1002189	78
1703	The free energy landscape of small molecule unbinding. <b>2011</b> , 7, e1002002	78
1702	"Fluctuograms" reveal the intermittent intra-protein communication in subtilisin Carlsberg and correlate mechanical coupling with co-evolution. <b>2011</b> , 7, e1002023	16
1701	Interconversion of functional motions between mesophilic and thermophilic adenylate kinases. <b>2011</b> , 7, e1002103	18

1700	Structural insights into the inhibition of cytosolic 5'-nucleotidase II (cN-II) by ribonucleoside 5'-monophosphate analogues. <b>2011</b> , 7, e1002295	20
1699	Computational methods for studying serpin conformational change and structural plasticity. <b>2011</b> , 501, 295-323	5
1698	The Class D beta-lactamase family: residues governing the maintenance and diversity of function. <b>2011</b> , 24, 801-9	20
1697	Hydrophobic residues in small ankyrin 1 participate in binding to obscurin. <b>2012</b> , 29, 36-51	6
1696	Beyond the binding site: the role of the IIIIloop and extra-domain structures in PDZ domains. <b>2012</b> , 8, e1002429	35
1695	Unraveling the structural complexity in a single-stranded RNA tail: implications for efficient ligand binding in the prequeuosine riboswitch. <b>2012</b> , 40, 1345-55	46
1694	Ligand-dependent conformations and dynamics of the serotonin 5-HT(2A) receptor determine its activation and membrane-driven oligomerization properties. <b>2012</b> , 8, e1002473	84
1693	The isolation and characterization of I-glucogallin as a novel aldose reductase inhibitor from Emblica officinalis. <b>2012</b> , 7, e31399	67
1692	Residual dipolar couplings measured in unfolded proteins are sensitive to amino-acid-specific geometries as well as local conformational sampling. <b>2012</b> , 40, 989-94	9
1691	A scoring function based on solvation thermodynamics for protein structure prediction. <b>2012</b> , 8, 127-38	1
1690	Molecular basis of calcium-sensitizing and desensitizing mutations of the human cardiac troponin C regulatory domain: a multi-scale simulation study. <b>2012</b> , 8, e1002777	27
1689	Strandwise translocation of a DNA glycosylase on undamaged DNA. <b>2012</b> , 109, 1086-91	31
1688	SwissSidechain: a molecular and structural database of non-natural sidechains. <b>2013</b> , 41, D327-32	74
1687	Sequence determinants of a microtubule tip localization signal (MtLS). <b>2012</b> , 287, 28227-42	36
1686	An integrated study of tyrosinase inhibition by rutin: progress using a computational simulation. <b>2012</b> , 29, 999-1012	57
1685	The molecular basis for selective inhibition of unconventional mRNA splicing by an IRE1-binding small molecule. <b>2012</b> , 109, E869-78	<b>3</b> 60
1684	A limited 4 🛮 🖟 adial displacement of the S4-S5 linker is sufficient for internal gate closing in Kv channels. <b>2012</b> , 287, 40091-8	21
1683	STAP Refinement of the NMR database: a database of 2405 refined solution NMR structures. <b>2012</b> , 40, D525-30	12

## (2012-2012)

1682	Sampling the conformational energy landscape of a hyperthermophilic protein by engineering key substitutions. <b>2012</b> , 29, 1683-94	23
1681	Improved predictions of transcription factor binding sites using physicochemical features of DNA. <b>2012</b> , 40, e175	25
1680	Computational mapping reveals dramatic effect of Hoogsteen breathing on duplex DNA reactivity with formaldehyde. <b>2012</b> , 40, 7644-52	27
1679	CHARMM Additive All-Atom Force Field for Phosphate and Sulfate Linked to Carbohydrates. <b>2012</b> , 8, 759-776	81
1678	Estimation of the binding free energy by Linear Interaction Energy models. 2012, 12, 551-61	3
1677	iAPBS: a programming interface to Adaptive Poisson-Boltzmann Solver (APBS). <b>2012</b> , 5,	37
1676	Misfolded proteins. <b>2012</b> , 141-164	2
1675	Glycan fragment database: a database of PDB-based glycan 3D structures. <b>2013</b> , 41, D470-4	41
1674	Note: FixSol solvation model and FIXPVA2 tessellation scheme. <b>2012</b> , 137, 246101	15
1673	Mechanism of BAG1 repair on Parkinson's disease-linked DJ1 mutation. <b>2012</b> , 30, 1-12	12
1672	Combining computational chemistry and crystallography for a better understanding of the structure of cellulose. <b>2012</b> , 67, 19-93	25
1671	Peptide kinetics from picoseconds to microseconds using boxed molecular dynamics: power law rate coefficients in cyclisation reactions. <b>2012</b> , 137, 165102	20
1670	Dynamics and energetics of hydrophobically confined water. <b>2012</b> , 85, 051506	15
1669	Charge-leveling and proper treatment of long-range electrostatics in all-atom molecular dynamics at constant pH. <b>2012</b> , 137, 184105	61
1668	Generalized essential energy space random walks to more effectively accelerate solute sampling in aqueous environment. <b>2012</b> , 136, 044103	13
1667	Structure and reorientational dynamics of angiotensin I and II: a microscopic physical insight. <b>2012</b> , 29, 671-90	7
1666	Accounting for the kinetics in order parameter analysis: lessons from theoretical models and a disordered peptide. <b>2012</b> , 137, 194101	14
1665	Transmembrane helix assembly by window exchange umbrella sampling. <b>2012</b> , 108, 108102	51

1664	Nectin ectodomain structures reveal a canonical adhesive interface. <b>2012</b> , 19, 906-15	83
1663	Synergistic substrate binding determines the stoichiometry of transport of a prokaryotic H(+)/Cl(-) exchanger. <b>2012</b> , 19, 525-31, S1	58
1662	Hallmarks of processivity in glycoside hydrolases from crystallographic and computational studies of the Serratia marcescens chitinases. <b>2012</b> , 287, 36322-30	81
1661	Enforced presentation of an extrahelical guanine to the lesion recognition pocket of human 8-oxoguanine glycosylase, hOGG1. <b>2012</b> , 287, 24916-28	44
1660	Computational investigation of glycosylation effects on a family 1 carbohydrate-binding module. <b>2012</b> , 287, 3147-55	52
1659	Product binding varies dramatically between processive and nonprocessive cellulase enzymes. <b>2012</b> , 287, 24807-13	49
1658	Alternative pathways for association and dissociation of the calmodulin-binding domain of plasma membrane Ca(2+)-ATPase isoform 4b (PMCA4b). <b>2012</b> , 287, 29664-71	6
1657	Lesion processing by a repair enzyme is severely curtailed by residues needed to prevent aberrant activity on undamaged DNA. <b>2012</b> , 109, 8091-6	41
1656	The intertransmembrane region of Kaposi's sarcoma-associated herpesvirus modulator of immune recognition 2 contributes to B7-2 downregulation. <b>2012</b> , 86, 5288-96	11
1655	Computer simulations of helix folding in homo- and heteropeptides. <b>2012</b> , 38, 682-694	10
1654	The Effect of D-(-)-arabinose on Tyrosinase: An Integrated Study Using Computational Simulation and Inhibition Kinetics. <b>2012</b> , 2012, 731427	4
1653	Analyzing effects of naturally occurring missense mutations. <b>2012</b> , 2012, 805827	78
1652	Cannabinoids suppress inflammatory and neuropathic pain by targeting $\pm 3$ glycine receptors. <b>2012</b> , 209, 1121-34	159
1651	Correlation of molecular and functional effects of mutations in cardiac troponin T linked to familial hypertrophic cardiomyopathy: an integrative in silico/in vitro approach. <b>2012</b> , 287, 14515-23	32
	hypertrophic cardiomyopathy. an integrative in suco/in vicro approach. <b>2012</b> , 287, 14515-25	
1650	Distant cytosolic residues mediate a two-way molecular switch that controls the modulation of inwardly rectifying potassium (Kir) channels by cholesterol and phosphatidylinositol 4,5-bisphosphate (PI(4,5)P(2)). <b>2012</b> , 287, 40266-78	24
1650 1649	Distant cytosolic residues mediate a two-way molecular switch that controls the modulation of inwardly rectifying potassium (Kir) channels by cholesterol and phosphatidylinositol	
	Distant cytosolic residues mediate a two-way molecular switch that controls the modulation of inwardly rectifying potassium (Kir) channels by cholesterol and phosphatidylinositol 4,5-bisphosphate (PI(4,5)P(2)). 2012, 287, 40266-78  The antibodies against the computationally designed mimic of the glycoprotein hormone receptor transmembrane domain provide insights into receptor activation and suppress the constitutively	24

1646	Rational prediction with molecular dynamics for hit identification. <b>2012</b> , 12, 2002-12	21
1645	Solvent Effect on the Fluorescence Spectra of Coumarin 120 in Water: A Combined Quantum Mechanical and Molecular Mechanical Study. <b>2012</b> , 81, SA024	1
1644	Polarizable molecular dynamics simulations of aqueous dipeptides. <b>2012</b> , 116, 8733-40	8
1643	Characterization of a viral phosphoprotein binding site on the surface of the respiratory syncytial nucleoprotein. <b>2012</b> , 86, 8375-87	41
1642	Interatomic Potential Development. <b>2012</b> , 267-291	6
1641	Close intramolecular sulfur-oxygen contacts: modified force field parameters for improved conformation generation. <b>2012</b> , 26, 1195-205	18
1640	Multiscale macromolecular simulation: role of evolving ensembles. <b>2012</b> , 52, 2638-49	11
1639	Exploring residue component contributions to dynamical network models of allostery. <b>2012</b> , 8, 2949-2961	122
1638	Peptide nanovesicles formed by the self-assembly of branched amphiphilic peptides. <b>2012</b> , 7, e45374	65
1637	Retaining glycosyltransferase mechanism studied by QM/MM methods: lipopolysaccharyl1,4-galactosyltransferase C transfers -galactose via an oxocarbenium ion-like transition state. <b>2012</b> , 134, 4743-52	77
1636	Water structure, dynamics, and spectral signatures: changes upon model cavity-ligand recognition. <b>2012</b> , 116, 13774-80	12
1635	Determining Geometrically Stable Domains in Molecular Conformation Sets. <b>2012</b> , 8, 2588-99	18
1634	Biomolecular electrostatics and solvation: a computational perspective. <b>2012</b> , 45, 427-91	132
1633	Computing the thermodynamic contributions of interfacial water. <b>2012</b> , 819, 393-404	42
1632	Ab initio MO Theory [An Important Tool in Foldamer Research: Prediction of Helices in Oligomers of EAmino Acids. <b>2012</b> , 95, 2348-2383	38
1631	Atomistic simulations of pH-dependent self-assembly of micelle and bilayer from fatty acids. <b>2012</b> , 137, 194902	36
1630	Homology modeling of cannabinoid receptors: discovery of cannabinoid analogues for therapeutic use. <b>2012</b> , 819, 595-613	8
1629	Comparison of Three Chain-of-States Methods: Nudged Elastic Band and Replica Path with Restraints or Constraints. <b>2012</b> , 8, 5035-5051	20

1628	Thirty-five years of biomolecular simulation: development of methodology, force fields and software. <b>2012</b> , 38, 1271-1281		18
1627	Understanding Protein-Surface Interactions at the Atomistic Level through the Synergistic Development of Experimental and Molecular Simulation Methods. <b>2012</b> , 197-228		2
1626	Rigid Body Energy Minimization on Manifolds for Molecular Docking. <b>2012</b> , 8, 4374-4380		21
1625	Introduction to ion channels and disease. <b>2012</b> , 112, 6215-7		20
1624	Hybrid Quantum and Classical Simulations of the Formate Dehydrogenase Catalyzed Hydride Transfer Reaction on an Accurate Semiempirical Potential Energy Surface. <b>2012</b> , 8, 4786-96		24
1623	Charge Optimization Theory for Induced-Fit Ligands. <b>2012</b> , 8, 4580-4592		6
1622	Simple structure-based approach for predicting the activity of inhibitors of beta-secretase (BACE1) associated with Alzheimer's disease. <b>2012</b> , 52, 3302-7		19
1621	An enzyme-initiated Smiles rearrangement enables the development of an assay of MshB, the GlcNAc-Ins deacetylase of mycothiol biosynthesis. <b>2012</b> , 10, 5278-88		4
1620	Molecular dynamics simulations of the Cx26 hemichannel: insights into voltage-dependent loop-gating. <b>2012</b> , 102, 1341-51		32
1619	Relaxation of the rigid backbone of an oligoamide-foldamer-based $\oplus$ -helix mimetic: identification of potent Bcl-xL inhibitors. <b>2012</b> , 10, 2928-33		53
1618	Adsorption of sulfite oxidase on self-assembled monolayers from molecular dynamics simulations. <b>2012</b> , 28, 5761-9		16
1617	Automation of the CHARMM General Force Field (CGenFF) II: assignment of bonded parameters and partial atomic charges. <b>2012</b> , 52, 3155-68		852
1616	Free energy landscapes of the $\oplus$ -d- and $\Box$ -d-glucopyranose conformations in both vacuum and aqueous solution. <b>2012</b> , 38, 1186-1197		5
1615	Predicted structure of agonist-bound glucagon-like peptide 1 receptor, a class B G protein-coupled receptor. <b>2012</b> , 109, 19988-93		41
1614	Out-of-register 🛭 sheets suggest a pathway to toxic amyloid aggregates. <b>2012</b> , 109, 20913-8		149
1613	Molecular dynamics simulation of HIV-1 fusion domain-membrane complexes: Insight into the N-terminal gp41 fusion mechanism. <b>2012</b> , 170, 9-16		12
1612	Structural model of channelrhodopsin. <b>2012</b> , 287, 7456-66		37
1611	Simulation of multiphase systems utilizing independent force fields to control intraphase and interphase behavior. <i>Journal of Computational Chemistry</i> , <b>2012</b> , 33, 1458-66	3.5	21

1010	Oxygen migration pathways in NO-bound truncated hemoglobin. <b>2012</b> , 13, 4276-86	20
1609	Homology modeling of the human 5-HT1A, 5-HT 2A, D1, and D2 receptors: model refinement with molecular dynamics simulations and docking evaluation. <b>2012</b> , 18, 3639-55	24
1608	Very large residual dipolar couplings from deuterated ubiquitin. <b>2012</b> , 54, 53-67	6
1607	A hybrid modeling strategy using Nuclear Overhauser Effect data with contact information. <b>2012</b> , 554, 190-194	2
1606	Optimization of the CHARMM additive force field for DNA: Improved treatment of the BI/BII conformational equilibrium. <b>2012</b> , 8, 348-362	348
1605	Using the unfolded state as the reference state improves the performance of statistical potentials. <b>2012</b> , 103, 1950-9	4
1604	Comparison of Structure-based Tools for the Prediction of Ligand Binding Site Residues in Apo-structures. <b>2012</b> , 11, 115-126	3
1603	Rotational velocity rescaling of molecular dynamics trajectories for direct prediction of protein NMR relaxation. <b>2012</b> , 168-169, 28-39	14
1602	Towards the prediction of order parameters from molecular dynamics simulations in proteins. <b>2012</b> , 136, 164101	15
1601	Molecular dynamics trajectory compression with a coarse-grained model. <b>2012</b> , 9, 476-86	6
	Molecular dynamics trajectory compression with a coarse-grained model. <b>2012</b> , 9, 476-86  Reaction dynamics of CN radicals with tetrahydrofuran in liquid solutions. <b>2012</b> , 14, 10424-37	20
1600	Reaction dynamics of CN radicals with tetrahydrofuran in liquid solutions. <b>2012</b> , 14, 10424-37  The natural DNA bending angle in the lac repressor headpiece-O1 operator complex is determined	
1600 1599	Reaction dynamics of CN radicals with tetrahydrofuran in liquid solutions. <b>2012</b> , 14, 10424-37  The natural DNA bending angle in the lac repressor headpiece-O1 operator complex is determined by protein-DNA contacts and water release. <b>2012</b> , 14, 2070-7  Fragment-based quantum mechanical methods for periodic systems with Ewald summation and	20
1600 1599 1598	Reaction dynamics of CN radicals with tetrahydrofuran in liquid solutions. 2012, 14, 10424-37  The natural DNA bending angle in the lac repressor headpiece-O1 operator complex is determined by protein-DNA contacts and water release. 2012, 14, 2070-7  Fragment-based quantum mechanical methods for periodic systems with Ewald summation and mean image charge convention for long-range electrostatic interactions. 2012, 14, 7821-9  Role of spatial ionic distribution on the energetics of hydrophobic assembly and properties of the	20 7 21
1600 1599 1598 1597	Reaction dynamics of CN radicals with tetrahydrofuran in liquid solutions. 2012, 14, 10424-37  The natural DNA bending angle in the lac repressor headpiece-O1 operator complex is determined by protein-DNA contacts and water release. 2012, 14, 2070-7  Fragment-based quantum mechanical methods for periodic systems with Ewald summation and mean image charge convention for long-range electrostatic interactions. 2012, 14, 7821-9  Role of spatial ionic distribution on the energetics of hydrophobic assembly and properties of the water/hydrophobe interface. 2012, 14, 1892-906  Practically Efficient and Robust Free Energy Calculations: Double-Integration Orthogonal Space	20 7 21 10
1600 1599 1598 1597 1596	Reaction dynamics of CN radicals with tetrahydrofuran in liquid solutions. 2012, 14, 10424-37  The natural DNA bending angle in the lac repressor headpiece-O1 operator complex is determined by protein-DNA contacts and water release. 2012, 14, 2070-7  Fragment-based quantum mechanical methods for periodic systems with Ewald summation and mean image charge convention for long-range electrostatic interactions. 2012, 14, 7821-9  Role of spatial ionic distribution on the energetics of hydrophobic assembly and properties of the water/hydrophobe interface. 2012, 14, 1892-906  Practically Efficient and Robust Free Energy Calculations: Double-Integration Orthogonal Space Tempering. 2012, 8, 810-23  Chloroperoxidase-catalyzed epoxidation of cis-II-methylstyrene: distal pocket flexibility tunes	20 7 21 10 70

1592	Molecular dynamics simulation of nitric oxide in myoglobin. <b>2012</b> , 116, 4154-62	12
1591	Traditional Chinese medicine as dual guardians against hypertension and cancer?. <b>2012</b> , 30, 299-317	11
1590	Molecular dynamics approaches estimate the binding energy of HIV-1 integrase inhibitors and correlate with in vitro activity. <b>2012</b> , 56, 411-9	37
1589	PredyFlexy: flexibility and local structure prediction from sequence. <b>2012</b> , 40, W317-22	69
1588	Conformational equilibrium of N-myristoylated cAMP-dependent protein kinase A by molecular dynamics simulations. <b>2012</b> , 51, 10186-96	26
1587	Correlating protein hot spot surface analysis using ProBiS with simulated free energies of protein-protein interfacial residues. <b>2012</b> , 52, 2541-9	4
1586	Transannular Diels-Alder reactivities of 14-membered macrocylic trienes and their relationship with the conformational preferences of the reactants: a combined quantum chemical and molecular dynamics study. <b>2012</b> , 77, 5371-80	7
1585	Mass Modulation of Protein Dynamics Associated with Barrier Crossing in Purine Nucleoside Phosphorylase. <b>2012</b> , 3, 3538-3544	43
1584	Maintain rigid structures in Verlet based cartesian molecular dynamics simulations. <b>2012</b> , 137, 134110	14
1583	Recent trends and applications in 3D virtual screening. <b>2012</b> , 15, 749-69	12
1583 1582	Recent trends and applications in 3D virtual screening. 2012, 15, 749-69  Efficient calculation of molecular configurational entropies using an information theoretic approximation. 2012, 116, 2891-904	12 67
	Efficient calculation of molecular configurational entropies using an information theoretic	
1582	Efficient calculation of molecular configurational entropies using an information theoretic approximation. <b>2012</b> , 116, 2891-904  Effects of two solvent conditions on the free energy landscape of the BBL peripheral subunit	67
1582 1581	Efficient calculation of molecular configurational entropies using an information theoretic approximation. 2012, 116, 2891-904  Effects of two solvent conditions on the free energy landscape of the BBL peripheral subunit binding domain. 2012, 116, 646-52  Cation-Land Einteractions in Aqueous Solution Studied Using Polarizable Potential Models. 2012	67
1582 1581 1580	Efficient calculation of molecular configurational entropies using an information theoretic approximation. 2012, 116, 2891-904  Effects of two solvent conditions on the free energy landscape of the BBL peripheral subunit binding domain. 2012, 116, 646-52  Cation-land Einteractions in Aqueous Solution Studied Using Polarizable Potential Models. 2012, 8, 182-93  Efficient Conformational Sampling in Explicit Solvent Using a Hybrid Replica Exchange Molecular	67 4 58
1582 1581 1580 1579	Efficient calculation of molecular configurational entropies using an information theoretic approximation. 2012, 116, 2891-904  Effects of two solvent conditions on the free energy landscape of the BBL peripheral subunit binding domain. 2012, 116, 646-52  Cation-land Einteractions in Aqueous Solution Studied Using Polarizable Potential Models. 2012, 8, 182-93  Efficient Conformational Sampling in Explicit Solvent Using a Hybrid Replica Exchange Molecular Dynamics Method. 2012, 8, 677-87  Inhibition of biocatalysis in [Fe-Fe] hydrogenase by oxygen: molecular dynamics and density	67 4 58 21
1582 1581 1580 1579	Efficient calculation of molecular configurational entropies using an information theoretic approximation. 2012, 116, 2891-904  Effects of two solvent conditions on the free energy landscape of the BBL peripheral subunit binding domain. 2012, 116, 646-52  Cation-land Einteractions in Aqueous Solution Studied Using Polarizable Potential Models. 2012, 8, 182-93  Efficient Conformational Sampling in Explicit Solvent Using a Hybrid Replica Exchange Molecular Dynamics Method. 2012, 8, 677-87  Inhibition of biocatalysis in [Fe-Fe] hydrogenase by oxygen: molecular dynamics and density functional theory calculations. 2012, 7, 1268-75	67 4 58 21 23

1574	A variable light domain fluorogen activating protein homodimerizes to activate dimethylindole red. <b>2012</b> , 51, 2471-85	19
1573	Structure and elasticity of lipid membranes with genistein and daidzein bioflavinoids using X-ray scattering and MD simulations. <b>2012</b> , 116, 3918-27	51
1572	Protein dynamics and ion traffic in bacterioferritin. <b>2012</b> , 51, 9900-10	17
1571	How Does Darunavir Prevent HIV-1 Protease Dimerization?. <b>2012</b> , 8, 1786-94	16
1570	QM/MM study on the catalytic mechanism of heme-containing aliphatic aldoxime dehydratase. <b>2012</b> , 116, 5689-93	13
1569	Variable charge reactive potential for hydrocarbons to simulate organic-copper interactions. <b>2012</b> , 116, 7976-91	76
1568	QM/MM analysis suggests that Alkaline Phosphatase (AP) and nucleotide pyrophosphatase/phosphodiesterase slightly tighten the transition state for phosphate diester hydrolysis relative to solution: implication for catalytic promiscuity in the AP superfamily. 2012, 134, 229-46	66
1567	Constant pH Molecular Dynamics Simulations of Nucleic Acids in Explicit Solvent. <b>2012</b> , 8, 36-46	73
1566	Dynamics of water/methanol mixtures at functionalized chromatographic interfaces. <b>2012</b> , 116, 10951-9	17
1565	Novel protease inhibitors via computational redesign of subtilisin BPN' propeptide. <b>2012</b> , 51, 8247-55	2
1564	Implementation of the solvent macromolecule boundary potential and application to model and realistic enzyme systems. <b>2012</b> , 116, 12522-34	14
1563	Conformational selection by the aIF2 GTPase: a molecular dynamics study of functional pathways. <b>2012</b> , 51, 353-61	8
1562	Normal mode analysis of the spectral density of the Fenna-Matthews-Olson light-harvesting protein: how the protein dissipates the excess energy of excitons. <b>2012</b> , 116, 14565-80	94
1561	Structural intermediates in a model of the substrate translocation path of the bacterial glutamate transporter homologue GltPh. <b>2012</b> , 116, 5372-83	40
1560	Assessment of Atomic Charge Models for Gas-Phase Computations on Polypeptides. <b>2012</b> , 8, 661-76	60
1559	Druggability Assessment of Allosteric Proteins by Dynamics Simulations in the Presence of Probe Molecules. <b>2012</b> , 8, 2435-2447	113
1558	From Molecular Phylogenetics to Quantum Chemistry: Discovering Enzyme Design Principles through Computation. <b>2012</b> , 2, e201209018	2
1557	Engineering protein therapeutics: predictive performances of a structure-based virtual affinity maturation protocol. <b>2012</b> , 52, 2204-14	5

1556	Electrostatically guided dynamicsthe root of fidelity in a promiscuous terpene synthase?. <b>2012</b> , 134, 19454-62	70
1555	Enhanced Sampling in Free Energy Calculations: Combining SGLD with the Bennett's Acceptance Ratio and Enveloping Distribution Sampling Methods. <b>2012</b> , 8, 3650-62	16
1554	Intrinsic energy landscapes of amino acid side-chains. <b>2012</b> , 52, 1559-72	17
1553	Mechanism of Cd2+ coordination during slow inactivation in potassium channels. <b>2012</b> , 20, 1332-42	22
1552	A hybrid elastic band string algorithm for studies of enzymatic reactions. <b>2012</b> , 14, 12544-53	18
1551	Role of hydrophobic core on the thermal stability of proteins - molecular dynamics simulations on a single point mutant of Sso7d abstract. <b>2012</b> , 29, 961-71	15
1550	A Local Rigid Body Framework for Global Optimization of Biomolecules. <b>2012</b> , 8, 5159-65	32
1549	Bond-order potentials with split-charge equilibration: application to C-, H-, and O-containing systems. <b>2012</b> , 136, 164701	23
1548	Replica exchanging self-guided Langevin dynamics for efficient and accurate conformational sampling. <b>2012</b> , 137, 044106	14
1547	Discovery of a novel chemotype of tyrosine kinase inhibitors by fragment-based docking and molecular dynamics. <b>2012</b> , 3, 834-8	35
1546	Caffeine and sugars interact in aqueous solutions: a simulation and NMR study. <b>2012</b> , 116, 11701-11	38
1545	Free Energy Guided Sampling. <b>2012</b> , 8, 2134-40	21
1544	Theoretical analysis of the catalytic mechanism of Helicobacter pylori glutamate racemase. <b>2012</b> , 116, 12406-14	12
1543	Collective Reaction Coordinate for Hybrid Quantum and Molecular Mechanics Simulations: A Case Study of the Hydride Transfer in Dihydrofolate Reductase. <b>2012</b> , 8, 2484-96	33
1542	LAMBADA and InflateGRO2: efficient membrane alignment and insertion of membrane proteins for molecular dynamics simulations. <b>2012</b> , 52, 2657-69	97
1541	Molecular Dynamics Simulations of Phosphatidylcholine Membranes: A Comparative Force Field Study. <b>2012</b> , 8, 4593-609	154
1540	Computational and experimental analysis of the transmembrane domain 4/5 dimerization interface of the serotonin 5-HT(1A) receptor. <b>2012</b> , 82, 448-63	41
1539	Trigger factor slows co-translational folding through kinetic trapping while sterically protecting the nascent chain from aberrant cytosolic interactions. <b>2012</b> , 134, 10920-32	58

1538	Ionic strength effects on amyloid formation by amylin are a complicated interplay among Debye screening, ion selectivity, and Hofmeister effects. <b>2012</b> , 51, 8478-90	110
1537	Scalable Anisotropic Shape and Electrostatic Models for Biological Bromine Halogen Bonds. <b>2012</b> , 8, 2461-73	70
1536	Function of the D-alanine:D-alanine ligase lid loop: a molecular modeling and bioactivity study. <b>2012</b> , 55, 6849-56	12
1535	The folding transition state of protein L is extensive with nonnative interactions (and not small and polarized). <b>2012</b> , 420, 220-34	25
1534	Molecular effects of familial hypertrophic cardiomyopathy-related mutations in the TNT1 domain of cTnT. <b>2012</b> , 421, 54-66	27
1533	Electrostatically accelerated coupled binding and folding of intrinsically disordered proteins. <b>2012</b> , 422, 674-684	60
1532	An antiparallel actin dimer is associated with the endocytic pathway in mammalian cells. <b>2012</b> , 177, 70-80	10
1531	Evidence that the kinesin light chain domain contains tetratricopeptide repeat units. 2012, 177, 602-12	3
1530	Structural and biophysical properties of a synthetic channel-forming peptide: designing a clinically relevant anion selective pore. <b>2012</b> , 1818, 1039-48	15
1529	An ensemble dynamics approach to decipher solid-state NMR observables of membrane proteins. <b>2012</b> , 1818, 252-62	21
1528	Membrane models of E. coli containing cyclic moieties in the aliphatic lipid chain. <b>2012</b> , 1818, 1205-10	72
1527	Charge distribution and imperfect amphipathicity affect pore formation by antimicrobial peptides. <b>2012</b> , 1818, 1274-83	87
1526	Coupling between the voltage-sensing and pore domains in a voltage-gated potassium channel. <b>2012</b> , 1818, 1726-36	17
1525	Structural basis of anthrax edema factor neutralization by a neutralizing antibody. <b>2012</b> , 417, 324-9	10
1524	Deconstructing 14-phenylpropyloxymetopon: minimal requirements for binding to mu opioid receptors. <b>2012</b> , 20, 4556-63	2
1523	Structure-based design, synthesis, and biological evaluation of dihydroquinazoline-derived potent Is becretase inhibitors. <b>2012</b> , 22, 5460-5	16
1522	MurD ligase from Escherichia coli: C-terminal domain closing motion. <b>2012</b> , 979, 73-81	14
1521	QM/MM study on the spontaneous reactivation mechanism of (-)methamidophos-inhibited-acetylcholinesterase. <b>2012</b> , 980, 108-114	8

1520	Transformation of the dihedral corrective map for d-amino residues using the CHARMM force field. <b>2012</b> , 543, 142-147		1
1519	A computational study of Mg2+ dehydration in aqueous solution in the presence of HSIand other monovalent anions Insights to dolomite formation. <b>2012</b> , 88, 77-87		19
1518	Overview of computer modeling of cellulose. <b>2012</b> , 908, 11-22		4
1517	The peptide-receptive transition state of MHC class I molecules: insight from structure and molecular dynamics. <b>2012</b> , 189, 1391-9		45
1516	Unraveling A Trap-and-Trigger Mechanism in the pH-Sensitive Self-Assembly of Spider Silk Proteins. <b>2012</b> , 3, 658-662		38
1515	Binding hot-spots in an antibody-ssDNA interface: a molecular dynamics study. <b>2012</b> , 8, 3274-80		1
1514	Collapse of unfolded proteins in a mixture of denaturants. <b>2012</b> , 134, 18266-74		50
1513	DNA Bending through Large Angles Is Aided by Ionic Screening. <b>2012</b> , 8, 2145-56		31
1512	Discovery of tyrosine kinase inhibitors by docking into an inactive kinase conformation generated by molecular dynamics. <b>2012</b> , 7, 1983-90		31
1511	Comparing normal modes across different models and scales: Hessian reduction versus coarse-graining. <i>Journal of Computational Chemistry</i> , <b>2012</b> , 33, 2250-75	3.5	12
1510	SIMONA 1.0: an efficient and versatile framework for stochastic simulations of molecular and nanoscale systems. <i>Journal of Computational Chemistry</i> , <b>2012</b> , 33, 2602-13	3.5	21
1509	Optimization of designed armadillo repeat proteins by molecular dynamics simulations and NMR spectroscopy. <b>2012</b> , 21, 1298-314		28
1508	Calcium binding and allosteric signaling mechanisms for the sarcoplasmic reticulum Caʿl+ ATPase. <b>2012</b> , 21, 1429-43		21
1507	Nucleotide recognition by the initiation factor aIF5B: free energy simulations of a neoclassical GTPase. <b>2012</b> , 80, 2742-57		5
1506	Interaction of tetraphenylphosphonium and dodecyltriphenylphosphonium with lipid membranes and mitochondria. <b>2012</b> , 77, 1021-8		14
1505	Protein Nano-Object Integrator (ProNOI) for generating atomic style objects for molecular modeling. <b>2012</b> , 12, 31		4
1504	Epitope mapping by random peptide phage display reveals essential residues for vaccinia extracellular enveloped virion spread. <b>2012</b> , 9, 217		8
1503	ACPYPE - AnteChamber PYthon Parser interfacE. <b>2012</b> , 5, 367		1186

1502	Structural attributes for the recognition of weak and anomalous regions in coiled-coils of myosins and other motor proteins. <b>2012</b> , 5, 530	13
1501	Molecular dynamics and mutational analysis of the catalytic and translocation cycle of RNA polymerase. <b>2012</b> , 5, 11	32
1500	DelPhi: a comprehensive suite for DelPhi software and associated resources. <b>2012</b> , 5, 9	246
1499	Improving the CHARMM force field for polyunsaturated fatty acid chains. <b>2012</b> , 116, 9424-31	102
1498	Computer-assisted modeling of antibody variable domains. <b>2012</b> , 907, 39-55	4
1497	Prospects of Modulating Protein Protein Interactions. <b>2012</b> , 295-329	3
1496	Force field for monovalent, divalent, and trivalent cations developed under the solvent boundary potential. <b>2012</b> , 116, 11763-7	24
1495	Viral Packaging of Nucleic Acids. <b>2012</b> , 231-245	
1494	Site-Specific Fragment Identification Guided by Single-Step Free Energy Perturbation Calculations. <b>2012</b> , 8, 3513-3525	29
1493	Intrinsic contribution of the 2'-hydroxyl to RNA conformational heterogeneity. <b>2012</b> , 134, 2800-6	25
1492	Poly(vinyl alcohol) oligomer in dilute aqueous solution: a comparative molecular dynamics simulation study. <b>2012</b> , 116, 10008-19	22
1491	Carbohydrate recognition by the antiviral lectin cyanovirin-N. <b>2012</b> , 134, 19639-51	17
1490	Molecular dynamics studies of fluid/oil interfaces for improved oil recovery processes. <b>2012</b> , 116, 14667-76	82
1489	On the morphology of viral capsids: elastic properties and buckling transitions. <b>2012</b> , 116, 8604-9	33
1488	Sequence/structure relationships in aromatic dipeptide hydrogels formed under thermodynamic control by enzyme-assisted self-assembly. <b>2012</b> , 8, 5595	75
1487	Water-Driven Cavity-Ligand Binding: Comparison of Thermodynamic Signatures from Coarse-Grained and Atomic-Level Simulations. <b>2012</b> , 8, 3696-704	41
1486	A molecular simulation based assessment of binding of metal ions on micelles. <b>2012</b> , 28, 11329-36	9
1485	Molecular dynamics. <b>2012</b> , 929, 243-85	20

1484	The tension of a curved surface from simulation. <b>2012</b> , 137, 234101	16
1483	The increasing role of QM/MM in drug discovery. <b>2012</b> , 87, 337-62	39
1482	Quantifying hub-like behavior in protein folding networks. <b>2012</b> , 8, 3044-3052	21
1481	Unlocking the binding and reaction mechanism of hydroxyurea substrates as biological nitric oxide donors. <b>2012</b> , 52, 1288-97	15
1480	A sulfoximine-based inhibitor of human asparagine synthetase kills L-asparaginase-resistant leukemia cells. <b>2012</b> , 20, 5915-27	32
1479	Depth of ⊞-synuclein in a bilayer determined by fluorescence, neutron reflectometry, and computation. <b>2012</b> , 102, 613-21	78
1478	Minimalist model for force-dependent DNA replication. <b>2012</b> , 102, 810-8	4
1477	Thermodynamic coupling of protonation and conformational equilibria in proteins: theory and simulation. <b>2012</b> , 102, 1590-7	40
1476	NMR observable-based structure refinement of DAP12-NKG2C activating immunoreceptor complex in explicit membranes. <b>2012</b> , 102, L27-9	23
1475	Influence of hydrophobic mismatch on structures and dynamics of gramicidin a and lipid bilayers. <b>2012</b> , 102, 1551-60	78
1474	Prying open single GroES ring complexes by force reveals cooperativity across domains. <b>2012</b> , 102, 1961-8	1
1473	The influenza fusion peptide adopts a flexible flat V conformation in membranes. <b>2012</b> , 102, 2270-8	11
1472	Multi-ion distributions in the cytoplasmic domain of inward rectifier potassium channels. <b>2012</b> , 103, 434-443	6
1471	Rapid calculation of protein pKa values using Rosetta. <b>2012</b> , 103, 587-595	51
1470	Inclusion of many-body effects in the additive CHARMM protein CMAP potential results in enhanced cooperativity of ⊞-helix and ⊡hairpin formation. <b>2012</b> , 103, 1045-51	105
1469	Ion-controlled conformational dynamics in the outward-open transition from an occluded state of LeuT. <b>2012</b> , 103, 878-88	77
1468	Weak intra-ring allosteric communications of the archaeal chaperonin thermosome revealed by normal mode analysis. <b>2012</b> , 103, 1285-95	9
1467	Molecular dynamics of class A 🛭 lactamases-effects of substrate binding. <b>2012</b> , 103, 1790-801	12

1466	Towards alpha-glucosidase folding induced by trifluoroethanol: Kinetics and computational prediction. <b>2012</b> , 47, 2284-2290	11
1465	Inhibitory effect of Zn2+ on ⊞-glucosidase: Inhibition kinetics and molecular dynamics simulation. <b>2012</b> , 47, 2510-2517	12
1464	Propeptides are sufficient to regulate organelle-specific pH-dependent activation of furin and proprotein convertase 1/3. <b>2012</b> , 423, 47-62	21
1463	Membrane-binding mechanism of a peripheral membrane protein through microsecond molecular dynamics simulations. <b>2012</b> , 423, 847-61	32
1462	Implementation of the force decomposition machine for molecular dynamics simulations. <b>2012</b> , 38, 243-7	1
1461	9.6 New Technologies for Molecular Dynamics Simulations. <b>2012</b> , 86-104	3
1460	9.11 Molecular Electrostatics and Solvent Effects. <b>2012</b> , 190-228	1
1459	9.9 Quantum Mechanical Methods for Enzyme Modeling: Accurate Computation of Kinetic Isotope Effects. <b>2012</b> , 149-161	
1458	Chapter 4:Intrinsic Motions of DNA Polymerases Underlie Their Remarkable Specificity and Selectivity and Suggest a Hybrid Substrate Binding Mechanism. 81-110	2
1457	Understanding ion sensing in Zn(II) porphyrins: spectroscopic and computational studies of nitrite/nitrate binding. <b>2012</b> , 51, 4756-62	9
1456	Charge Group Partitioning in Biomolecular Simulation. <b>2012</b> , 29-43	5
1455	The -Cys-X1-X2-Cys- motif of reduced glutaredoxins adopts a consensus structure that explains the low pK(a) of its catalytic cysteine. <b>2012</b> , 51, 8189-207	4
1454	Assessment of Common Simulation Protocols for Simulations of Nanopores, Membrane Proteins, and Channels. <b>2012</b> , 8, 2905-11	50
1453	Update of the cholesterol force field parameters in CHARMM. <b>2012</b> , 116, 203-10	147
1452	Residue-residue contacts: application to analysis of secondary structure interactions. <b>2013</b> , 932, 159-73	1
1451	Molecular modeling of lipase binding to a substrate-water interface. <b>2012</b> , 861, 313-27	3
1450	Chapter 3:Towards Biomolecular Simulations with Explicit Inclusion of Polarizability: Development of a CHARMM Polarizable Force Field based on the Classical Drude Oscillator Model. <b>2012</b> , 23-50	4
1449	Chapter 4:Integral Equation Theory of Biomolecules and Electrolytes. <b>2012</b> , 51-86	12

1448	Theoretical study of the mechanism of the hydride transfer between ferredoxin-NADP+ reductase and NADP+: the role of Tyr303. <b>2012</b> , 134, 20544-53	30
1447	The Role of Atomic Polarization in the Thermodynamics of Chloroform Partitioning to Lipid Bilayers. <b>2012</b> , 8, 618-28	42
1446	The molecular mechanism underlying mechanical anisotropy of the protein GB1. 2012, 103, 2361-8	27
1445	Molecular dynamics simulation in virus research. <b>2012</b> , 3, 258	36
1444	Molecular dynamics study of the role of the spine of hydration in DNA A-tracts in determining nucleosome occupancy. <b>2012</b> , 116, 13672-81	14
1443	Synergistic folding of two intrinsically disordered proteins: searching for conformational selection. <b>2012</b> , 8, 198-209	47
1442	A theoretical study of the mechanism of the nucleotidyl transfer reaction catalyzed by yeast RNA polymerase II. <b>2012</b> , 55, 1887-1894	6
1441	Optimization of CHARMM force field parameters for the chalcone fragment. <b>2012</b> , 55, 2580-2586	
1440	Development and applications of the ABEEM fluctuating charge molecular force field in the ion-containing systems. <b>2012</b> , 55, 2471-2484	21
1439	A review of protein adsorption on bioceramics. <b>2012</b> , 2, 259-77	218
1439 1438	A review of protein adsorption on bioceramics. <b>2012</b> , 2, 259-77  New ketomethylene inhibitor analogues: synthesis and assessment of structural determinants for N-domain selective inhibition of angiotensin-converting enzyme. <b>2012</b> , 393, 485-93	218 9
	New ketomethylene inhibitor analogues: synthesis and assessment of structural determinants for	
1438	New ketomethylene inhibitor analogues: synthesis and assessment of structural determinants for N-domain selective inhibition of angiotensin-converting enzyme. <b>2012</b> , 393, 485-93  Optimization of the additive CHARMM all-atom protein force field targeting improved sampling of	9
1438 1437	New ketomethylene inhibitor analogues: synthesis and assessment of structural determinants for N-domain selective inhibition of angiotensin-converting enzyme. <b>2012</b> , 393, 485-93  Optimization of the additive CHARMM all-atom protein force field targeting improved sampling of the backbone [II] and side-chain (1) and (2) dihedral angles. <b>2012</b> , 8, 3257-3273  Exome sequencing identifies recurrent somatic MAP2K1 and MAP2K2 mutations in melanoma.	9 2511
1438 1437 1436	New ketomethylene inhibitor analogues: synthesis and assessment of structural determinants for N-domain selective inhibition of angiotensin-converting enzyme. 2012, 393, 485-93  Optimization of the additive CHARMM all-atom protein force field targeting improved sampling of the backbone [I]and side-chain (I) and (D) dihedral angles. 2012, 8, 3257-3273  Exome sequencing identifies recurrent somatic MAP2K1 and MAP2K2 mutations in melanoma. 2011, 44, 133-9  Direct hydride shift mechanism and stereoselectivity of P450nor confirmed by QM/MM	9 2511 313
1438 1437 1436 1435	New ketomethylene inhibitor analogues: synthesis and assessment of structural determinants for N-domain selective inhibition of angiotensin-converting enzyme. 2012, 393, 485-93  Optimization of the additive CHARMM all-atom protein force field targeting improved sampling of the backbone (Dand side-chain (1) and (2) dihedral angles. 2012, 8, 3257-3273  Exome sequencing identifies recurrent somatic MAP2K1 and MAP2K2 mutations in melanoma. 2011, 44, 133-9  Direct hydride shift mechanism and stereoselectivity of P450nor confirmed by QM/MM calculations. 2012, 116, 872-85  Analysis and elimination of a bias in targeted molecular dynamics simulations of conformational	9 2511 313 20
1438 1437 1436 1435	New ketomethylene inhibitor analogues: synthesis and assessment of structural determinants for N-domain selective inhibition of angiotensin-converting enzyme. 2012, 393, 485-93  Optimization of the additive CHARMM all-atom protein force field targeting improved sampling of the backbone [Land side-chain (I1) and (I2) dihedral angles. 2012, 8, 3257-3273  Exome sequencing identifies recurrent somatic MAP2K1 and MAP2K2 mutations in melanoma. 2011, 44, 133-9  Direct hydride shift mechanism and stereoselectivity of P450nor confirmed by QM/MM calculations. 2012, 116, 872-85  Analysis and elimination of a bias in targeted molecular dynamics simulations of conformational transitions: application to calmodulin. 2012, 116, 8584-603	9 2511 313 20 42

1430	Molecular dynamics simulations of Ago silencing complexes reveal a large repertoire of admissible 'seed-less' targets. <b>2012</b> , 2, 569	54
1429	Computational design of a carbon nanotube fluorofullerene biosensor. <b>2012</b> , 12, 13720-35	6
1428	Pressure effects on enzyme-catalyzed quantum tunneling events arise from protein-specific structural and dynamic changes. <b>2012</b> , 134, 9749-54	23
1427	A computational study of calcium(II) and copper(II) ion binding to the hyaluronate molecule. <b>2012</b> , 13, 12036-45	3
1426	How strongly does trehalose interact with lysozyme in the solid state? Insights from molecular dynamics simulation and inelastic neutron scattering. <b>2012</b> , 116, 11103-16	46
1425	Theoretical aspects of indirect spin-spin couplings. <b>2012</b> , 119-147	1
1424	Efficient and Unbiased Sampling of Biomolecular Systems in the Canonical Ensemble: A Review of Self-Guided Langevin Dynamics. <b>2012</b> , 150, 255-326	29
1423	Chemical optimization of new ligands of the low-density lipoprotein receptor as potential vectors for central nervous system targeting. <b>2012</b> , 55, 2227-41	53
1422	Momentum Distribution as a Fingerprint of Quantum Delocalization in Enzymatic Reactions: Open-Chain Path-Integral Simulations of Model Systems and the Hydride Transfer in Dihydrofolate Reductase. <b>2012</b> , 8, 1223-34	20
1421	Calculation of Free Energy Landscape in Multi-Dimensions with Hamiltonian-Exchange Umbrella Sampling on Petascale Supercomputer. <b>2012</b> , 8, 4672-80	76
1420	Comparing reduced partial charge models with polarizable simulations of ionic liquids. <b>2012</b> , 14, 3089-102	198
1419	Computational Drug Discovery and Design. 2012,	19
1418	High-throughput virtual screening lead to discovery of non-peptidic inhibitors of West Nile virus NS3 protease. <b>2012</b> , 819, 615-23	1
1417	Structural stability-chromatographic retention relationship on exenatide diastereomer separation. <b>2012</b> , 404, 2437-44	3
1416	MDMS: Molecular Dynamics Meta-Simulator for evaluating exchange type sampling methods. <b>2012</b> , 545, 118-124	5
1415	In silico engineering of aggregation-prone recombinant proteins for substrate recognition by the chaperonin GroEL. <b>2012</b> , 13 Suppl 7, S22	2
1414	Discrete molecular dynamics: an efficient and versatile simulation method for fine protein characterization. <b>2012</b> , 116, 8375-82	140
1413	Probing structural features of Alzheimer's amyloid-🏿 pores in bilayers using site-specific amino acid substitutions. <b>2012</b> , 51, 776-85	41

1412	The effect of fucoidan on tyrosinase: computational molecular dynamics integrating inhibition kinetics. <b>2012</b> , 30, 460-73	24
1411	Putting the pieces together: integrative modeling platform software for structure determination of macromolecular assemblies. <b>2012</b> , 10, e1001244	362
1410	Kinetic rate constant prediction supports the conformational selection mechanism of protein binding. <b>2012</b> , 8, e1002351	43
1409	Molecular dynamics studies of the nucleoprotein of influenza A virus: role of the protein flexibility in RNA binding. <b>2012</b> , 7, e30038	29
1408	Effects of ligands on unfolding of the amyloid I-peptide central helix: mechanistic insights from molecular dynamics simulations. <b>2012</b> , 7, e30510	17
1407	Structure-based high-throughput epitope analysis of hexon proteins in B and C species human adenoviruses (HAdVs). <b>2012</b> , 7, e32938	13
1406	In silico investigation of potential SRC kinase ligands from traditional Chinese medicine. <b>2012</b> , 7, e33728	20
1405	Structural analysis of a peptide fragment of transmembrane transporter protein bilitranslocase. <b>2012</b> , 7, e38967	14
1404	Simulation vs. reality: a comparison of in silico distance predictions with DEER and FRET measurements. <b>2012</b> , 7, e39492	57
1403	In silico identification of potent pancreatic triacylglycerol lipase inhibitors from traditional Chinese medicine. <b>2012</b> , 7, e43932	20
1402	Structural basis of type 2A von Willebrand disease investigated by molecular dynamics simulations and experiments. <b>2012</b> , 7, e45207	12
1401	The mutation V42M distorts the compact packing of the human gamma-S-crystallin molecule, resulting in congenital cataract. <b>2012</b> , 7, e51401	17
1400	Structural Bioinformatics of Proteins: Predicting the Tertiary and Quaternary Structure of Proteins from Sequence. <b>2012</b> ,	1
1399	The Molecular Structure and Conformational Dynamics of Chitosan Polymers: An Integrated Perspective from Experiments and Computational Simulations. <b>2012</b> ,	3
1398	In Silico and In Vitro Comparison of HIV-1 Subtypes B and CRF02_AG Integrases Susceptibility to Integrase Strand Transfer Inhibitors. <b>2012</b> , 2012, 548657	5
1397	Reaction Path Optimization and Sampling Methods and Their Applications for Rare Events. 2012,	1
1396	Structure based virtual screening of novel inhibitors against multidrug resistant superbugs. <b>2012</b> , 8, 420-5	8
1395	Molecular Simulation with Discrete Fast Fourier Transform. 2012,	

1394	Familial Hypertrophic Cardiomyopathy-Related Troponin Mutations and Sudden Cardiac Death. <b>2012</b> ,	1
1393	Exploring Protein-Protein and Protein-Ligand Interactions in the Immune System using Molecular Dynamics and Continuum Electrostatics. <b>2012</b> , 2, 324-343	16
1392	Structural biology of factor VIIa/tissue factor initiated coagulation. <b>2012</b> , 17, 2476-94	32
1391	The use of glycoinformatics in glycochemistry. <b>2012</b> , 8, 915-29	20
1390	Interactions of oligomers of organic polyethers with histidine amino acid. <b>2012</b> , 26, 532-40	7
1389	Computational studies of LXR molecular interactions reveal an allosteric communication pathway. <b>2012</b> , 80, 294-306	14
1388	Minimal ensembles of side chain conformers for modeling protein-protein interactions. <b>2012</b> , 80, 591-601	25
1387	Ligand-induced formation of transient dimers of mammalian 12/15-lipoxygenase: a key to allosteric behavior of this class of enzymes?. <b>2012</b> , 80, 703-12	24
1386	Synergistic use of NMR and MD simulations to study the structural heterogeneity of proteins. <b>2012</b> , 2, 466-478	20
1385	Recent Developments and Applications of the CHARMM force fields. <b>2012</b> , 2, 167-185	139
1385	Recent Developments and Applications of the CHARMM force fields. <b>2012</b> , 2, 167-185  Recent trends in conformational analysis. <b>2012</b> , 2, 613-641	139 55
1384	Recent trends in conformational analysis. <b>2012</b> , 2, 613-641  Conformational selection through electrostatics: Free energy simulations of GTP and GDP binding	55
1384	Recent trends in conformational analysis. <b>2012</b> , 2, 613-641  Conformational selection through electrostatics: Free energy simulations of GTP and GDP binding to archaeal initiation factor 2. <b>2012</b> , 80, 1264-82  Inhibition of interdomain motion in g-actin by the natural product latrunculin: a molecular dynamics	55 8
1384 1383 1382	Recent trends in conformational analysis. <b>2012</b> , 2, 613-641  Conformational selection through electrostatics: Free energy simulations of GTP and GDP binding to archaeal initiation factor 2. <b>2012</b> , 80, 1264-82  Inhibition of interdomain motion in g-actin by the natural product latrunculin: a molecular dynamics study. <b>2012</b> , 80, 1998-2008	<ul><li>55</li><li>8</li><li>6</li></ul>
1384 1383 1382	Recent trends in conformational analysis. 2012, 2, 613-641  Conformational selection through electrostatics: Free energy simulations of GTP and GDP binding to archaeal initiation factor 2. 2012, 80, 1264-82  Inhibition of interdomain motion in g-actin by the natural product latrunculin: a molecular dynamics study. 2012, 80, 1998-2008  Peptide binding to the PDZ3 domain by conformational selection. 2012, 80, 2562-72  The Structure, Thermodynamics and Solubility of Organic Crystals from Simulation with a	55 8 6
1384 1383 1382 1381	Recent trends in conformational analysis. 2012, 2, 613-641  Conformational selection through electrostatics: Free energy simulations of GTP and GDP binding to archaeal initiation factor 2. 2012, 80, 1264-82  Inhibition of interdomain motion in g-actin by the natural product latrunculin: a molecular dynamics study. 2012, 80, 1998-2008  Peptide binding to the PDZ3 domain by conformational selection. 2012, 80, 2562-72  The Structure, Thermodynamics and Solubility of Organic Crystals from Simulation with a Polarizable Force Field. 2012, 8, 1721-1736	55 8 6 13 65

1376	Balancing target flexibility and target denaturation in computational fragment-based inhibitor discovery. <i>Journal of Computational Chemistry</i> , <b>2012</b> , 33, 1880-91	3.5	32
1375	Photocontrol of reversible amyloid formation with a minimal-design peptide. <b>2012</b> , 116, 8961-73		17
1374	Phenylalanine assembly into toxic fibrils suggests amyloid etiology in phenylketonuria. <b>2012</b> , 8, 701-6		266
1373	Predicting folding free energy changes upon single point mutations. <b>2012</b> , 28, 664-71		67
1372	Magnesium Ion-Water Coordination and Exchange in Biomolecular Simulations. <b>2012</b> , 8, 1493-502		257
1371	Biomolecular dynamics: order-disorder transitions and energy landscapes. <b>2012</b> , 75, 076601		91
1370	GPU/CPU Algorithm for Generalized Born/Solvent-Accessible Surface Area Implicit Solvent Calculations. <b>2012</b> , 8, 2521-2530		37
1369	Opening and closing of the bacterial RNA polymerase clamp. <b>2012</b> , 337, 591-5		160
1368	Expanding molecular modeling and design tools to non-natural sidechains. <i>Journal of Computational Chemistry</i> , <b>2012</b> , 33, 1525-35	3.5	21
1367	Atomic multipoles: electrostatic potential fit, local reference axis systems, and conformational dependence. <i>Journal of Computational Chemistry</i> , <b>2012</b> , 33, 1673-88	3.5	52
1366	Force field development for cofactors in the photosystem II. <i>Journal of Computational Chemistry</i> , <b>2012</b> , 33, 1969-80	3.5	40
1365	A simplified homology-model builder toward highly protein-like structures: an inspection of restraining potentials. <i>Journal of Computational Chemistry</i> , <b>2012</b> , 33, 1927-35	3.5	42
1364	Highly efficient and exact method for parallelization of grid-based algorithms and its implementation in DelPhi. <i>Journal of Computational Chemistry</i> , <b>2012</b> , 33, 1960-6	3.5	34
1363	nMoldyn 3: using task farming for a parallel spectroscopy-oriented analysis of molecular dynamics simulations. <i>Journal of Computational Chemistry</i> , <b>2012</b> , 33, 2043-8	3.5	43
1362	Extension of the CHARMM General Force Field to sulfonyl-containing compounds and its utility in biomolecular simulations. <i>Journal of Computational Chemistry</i> , <b>2012</b> , 33, 2451-68	3.5	447
1361	Conformational Dynamics of a Central Trisaccharide Fragment of the LeaLex Tumor Associated Antigen Studied by NMR Spectroscopy and Molecular Dynamics Simulations. <b>2012</b> , 2012, 4705-4715		10
1360	Computational prediction of 1H and 13C chemical shifts: a useful tool for natural product, mechanistic, and synthetic organic chemistry. <b>2012</b> , 112, 1839-62		809
1359	Nanodiamonds in sugar rings: an experimental and theoretical investigation of cyclodextrin-nanodiamond inclusion complexes. <b>2012</b> , 10, 4524-30		42

1358	Quantum mechanical/molecular mechanical study on the mechanism of the enzymatic Baeyer-Villiger reaction. <b>2012</b> , 134, 2732-41	83
1357	Characterization of the Reaction Path and Transition States for RNA Transphosphorylation Models from Theory and Experiment. <b>2012</b> , 124, 671-675	3
1356	Investigating the halochromic properties of azo dyes in an aqueous environment by using a combined experimental and theoretical approach. <b>2012</b> , 18, 8120-9	35
1355	Studies on differential nuclear translocation mechanism and assembly of the three subunits of the Arabidopsis thaliana transcription factor NF-Y. <b>2012</b> , 5, 876-88	75
1354	Stability and Mobility of Functionalized Silica Nanoparticles for Enhanced Oil Recovery Applications. <b>2012</b> ,	65
1353	Molecular Dynamics Simulation: From ♠b Initioᡅo ᠒oarse Grained□ <b>2012</b> , 195-238	10
1352	Applications of Computational Methods to Simulations of Proteins Dynamics. <b>2012</b> , 1127-1153	4
1351	Pharmacophore modeling, molecular docking, and molecular dynamics simulation approaches for identifying new lead compounds for inhibiting aldose reductase 2. <b>2012</b> , 18, 3267-82	15
1350	Correlation between biological activity and binding energy in systems of integrin with cyclic RGD-containing binders: a QM/MM molecular dynamics study. <b>2012</b> , 18, 4917-27	9
1349	The Amber ff99 Force Field Predicts Relative Free Energy Changes for RNA Helix Formation. <b>2012</b> , 8, 2497-2505	30
1348	Virtual target screening: validation using kinase inhibitors. <b>2012</b> , 52, 2192-203	21
1347	Studies on the conformational flexibility of ∃-L-rhamnose-containing oligosaccharides using 13C-site-specific labeling, NMR spectroscopy and molecular simulations: implications for the three-dimensional structure of bacterial rhamnan polysaccharides. <b>2012</b> , 10, 2453-63	14
1346	Isomerization mechanism of the HcRed fluorescent protein chromophore. <b>2012</b> , 14, 11413-24	20
1345	Comparison of Cellulose IIISimulations with Three Carbohydrate Force Fields. <b>2012</b> , 8, 735-48	101
1344	Density of states-based molecular simulations. <b>2012</b> , 3, 369-94	46
1343	Platinated DNA affects zinc finger conformation. Interaction of a platinated single-stranded oligonucleotide and the C-terminal zinc finger of nucleocapsid protein HIVNCp7. <b>2012</b> , 51, 1752-61	14
1342	Computational prediction of metabolism: sites, products, SAR, P450 enzyme dynamics, and mechanisms. <b>2012</b> , 52, 617-48	212
1341	Application of binding free energy calculations to prediction of binding modes and affinities of MDM2 and MDMX inhibitors. <b>2012</b> , 52, 1821-32	27

1340	Recent advances in computational actinoid chemistry. <b>2012</b> , 41, 5836-65	104
1339	An assessment of computational methods for obtaining structural information of moderately flexible biomolecules from ion mobility spectrometry. <b>2012</b> , 23, 792-805	27
1338	Predicting binding affinities of host-guest systems in the SAMPL3 blind challenge: the performance of relative free energy calculations. <b>2012</b> , 26, 543-50	25
1337	Subunit F modulates ATP binding and migration in the nucleotide-binding subunit B of the A(1)A(O) ATP synthase of Methanosarcina mazei $G\square$ 1. <b>2012</b> , 44, 213-24	3
1336	Goal-Oriented Adaptivity and Multilevel Preconditioning for the Poisson-Boltzmann Equation. <b>2012</b> , 52, 202-225	9
1335	Interaction of nucleic acids with carbon nanotubes and dendrimers. <b>2012</b> , 37, 457-74	43
1334	Weakly hydrated surfaces and the binding interactions of small biological solutes. <b>2012</b> , 41, 369-77	13
1333	Improving the acidic stability of a methyl parathion hydrolase by changing basic residues to acidic residues. <b>2012</b> , 34, 1115-21	7
1332	Structural modelling and dynamics of proteins for insights into drug interactions. <b>2012</b> , 64, 323-43	24
1331	Molecular dynamics simulations of the interaction of glucose with imidazole in aqueous solution. <b>2012</b> , 349, 73-7	16
1330	Transition path sampling of protein conformational changes. <b>2012</b> , 396, 30-44	25
1329	Large-scale motions in the adenylate kinase solution ensemble: coarse-grained simulations and comparison with solution X-ray scattering. <b>2012</b> , 396, 84-91	26
1328	Molecular dynamics study of ethanol solvated by water on the Pt (1 1 1) surface. <b>2012</b> , 402, 41-47	5
1327	Kinetics of proton release and uptake by channelrhodopsin-2. <b>2012</b> , 586, 1344-8	26
1326	HPAM: Hirshfeld Partitioned Atomic Multipoles. <b>2012</b> , 183, 390-397	13
1325	Solvation Structure and Energetics of Single Ions at the Aqueous Liquid-Vapor Interface. <b>2012</b> , 527, 22-26	15
1324	Refined structure-based simulation of plant light-harvesting complex II: linear optical spectra of trimers and aggregates. <b>2012</b> , 1817, 1446-60	42
1323	Increased endothelial cell selectivity of triazole-bridged dihalogenated A-ring analogues of combretastatin A-1. <b>2012</b> , 20, 1749-59	17

1322	Influence of the membrane dipole potential on peptide binding to lipid bilayers. 2012, 161, 1-7		33
1321	Influence of the enzyme phosphorylation state and the substrate on PKA enzyme dynamics. <b>2012</b> , 161, 17-28		9
1320	Experimentally assessing molecular dynamics sampling of the protein native state conformational distribution. <b>2012</b> , 163-164, 21-34		7
1319	Importance of local interactions for the stability of inhibitory helix 1 in apo Ets-1. <b>2012</b> , 165-166, 74-8		12
1318	Molecular dynamics in drug design: new generations of compstatin analogs. 2012, 79, 703-18		31
1317	Contribution of both catalytic constant and Michaelis constant to CALB enantioselectivity: Use of FEP calculations for prediction studies. <b>2012</b> , 76, 29-36		4
1316	An efficient null model for conformational fluctuations in proteins. <b>2012</b> , 20, 1028-39		7
1315	A position-specific distance-dependent statistical potential for protein structure and functional study. <b>2012</b> , 20, 1118-26		48
1314	Molecular modeling of Bt Cry1Ac (DI-DII)-ASAL (Allium sativum lectin)-fusion protein and its interaction with aminopeptidase N (APN) receptor of Manduca sexta. <b>2012</b> , 33, 61-76		13
1313	Identification of CK2 inhibitors with new scaffolds by a hybrid virtual screening approach based on Bayesian model; pharmacophore hypothesis and molecular docking. <b>2012</b> , 36, 42-7		16
1312	Molecular dynamics simulation study of tubulin dimer interaction with cytostatics. <b>2012</b> , 46, 316-321		5
1311	Modelling zwitterions in solution: 3-fluoro-Eminobutyric acid (3F-GABA). <b>2012</b> , 18, 184-95		11
1310	Web interface for Brownian dynamics simulation of ion transport and its applications to beta-barrel pores. <i>Journal of Computational Chemistry</i> , <b>2012</b> , 33, 331-9	3.5	38
1309	MATCH: an atom-typing toolset for molecular mechanics force fields. <i>Journal of Computational Chemistry</i> , <b>2012</b> , 33, 189-202	3.5	115
1308	Thermodynamics and kinetics of large-time-step molecular dynamics. <i>Journal of Computational Chemistry</i> , <b>2012</b> , 33, 475-83	3.5	10
1307	Potential of mean force of water-proton bath and molecular dynamic simulation of proteins at constant pH. <i>Journal of Computational Chemistry</i> , <b>2012</b> , 33, 832-42	3.5	14
1306	Cellulose-builder: a toolkit for building crystalline structures of cellulose. <i>Journal of Computational Chemistry</i> , <b>2012</b> , 33, 1338-46	3.5	119
1305	Photodissociation dynamics of ClCN at different wavelengths. <b>2012</b> , 13, 305-13		4

1304	Characterization of the reaction path and transition states for RNA transphosphorylation models from theory and experiment. <b>2012</b> , 51, 647-51	43
1303	Toward molecular models of proton pumping: Challenges, methods and relevant applications. <b>2012</b> , 55, 3-18	6
1302	Studying interfacial reactions of cholesterol sulfate in an unsaturated phosphatidylglycerol layer with ozone using field induced droplet ionization mass spectrometry. <b>2012</b> , 23, 141-52	14
1301	Structure-based simulation of linear optical spectra of the CP43 core antenna of photosystem II. <b>2012</b> , 111, 87-101	33
1300	Determination of enthalpies (Heats) of formation. <b>2013</b> , 3, 21-36	18
1299	Is it possible to stabilize a thermophilic protein further using sequences and structures of mesophilic proteins: a theoretical case study concerning DgAS. <b>2013</b> , 10, 26	2
1298	Nanomaterials Imaging Techniques, Surface Studies, and Applications. 2013,	2
1297	Study of Nanocomposites of Amino Acids and Organic Polyethers by Means of Mass Spectrometry and Molecular Dynamics Simulation. <b>2013</b> , 327-338	1
1296	CHARMM36 all-atom additive protein force field: validation based on comparison to NMR data. <i>Journal of Computational Chemistry</i> , <b>2013</b> , 34, 2135-45	1487
1295	Gestalt-binding of tropomyosin on actin during thin filament activation. <b>2013</b> , 34, 155-63	49
1294	A time-dependent DFT/molecular dynamics study of the proton-wire responsible for the red fluorescence in the LSSmKate2 protein. <b>2013</b> , 132, 1	10
1293	Disruption of intrinsic motions as a mechanism for enzyme inhibition. <b>2013</b> , 105, 494-501	2
1292	Inactivation and conformational changes in methyl parathion hydrolase in 2,2,2-trifluoroethanol solutions: Inactivation kinetics and molecular dynamics simulation. <b>2013</b> , 48, 625-632	4
1291	Computational study of the structure and electronic circular dichroism spectroscopy of blue copper proteins. <b>2013</b> , 117, 8105-12	7
1290	The conformation of a ribose derivative in aqueous solution: a neutron-scattering and molecular dynamics study. <b>2013</b> , 99, 739-45	3
1289	Design, synthesis and biological evaluation of novel mansonone E derivatives prepared via CuAAC click chemistry as topoisomerase II inhibitors. <b>2013</b> , 68, 58-71	22
1288	Lipid-Protein Interactions. 2013,	20
1287	DNA binding and bending by Sac7d is stepwise. <b>2013</b> , 14, 1434-7	12

1286 Molecular Mechanics. **2013**, 263-277

1285	Conformational disorder enhances electron transfer through alkyl monolayers: ferrocene on conductive diamond. <b>2013</b> , 135, 5751-61		52
1284	AUTOMATED FORCE FIELD PARAMETERIZATION FOR NON-POLARIZABLE AND POLARIZABLE ATOMIC MODELS BASED ON TARGET DATA. <b>2013</b> , 9,		172
1283	Grcarma: A fully automated task-oriented interface for the analysis of molecular dynamics trajectories. <i>Journal of Computational Chemistry</i> , <b>2013</b> , 34, 2310-2	3.5	81
1282	Model-based design of synthetic, biological systems. <b>2013</b> , 103, 2-11		15
1281	Routine Microsecond Molecular Dynamics Simulations with AMBER on GPUs. 2. Explicit Solvent Particle Mesh Ewald. <b>2013</b> , 9, 3878-88		1740
1280	A conformational intermediate in glutamate receptor activation. <b>2013</b> , 79, 492-503		34
1279	Towards an understanding of channelrhodopsin function: simulations lead to novel insights of the channel mechanism. <b>2013</b> , 425, 1795-814		58
1278	MAPs: a database of modular antibody parts for predicting tertiary structures and designing affinity matured antibodies. <b>2013</b> , 14, 168		21
1277	The novel BH3 ⊞-helix mimetic JY-1-106 induces apoptosis in a subset of cancer cells (lung cancer, colon cancer and mesothelioma) by disrupting Bcl-xL and Mcl-1 protein-protein interactions with Bak. <b>2013</b> , 12, 42		69
1276	Recent advances in computational predictions of NMR parameters for the structure elucidation of carbohydrates: methods and limitations. <b>2013</b> , 42, 8376-415		93
1275	Cooperative stabilization of Zn(2+):DNA complexes through netropsin binding in the minor groove of FdU-substituted DNA. <b>2013</b> , 31, 1301-10		11
1274	Improving stability of nitrile hydratase by bridging the salt-bridges in specific thermal-sensitive regions. <b>2012</b> , 164, 354-62		64
1273	Recent Progress in Density Functional Methodology for Biomolecular Modeling. 2013, 1-64		7
1272	Molecular Dynamics Simulations Provide Atomistic Insight into Hydrogen Exchange Mass Spectrometry Experiments. <b>2013</b> , 9, 658-69		23
1271	Theoretical study of HOCl-catalyzed keto-enol tautomerization of I-cyclopentanedione in an explicit water environment. <b>2013</b> , 117, 8437-48		13
1270	Endoglucanase peripheral loops facilitate complexation of glucan chains on cellulose via adaptive coupling to the emergent substrate structures. <b>2013</b> , 117, 10750-8		14
1269	Simulating the mechanism of antimicrobial lipopeptides with all-atom molecular dynamics. <b>2013</b> , 52, 5604-10		32

1268	Nucleotide-dependent control of internal strains in ring-shaped AAA+ motors. 2013, 6, 65-73	7
1267	Atomistic and Coarse-Grained Molecular Dynamics Simulations of Membrane Proteins. 2013, 193-206	1
1266	Bifurcated hydrogen bonding and asymmetric fluctuations in a carbohydrate crystal studied via X-ray crystallography and computational analysis. <b>2013</b> , 117, 7546-53	5
1265	PTRAJ and CPPTRAJ: Software for Processing and Analysis of Molecular Dynamics Trajectory Data. <b>2013</b> , 9, 3084-95	3066
1264	Discovery of ZAP70 inhibitors by high-throughput docking into a conformation of its kinase domain generated by molecular dynamics. <b>2013</b> , 23, 5721-6	69
1263	Expanding the frontiers of protein-protein modeling: from docking and scoring to binding affinity predictions and other challenges. <b>2013</b> , 81, 2192-200	20
1262	DNA bending propensity in the presence of base mismatches: implications for DNA repair. <b>2013</b> , 117, 6194-205	31
1261	Unraveling protein-protein interactions in clathrin assemblies via atomic force spectroscopy. <b>2013</b> , 59, 316-27	4
1260	Comparison of volume and surface area nonpolar solvation free energy terms for implicit solvent simulations. <b>2013</b> , 139, 044119	18
1259	Overcoming the Rare Event Sampling Problem in Biological Systems with Infinite Swapping. <b>2013</b> , 9, 4215-24	18
1258	Simulations of anionic lipid membranes: development of interaction-specific ion parameters and validation using NMR data. <b>2013</b> , 117, 10183-92	130
1257	3D electron tomography of pretreated biomass informs atomic modeling of cellulose microfibrils. <b>2013</b> , 7, 8011-9	60
1256	The different interactions of lysine and arginine side chains with lipid membranes. 2013, 117, 11906-20	176
1255	Development and Optimization of a New Force Field for Flexible Aluminosilicates, Enabling Fast Molecular Dynamics Simulations on Parallel Architectures. <b>2013</b> , 117, 503-509	17
1254	Insight into the degradation of type-I collagen fibrils by MMP-8. <b>2013</b> , 425, 1815-25	36
1253	Perspective: Coarse-grained models for biomolecular systems. <b>2013</b> , 139, 090901	532
1252	What Is the Dielectric Constant of a Protein When Its Backbone Is Fixed?. <b>2013</b> , 9, 4603-8	14
1251	Mechanism and Kinetics of Acetyl-Lysine Binding to Bromodomains. <b>2013</b> , 9, 4225-32	24

1250	An implementation of hydrophobic force in implicit solvent molecular dynamics simulation for packed proteins. <b>2013</b> , 19, 2605-12	4
1249	Quantum mechanics/molecular mechanics dual Hamiltonian free energy perturbation. <b>2013</b> , 139, 064105	33
1248	Amine oxidation mediated by lysine-specific demethylase 1: quantum mechanics/molecular mechanics insights into mechanism and role of lysine 661. <b>2013</b> , 135, 13400-13	34
1247	Polarizable empirical force field for acyclic polyalcohols based on the classical Drude oscillator. <b>2013</b> , 99, 724-38	45
1246	Structural landscape of the proline-rich domain of Sos1 nucleotide exchange factor. <b>2013</b> , 175-176, 54-62	6
1245	In silico study of Aquaporin V: Effects and affinity of the central pore-occluding lipid. 2013, 171, 24-30	22
1244	Accurate high-throughput structure mapping and prediction with transition metal ion FRET. <b>2013</b> , 21, 9-19	21
1243	Inclusion of lateral pressure/curvature stress effects in implicit membrane models. 2013, 104, 643-54	27
1242	Inhibition of tyrosinase by gastrodin: An integrated kinetic-computational simulation analysis. <b>2013</b> , 48, 162-168	12
1241	Molecular energetics in the capsomere of virus-like particle revealed by molecular dynamics simulations. <b>2013</b> , 117, 5411-21	13
1240	Principles of Shape-Driven Nanostructure Design via Self-Assembly of Protein Building Blocks. <b>2013</b> , 171-189	
1239	Glycerol modulates water permeation through Escherichia coli aquaglyceroporin GlpF. <b>2013</b> , 1828, 1786-93	24
1238	Periodic boundary conditions for QM/MM calculations: Ewald summation for extended Gaussian basis sets. <b>2013</b> , 139, 244108	38
1237	Simulation study of ion pairing in concentrated aqueous salt solutions with a polarizable force field. <b>2013</b> , 160, 135-49; discussion 207-24	86
1236	Optimization of 3D Poisson-Nernst-Planck model for fast evaluation of diverse protein channels. <b>2013</b> , 81, 1802-22	7
1235	Absolute free energies of biomolecules from unperturbed ensembles. <i>Journal of Computational Chemistry</i> , <b>2013</b> , 34, 2726-41	12
1234	Liquid-vapor interfacial properties of aqueous solutions of guanidinium and methyl guanidinium chloride: influence of molecular orientation on interface fluctuations. <b>2013</b> , 117, 11719-31	13
1233	The mechanism by which a propeptide-encoded pH sensor regulates spatiotemporal activation of furin. <b>2013</b> , 288, 19154-65	19

1232	Energetic and structural details of the trigger-loop closing transition in RNA polymerase II. <b>2013</b> , 105, 767-75	25
1231	Characterizing a histidine switch controlling pH-dependent conformational changes of the influenza virus hemagglutinin. <b>2013</b> , 105, 993-1003	16
1230	Different hydration patterns in the pores of AmtB and RhCG could determine their transport mechanisms. <b>2013</b> , 52, 7091-8	10
1229	Direct observation of amyloid nucleation under nanomechanical stretching. <b>2013</b> , 7, 7734-43	18
1228	All-atom molecular dynamics simulation of photosystem II embedded in thylakoid membrane. <b>2013</b> , 135, 15670-3	65
1227	Acetylation of (R,S)-propranolol catalyzed by Candida antarctica lipase B: An experimental and computational study. <b>2013</b> , 98, 21-29	15
1226	Catalytic mechanism of the glycyl radical enzyme 4-hydroxyphenylacetate decarboxylase from continuum electrostatic and QC/MM calculations. <b>2013</b> , 135, 14574-85	25
1225	Accurate and efficient integration for molecular dynamics simulations at constant temperature and pressure. <b>2013</b> , 139, 164106	96
1224	Sensitivity-enhanced solid-state NMR detection of expansin's target in plant cell walls. <b>2013</b> , 110, 16444-9	171
1223	Native contacts determine protein folding mechanisms in atomistic simulations. <b>2013</b> , 110, 17874-9	332
1222	Specific and non-specific protein association in solution: computation of solvent effects and prediction of first-encounter modes for efficient configurational bias Monte Carlo simulations. <b>2013</b> , 117, 12360-74	15
1221	ESR1 ligand-binding domain mutations in hormone-resistant breast cancer. <b>2013</b> , 45, 1439-45	754
<b>122</b> 0	Evolutionary Algorithm in the Optimization of a Coarse-Grained Force Field. 2013, 9, 4874-89	23
1219	A comparative Kirkwood-Buff study of aqueous methanol solutions modeled by the CHARMM additive and Drude polarizable force fields. <b>2013</b> , 117, 10572-80	11
1218	Functional and structural interaction of (-)-reboxetine with the human $\oplus 4\square$ nicotinic acetylcholine receptor. <b>2013</b> , 344, 113-23	11
1217	Ubiquitin: molecular modeling and simulations. <b>2013</b> , 46, 29-40	15
1216	Multipole-Based Force Fields from ab Initio Interaction Energies and the Need for Jointly Refitting All Intermolecular Parameters. <b>2013</b> , 9, 1499-511	32
1215	Force Field for Peptides and Proteins based on the Classical Drude Oscillator. <b>2013</b> , 9, 5430-5449	274

1214	Selective inhibition of the West Nile virus methyltransferase by nucleoside analogs. <b>2013</b> , 97, 232-9		44
1213	Crystal structure and computational characterization of the lytic polysaccharide monooxygenase GH61D from the Basidiomycota fungus Phanerochaete chrysosporium. <b>2013</b> , 288, 12828-39		131
1212	Energetics of Multi-Ion Conduction Pathways in Potassium Ion Channels. <b>2013</b> , 9, 5176-5189		31
1211	Computational methods of studying the binding of toxins from venomous animals to biological ion channels: theory and applications. <b>2013</b> , 93, 767-802		42
<b>121</b> 0	Lennard-Jones Lattice Summation in Bilayer Simulations Has Critical Effects on Surface Tension and Lipid Properties. <b>2013</b> , 9, 3527-37		89
1209	QuanPol: a full spectrum and seamless QM/MM program. <i>Journal of Computational Chemistry</i> , <b>2013</b> , 34, 2816-33	3.5	29
1208	Conformational analysis of NMDA receptor GluN1, GluN2, and GluN3 ligand-binding domains reveals subtype-specific characteristics. <b>2013</b> , 21, 1788-99		73
1207	Computational methods for constructing protein structure models from 3D electron microscopy maps. <b>2013</b> , 184, 93-102		31
1206	Gastric intrinsic factor deficiency with combined GIF heterozygous mutations and FUT2 secretor variant. <b>2013</b> , 95, 995-1001		20
1205	Mechanism of activation of elongation factor Tu by ribosome: catalytic histidine activates GTP by protonation. <b>2013</b> , 19, 1218-25		18
1204	Analyzing the relationship between single base flipping and strand slippage near DNA duplex termini. <b>2013</b> , 117, 14320-8		3
1203	Conformation and dynamics at a flexible glycosidic linkage revealed by NMR spectroscopy and molecular dynamics simulations: analysis of □L-Fucp-(1->6)-□-D-Glcp-OMe in water solution. <b>2013</b> , 117, 14709-22		18
1202	Modeling active GPCR conformations. <b>2013</b> , 522, 21-35		11
1201	Branched oligopeptides form nanocapsules with lipid vesicle characteristics. <b>2013</b> , 29, 14648-54		20
1200	Dynamic Heterogeneous Dielectric Generalized Born (DHDGB): An implicit membrane model with a dynamically varying bilayer thickness. <b>2013</b> , 9, 1709-1719		40
1199	Photocontrolled nuclear-targeted drug delivery by single component photoresponsive fluorescent organic nanoparticles of acridin-9-methanol. <b>2013</b> , 24, 1828-39		35
1198	Molecular dynamics and NMR spectroscopy studies of E. coli lipopolysaccharide structure and dynamics. <b>2013</b> , 105, 1444-55		125
1197	On the nature of interactions between ionic liquids and small amino-acid-based biomolecules. <b>2013</b> , 14, 4044-64		55

1196	Charging free energy calculations using the Generalized Solvent Boundary Potential (GSBP) and periodic boundary condition: a comparative analysis using ion solvation and oxidation free energy in proteins. <b>2013</b> , 117, 2005-18	26
1195	Targeted conformational search with map-restrained self-guided Langevin dynamics: application to flexible fitting into electron microscopic density maps. <b>2013</b> , 183, 429-440	35
1194	A Y328C missense mutation in spermine synthase causes a mild form of Snyder-Robinson syndrome. <b>2013</b> , 22, 3789-97	26
1193	Molecular basis of lateral force spectroscopy nano-diagnostics: computational unbinding of autism related chemokine MCP-1 from IgG antibody. <b>2013</b> , 19, 4773-80	4
1192	Optimized CGenFF force-field parameters for acylphosphate and N-phosphonosulfonimidoyl functional groups. <b>2013</b> , 19, 5075-87	1
1191	Different effects of progesterone and estradiol on chimeric and wild type aldosterone synthase in vitro. <b>2013</b> , 11, 76	10
1190	Fast calculation of the infrared spectra of large biomolecules. <b>2013</b> , 42, 795-801	7
1189	The role of aromatic L-amino acid decarboxylase in bacillamide C biosynthesis by Bacillus atrophaeus C89. <b>2013</b> , 3, 1753	17
1188	Identification of Ligand Binding Site and Protein-Protein Interaction Area. 2013,	0
1187	Quantum and all-atom molecular dynamics simulations of protonation and divalent ion binding to phosphatidylinositol 4,5-bisphosphate (PIP2). <b>2013</b> , 117, 8322-9	31
1186	A structural and functional model for human bone sialoprotein. <b>2013</b> , 39, 108-17	19
1185	Hidden Conformation Events in DNA Base Extrusions: A Generalized Ensemble Path Optimization and Equilibrium Simulation Study. <b>2013</b> , 9,	15
1184	PRIMO: A Transferable Coarse-grained Force Field for Proteins. <b>2013</b> , 9, 3769-3788	71
1183	Computational protein design: the Proteus software and selected applications. <i>Journal of Computational Chemistry</i> , <b>2013</b> , 34, 2472-84	38
1182	Exploring the possible role of Glu286 in CcO by electrostatic energy computations combined with molecular dynamics. <b>2013</b> , 117, 12432-41	29
1181	A new structural technique for examining ion-neutral association in aqueous solution. <b>2013</b> , 160, 161-70; discussion 207-24	2
1180	Protein structural statistics with PSS. <b>2013</b> , 53, 2471-82	10
1179	Charge group partitioning in biomolecular simulation. <b>2013</b> , 20, 188-98	120

# (2013-2013)

1178	Mechanism of transient binding and release of substrate protein during the allosteric cycle of the p97 nanomachine. <b>2013</b> , 135, 14627-36		17
1177	CD44 receptor unfolding enhances binding by freeing basic amino acids to contact carbohydrate ligand. <b>2013</b> , 105, 1217-26		17
1176	Microscopic insights into the NMR relaxation-based protein conformational entropy meter. <b>2013</b> , 135, 15092-100		105
1175	The membrane protein LeuT in micellar systems: aggregation dynamics and detergent binding to the S2 site. <b>2013</b> , 135, 14266-75		29
1174	Molecular recognition of CXCR4 by a dual tropic HIV-1 gp120 V3 loop. <b>2013</b> , 105, 1502-14		39
1173	Conserved Walker A cysteines 431 and 1074 in human P-glycoprotein are accessible to thiol-specific agents in the apo and ADP-vanadate trapped conformations. <b>2013</b> , 52, 7327-38		8
1172	CHARMM-GUI micelle builder for pure/mixed micelle and protein/micelle complex systems. <b>2013</b> , 53, 2171-80		61
1171	Kirkwood-Buff analysis of aqueous N-methylacetamide and acetamide solutions modeled by the CHARMM additive and Drude polarizable force fields. <b>2013</b> , 139, 084509		29
1170	Effects of Nuclear Vibrations on the Energetics of Polythiophene: Quantized Energy Molecular Dynamics. <b>2013</b> , 66, 1021		5
1169	Fisher information metric for the Langevin equation and least informative models of continuous stochastic dynamics. <b>2013</b> , 139, 121931		13
1168	Detection of peptide-binding sites on protein surfaces: the first step toward the modeling and targeting of peptide-mediated interactions. <b>2013</b> , 81, 2096-105		71
1167	Role of conformational properties on the transannular DielsAlder reactivity of macrocyclic trienes with varying linker lengths. <b>2013</b> , 3, 15892		O
1166	Selective inhibition of the unfolded protein response: targeting catalytic sites for Schiff base modification. <b>2013</b> , 9, 2408-16		24
1165	H-loop histidine catalyzes ATP hydrolysis in the E. coli ABC-transporter HlyB. <b>2013</b> , 15, 15811-5		21
1164	Role of protein matrix rigidity and local polarization effects in the monovalent cation selectivity of crystallographic sites in the Na-coupled aspartate transporter Glt(Ph). <b>2013</b> , 15, 2397-404		8
1163	Statistical torsion angle potential energy functions for protein structure modeling: a bicubic interpolation approach. <b>2013</b> , 81, 1156-65		19
1162	Mapping the interactions of selected antibiotics and their Cu2+ complexes with the antigenomic II ribozyme. <b>2013</b> , 280, 2652-64		6
1161	Application of replica exchange umbrella sampling to protein structure refinement of nontemplate models. <i>Journal of Computational Chemistry</i> , <b>2013</b> , 34, 1785-93	3.5	7

1160	In-depth analysis of hyaline fibromatosis syndrome frameshift mutations at the same site reveal the necessity of personalized therapy. <b>2013</b> , 34, 1005-17	13
1159	Monte Carlo simulations of proteins at constant pH with generalized Born solvent, flexible sidechains, and an effective dielectric boundary. <i>Journal of Computational Chemistry</i> , <b>2013</b> , 34, 2742-56 <sup>3-5</sup>	28
1158	A microiterative intrinsic reaction coordinate method for large QM/MM systems. <b>2013</b> , 15, 14188-95	9
1157	Exploiting the capabilities of quantum chemical simulations to characterise the hydration of molecular compounds. <b>2013</b> , 3, 1606-1635	48
1156	Naturally and synthetically linked lys48 diubiquitin: a QM/MM study. <b>2013</b> , 3, 16122	13
1155	Structural and thermodynamic insight into Escherichia coli UvrABC-mediated incision of cluster diacetylaminofluorene adducts on the Narl sequence. <b>2013</b> , 26, 1251-62	11
1154	Stabilization of different types of transition states in a single enzyme active site: QM/MM analysis of enzymes in the alkaline phosphatase superfamily. <b>2013</b> , 135, 10457-69	77
1153	Two Dimensional Window Exchange Umbrella Sampling for Transmembrane Helix Assembly. <b>2013</b> , 9, 13-17	33
1152	Influence of ester-modified lipids on bilayer structure. <b>2013</b> , 29, 14196-203	14
1151	Peptide backbone sampling convergence with the adaptive biasing force algorithm. <b>2013</b> , 117, 518-26	19
1151 1150	Peptide backbone sampling convergence with the adaptive biasing force algorithm. <b>2013</b> , 117, 518-26  The water R1(I)NMRD profiles of a hydrated protein from molecular dynamics simulation. <b>2013</b> , 15, 14089-97	19 4
1150	The water R1(I)NMRD profiles of a hydrated protein from molecular dynamics simulation. 2013,	
1150	The water R1(I)NMRD profiles of a hydrated protein from molecular dynamics simulation. <b>2013</b> , 15, 14089-97	4
1150 1149	The water R1(I)NMRD profiles of a hydrated protein from molecular dynamics simulation. 2013, 15, 14089-97  Hierarchical Multiscale Modeling of Macromolecules and their Assemblies. 2013, 9, 4319-4335	6
1150 1149 1148	The water R1(I)NMRD profiles of a hydrated protein from molecular dynamics simulation. 2013, 15, 14089-97  Hierarchical Multiscale Modeling of Macromolecules and their Assemblies. 2013, 9, 4319-4335  Protein structure optimization with a "Lamarckian" ant colony algorithm. 2013, 10, 1548-52  Glycerol inhibits water permeation through Plasmodium falciparum aquaglyceroporin. 2013, 181, 71-6	4 6 3
1150 1149 1148 1147	The water R1(I)NMRD profiles of a hydrated protein from molecular dynamics simulation. 2013, 15, 14089-97  Hierarchical Multiscale Modeling of Macromolecules and their Assemblies. 2013, 9, 4319-4335  Protein structure optimization with a "Lamarckian" ant colony algorithm. 2013, 10, 1548-52  Glycerol inhibits water permeation through Plasmodium falciparum aquaglyceroporin. 2013, 181, 71-6	4 6 3 9
1150 1149 1148 1147 1146	The water R1(I)NMRD profiles of a hydrated protein from molecular dynamics simulation. 2013, 15, 14089-97  Hierarchical Multiscale Modeling of Macromolecules and their Assemblies. 2013, 9, 4319-4335  Protein structure optimization with a "Lamarckian" ant colony algorithm. 2013, 10, 1548-52  Glycerol inhibits water permeation through Plasmodium falciparum aquaglyceroporin. 2013, 181, 71-6  QM/MM simulations of vibrational spectra of bacteriorhodopsin and channelrhodopsin-2. 2013, 15, 6651-9  CHARMM-GUI Ligand Binder for absolute binding free energy calculations and its application. 2013,	4 6 3 9 21

1142	The backbone dynamics of the amyloid precursor protein transmembrane helix provides a rationale for the sequential cleavage mechanism of Execretase. <b>2013</b> , 135, 1317-29	57
1141	Cardiolipin Models for Molecular Simulations of Bacterial and Mitochondrial Membranes. <b>2013</b> , 9, 670-8	21
1140	Protein Structure Refinement through Structure Selection and Averaging from Molecular Dynamics Ensembles. <b>2013</b> , 9, 1294-1303	75
1139	Biomolecular Simulations. 2013,	17
1138	Dielectric constants of binary mixtures of propylene carbonate with dimethyl carbonate and ethylene carbonate from molecular dynamics simulation: comparison between non-polarizable and polarizable force fields. <b>2013</b> , 111, 277-285	9
1137	ESPResSo++: A modern multiscale simulation package for soft matter systems. <b>2013</b> , 184, 1129-1149	87
1136	Room temperature catalyst-free Knoevenagel condensation: facile access to isatinylidenerhodanines. <b>2013</b> , 54, 1700-1703	7
1135	Binding structures of tri-N-acetyl-I-glucosamine in hen egg white lysozyme using molecular dynamics with a polarizable force field. <i>Journal of Computational Chemistry</i> , <b>2013</b> , 34, 163-74	16
1134	An artificial neural network approach to improving the correlation between protein energetics and the backbone structure. <b>2013</b> , 13, 230-8	4
1133	Influence of pressure on the low-frequency vibrational modes of lysozyme and water: a complementary inelastic neutron scattering and molecular dynamics simulation study. <b>2013</b> , 81, 326-40	26
1132	Structure refinement of protein model decoys requires accurate side-chain placement. <b>2013</b> , 81, 469-78	13
1131	Understanding the basis of a class of paradoxical mutations in AraC through simulations. <b>2013</b> , 81, 490-8	2
1130	OpenMM 4: A Reusable, Extensible, Hardware Independent Library for High Performance Molecular Simulation. <b>2013</b> , 9, 461-469	440
1129	Quasiperiodic oscillation and possible Second Law violation in a nanosystem. <b>2013</b> , 571, 61-65	3
1128	Conformational thermodynamics of metal-ion binding to a protein. <b>2013</b> , 581, 91-95	16
1127	Increased carbonylation of the lipid phosphatase PTEN contributes to Akt2 activation in a murine model of early alcohol-induced steatosis. <b>2013</b> , 65, 680-692	60
1126	Replica exchange molecular dynamics simulations of an $\oplus / \oplus$ type small acid soluble protein (SASP). <b>2013</b> , 184, 17-21	2
1125	Cardiovascular effects of a novel selective Rho kinase inhibitor, 2-(1H-indazole-5-yl)amino-4-methoxy-6-piperazino triazine (DW1865). <b>2013</b> , 702, 218-26	24

1124	Toward the inhibitory effect of acetylsalicylic acid on tyrosinase: Integrating kinetics studies and computational simulations. <b>2013</b> , 48, 260-266	23
1123	Computational and theoretical methods for protein folding. <b>2013</b> , 52, 8601-24	42
1122	Quantum mechanical force field for water with explicit electronic polarization. 2013, 139, 054503	31
1121	Hemoglobin Bohr effects: atomic origin of the histidine residue contributions. <b>2013</b> , 52, 8539-55	21
1120	Protonation of trimethylamine N-oxide (TMAO) is required for stabilization of RNA tertiary structure. <b>2013</b> , 184, 8-16	20
1119	Structural elucidation of transmembrane transporter protein bilitranslocase: conformational analysis of the second transmembrane region TM2 by molecular dynamics and NMR spectroscopy. <b>2013</b> , 1828, 2609-19	6
1118	Evidence of colorectal cancer risk associated variant Lys25Ser in the proximity of human bone morphogenetic protein 2. <b>2013</b> , 522, 75-83	3
1117	The effect of validamycin A on tyrosinase: inhibition kinetics and computational simulation. <b>2013</b> , 55, 15-23	12
1116	The cost of living in the membrane: a case study of hydrophobic mismatch for the multi-segment protein LeuT. <b>2013</b> , 169, 27-38	38
1115	Conformational preferences of plumbagin with phenyl-1-thioglucoside conjugates in solution and bound to MshB determined by aromatic association. <b>2013</b> , 371, 52-60	8
1114	Effects of piperonylic acid on tyrosinase: Mixed-type inhibition kinetics and computational simulations. <b>2013</b> , 48, 1706-1714	23
1113	Coarse grained normal mode analysis vs. refined Gaussian Network Model for protein residue-level structural fluctuations. <b>2013</b> , 75, 124-60	27
1112	Ligand binding site identification by higher dimension molecular dynamics. <b>2013</b> , 53, 674-80	1
1111	Polarizable Interaction Model for Liquid, Supercritical, and Aqueous Ammonia. <b>2013</b> , 9, 2035-51	17
1110	Absolute hydration free energies of blocked amino acids: implications for protein solvation and stability. <b>2013</b> , 104, 453-62	46
1109	Conformational contribution to thermodynamics of binding in protein-peptide complexes through microscopic simulation. <b>2013</b> , 104, 1274-84	24
1108	Direct visualization of single ions in the Stern layer of calcite. <b>2013</b> , 29, 2207-16	133
1107	Molecular modelling and simulations in cancer research. <b>2013</b> , 1836, 1-14	33

# (2013-2013)

1106	Carnosine inhibits AL(42) aggregation by perturbing the H-bond network in and around the central hydrophobic cluster. <b>2013</b> , 14, 583-92	61
1105	Quantum mechanics/molecular mechanics modeling of fatty acid amide hydrolase reactivation distinguishes substrate from irreversible covalent inhibitors. <b>2013</b> , 56, 2500-12	28
1104	pH-selective mutagenesis of protein-protein interfaces: in silico design of therapeutic antibodies with prolonged half-life. <b>2013</b> , 81, 704-14	42
1103	Understanding photosynthetic light-harvesting: a bottom up theoretical approach. <b>2013</b> , 15, 3348-71	124
1102	High-throughput molecular dynamics simulations: toward a dynamic view of macromolecular structure. <b>2013</b> , 3, 364-377	6
1101	OSPREY: protein design with ensembles, flexibility, and provable algorithms. <b>2013</b> , 523, 87-107	94
1100	RNA 3D structure prediction by using a coarse-grained model and experimental data. <b>2013</b> , 117, 3135-44	57
1099	Exploring the mechanism of a regulatory SNP of KLK3 by molecular dynamics simulation. <b>2013</b> , 31, 426-40	3
1098	Protein fibrillation and nanoparticle interactions: opportunities and challenges. 2013, 5, 2570-88	116
1097	GROMACS 4.5: a high-throughput and highly parallel open source molecular simulation toolkit. <b>2013</b> , 29, 845-54	4786
1096	Towards Accurate Prediction of Protonation Equilibrium of Nucleic Acids. 2013, 4, 760-766	26
1095	Six-site polarizable model of water based on the classical Drude oscillator. <b>2013</b> , 138, 034508	92
1094	Silica surface features and their role in the adsorption of biomolecules: computational modeling and experiments. <b>2013</b> , 113, 4216-313	414
1093	PowerBorn: A Barnes-Hut Tree Implementation for Accurate and Efficient Born Radii Computation. <b>2013</b> , 9, 1489-98	8
1092	The simulation approach to lipid-protein interactions. <b>2013</b> , 974, 435-55	3
1091	Membrane interactions and pore formation by the antimicrobial peptide protegrin. <b>2013</b> , 104, 633-42	38
1090	Structure-based network analysis of an evolved G protein-coupled receptor homodimer interface. <b>2013</b> , 22, 745-54	9
1089	Effects of boldine on tyrosinase: Inhibition kinetics and computational simulation. <b>2013</b> , 48, 152-161	17

1088	Direct evidence for hydrogen bonding in glycans: a combined NMR and molecular dynamics study. <b>2013</b> , 117, 4860-9	40
1087	Impact of geometry optimization on base-base stacking interaction energies in the canonical A- and B-forms of DNA. <b>2013</b> , 117, 1560-8	12
1086	Assessing the quality of absolute hydration free energies among CHARMM-compatible ligand parameterization schemes. <i>Journal of Computational Chemistry</i> , <b>2013</b> , 34, 893-903	30
1085	Macrodomain-containing proteins are new mono-ADP-ribosylhydrolases. <b>2013</b> , 20, 502-7	229
1084	The Theory of Ultra-Coarse-Graining. 1. General Principles. <b>2013</b> , 9, 2466-80	114
1083	Investigating the malleability of RNA aptamers. <b>2013</b> , 63, 178-87	11
1082	A general method for constructing atomic-resolution RNA ensembles using NMR residual dipolar couplings: the basis for interhelical motions revealed. <b>2013</b> , 135, 5457-66	70
1081	Methylations of tryptophan-modified naphthoquinone affect its inhibitory potential toward Allaggregation. <b>2013</b> , 117, 1780-9	15
1080	A partition function-based weighting scheme in force field parameter development using ab initio calculation results in global configurational space. <i>Journal of Computational Chemistry</i> , <b>2013</b> , 34, 1271-8 $^{3.5}$	1
1079	Fluorescent photoremovable precursor (acridin-9-ylmethyl)ester: synthesis, photophysical, photochemical and biological applications. <b>2013</b> , 12, 1041-52	9
1078	Restrained-ensemble molecular dynamics simulations based on distance histograms from double electron-electron resonance spectroscopy. <b>2013</b> , 117, 4733-9	56
1077	Molecular dynamics simulation by GROMACS using GUI plugin for PyMOL. <b>2013</b> , 53, 1229-34	46
1076	Evolutionary and mechanistic insights into substrate and product accommodation of CTP:phosphocholine cytidylyltransferase from Plasmodium falciparum. <b>2013</b> , 280, 3132-48	15
1075	Pathways of Amyloid Fibril Formation Using a Simplified Peptide Model. <b>2013</b> , 305-331	
1074	New insights into the folding of a I-sheet miniprotein in a reduced space of collective hydrogen bond variables: application to a hydrodynamic analysis of the folding flow. <b>2013</b> , 117, 6092-105	23
1073	Ligand Binding Pathway Elucidation for Cryptophane Host-Guest Complexes. <b>2013</b> , 9, 2010-9	3
1072	Potential conformational heterogeneity of p53 bound to S100B(III). <b>2013</b> , 425, 999-1010	22
1071	Synthesis, modeling, and pharmacological evaluation of UMB 425, a mixed lagonist/lantagonist opioid analgesic with reduced tolerance liabilities. <b>2013</b> , 4, 1256-66	36

1070	Amphipathic ⊞-helix mimetics based on a 1,2-diphenylacetylene scaffold. <b>2013</b> , 15, 3234-7	36
1069	Self-Learning Adaptive Umbrella Sampling Method for the Determination of Free Energy Landscapes in Multiple Dimensions. <b>2013</b> , 9, 1885-1895	63
1068	Structures, dynamics, and stabilities of fully modified locked nucleic acid (□D-LNA and □-L-LNA) duplexes in comparison to pure DNA and RNA duplexes. <b>2013</b> , 117, 5556-64	21
1067	Intricate structural coordination and domain plasticity regulate activity of serine protease HtrA2. <b>2013</b> , 27, 3054-66	27
1066	Efficiency of Adaptive Temperature-Based Replica Exchange for Sampling Large-Scale Protein Conformational Transitions. <b>2013</b> , 9, 2849-56	24
1065	Temperature dependence and energetics of single ions at the aqueous liquid-vapor interface. <b>2013</b> , 117, 6512-23	22
1064	Simulating DNA by molecular dynamics: aims, methods, and validation. <b>2013</b> , 924, 445-68	8
1063	Classical molecular dynamics in a nutshell. <b>2013</b> , 924, 127-52	9
1062	Partial base flipping is sufficient for strand slippage near DNA duplex termini. <b>2013</b> , 135, 8274-82	11
1061	Computational approach to design small molecule inhibitors and identify SarA as a potential therapeutic candidate. <b>2013</b> , 22, 1856-1865	13
1060	Estimation of ligand efficacies of metabotropic glutamate receptors from conformational forces obtained from molecular dynamics simulations. <b>2013</b> , 53, 1337-49	3
1059	Two-Dimensional Infrared (2DIR) Spectroscopy of the Peptide Beta3s Folding. <b>2013</b> , 4, 1913-1917	4
1058	Conformational determinants of the activity of antiproliferative factor glycopeptide. <b>2013</b> , 53, 1127-37	11
1057	Role of Arg403 for thermostability and catalytic activity of rabbit 12/15-lipoxygenase. <b>2013</b> , 1831, 1079-88	14
1056	Continuous development of schemes for parallel computing of the electrostatics in biological systems: implementation in DelPhi. <i>Journal of Computational Chemistry</i> , <b>2013</b> , 34, 1949-60	21
1055	Structure and thermodynamic insights on acetylaminofluorene-modified deletion DNA duplexes as models for frameshift mutagenesis. <b>2013</b> , 26, 937-51	10
1054	Ligand binding and dynamics of the monomeric epidermal growth factor receptor ectodomain. <b>2013</b> , 81, 1931-43	11
1053	MD and QM/MM study on catalytic mechanism of a FAD-dependent enzyme ORF36: for nitro sugar biosynthesis. <b>2013</b> , 44, 9-16	8

1052	A simple but effective modeling strategy for structural properties of non-heme Fe(II) sites in proteins: test of force field models and application to proteins in the AlkB family. <i>Journal of Computational Chemistry</i> , <b>2013</b> , 34, 1620-35	3.5	9
1051	The effect of Zn(2+) on Pelodiscus sinensis creatine kinase: unfolding and aggregation studies. <b>2013</b> , 31, 572-90		6
1050	Improving the thermostability of methyl parathion hydrolase from Ochrobactrum sp. M231 using a computationally aided method. <b>2013</b> , 97, 2997-3006		27
1049	Of pendulums, polymers, and robots: Computational mechanics with constraints. <b>2013</b> , 81, 537-544		5
1048	Combined approaches for drug design points the way to novel proline racemase inhibitor candidates to fight Chagas' disease. <b>2013</b> , 8, e60955		13
1047	Molecular details of the activation of the Eppioid receptor. <b>2013</b> , 117, 7907-17		24
1046	Sophisticated modeling uncovers atomic DNA structure in bacteriophage 29 cavity. 2013, 104, 1840-1		
1045	Modular aspects of kinesin force generation machinery. <b>2013</b> , 104, 1969-78		29
1044	High-throughput identification of putative receptors for cancer-binding peptides using biopanning and microarray analysis. <b>2013</b> , 5, 342-50		5
1043	A Drude polarizable model for liquid hydrogen sulfide. <b>2013</b> , 117, 5222-9		18
1042	Thioredoxin-mimetic peptides (TXM) reverse auranofin induced apoptosis and restore insulin secretion in insulinoma cells. <b>2013</b> , 85, 977-90		25
1041	Matching of additive and polarizable force fields for multiscale condensed phase simulations. <b>2013</b> , 9, 2826-2837		23
1040	Quantum and classical simulations of orotidine monophosphate decarboxylase: support for a direct decarboxylation mechanism. <b>2013</b> , 52, 4382-90		22
1039	Probing the molecular determinant of the lipase-specific foldase Lif26 for the interaction with its cognate Lip26. <b>2013</b> , 53, 54-61		2
1038	From molecular dynamics to fluorescence anisotropy of fluorophores bound to oriented structures. <b>2013</b> , 232, 482-497		3
1037	Comprehensive experimental and computational analysis of binding energy hot spots at the NF-B essential modulator/IKK protein-protein interface. 2013, 135, 6242-56		40
1036	Spherical monovalent ions at aqueous liquid-vapor interfaces: interfacial stability and induced interface fluctuations. <b>2013</b> , 117, 11732-42		15
1035	Binding site dynamics and aromatic-carbohydrate interactions in processive and non-processive family 7 glycoside hydrolases. <b>2013</b> , 117, 4924-33		48

### (2013-2013)

1034	Glycoside hydrolase processivity is directly related to oligosaccharide binding free energy. <b>2013</b> , 135, 18831-9	71
1033	Acceleration of Semiempirical Quantum Mechanical Calculations by Extended Lagrangian Molecular Dynamics Approach. <b>2013</b> , 9, 3393-403	6
1032	Cooperativity and site selectivity in the ileal lipid binding protein. <b>2013</b> , 52, 4723-33	8
1031	Conformational freedom in tight binding enzymatic transition-state analogues. <b>2013</b> , 117, 9591-7	8
1030	Variational Optimization of an All-Atom Implicit Solvent Force Field to Match Explicit Solvent Simulation Data. <b>2013</b> , 9, 5641-5652	38
1029	Scoring multipole electrostatics in condensed-phase atomistic simulations. <b>2013</b> , 117, 5460-71	18
1028	How does catalase release nitric oxide? A computational structure-activity relationship study. <b>2013</b> , 53, 2951-61	5
1027	A coarse grain model for protein-surface interactions. <b>2013</b> , 139, 095102	34
1026	Molecular Dynamics Simulations Accelerated by GPU for Biological Macromolecules with a Non-Ewald Scheme for Electrostatic Interactions. <b>2013</b> , 9, 5599-609	43
1025	Membrane Packing Problems: A short Review on computational Membrane Modeling Methods and Tools. <b>2013</b> , 5, e201302014	31
1024	In silico-based combinatorial pharmacophore modelling and docking studies of GSK-3□and GK inhibitors of Hippophae. <b>2013</b> , 38, 805-14	18
1023	ATP transport through VDAC and the VDAC-tubulin complex probed by equilibrium and nonequilibrium MD simulations. <b>2013</b> , 52, 9246-56	45
1022	Understanding selectin counter-receptor binding from electrostatic energy computations and experimental binding studies. <b>2013</b> , 117, 16443-54	14
1021	Molecular Dynamics Investigation of Alkali Metal Ions in Liquid and Aqueous Ammonia. <b>2013</b> , 9, 2324-38	23
1020	Automated Optimization of Potential Parameters. 2013, 9, 3311-3320	27
1019	Generating reservoir conformations for replica exchange through the use of the conformational space annealing method. <b>2013</b> , 9, 1115-1124	11
1018	PNP diminishes guanosine glycosidic bond strength through restrictive ring pucker as a precursor to phosphorylation. <b>2013</b> , 117, 6019-26	1
1017	Cation-Interactions as lipid-specific anchors for phosphatidylinositol-specific phospholipase C. <b>2013</b> , 135, 5740-50	41

1016	A Polarizable Force-Field for Cholesterol and Sphingomyelin. <b>2013</b> , 9, 2498-503	19
1015	Conserved water molecules in family 1 glycosidases: a DXMS and molecular dynamics study. <b>2013</b> , 52, 5900-10	29
1014	Targeting protein tyrosine phosphatase SHP2 for the treatment of PTPN11-associated malignancies. <b>2013</b> , 12, 1738-48	33
1013	Effects of protonation state of Asp181 and position of active site water molecules on the conformation of PTP1B. <b>2013</b> , 81, 788-804	5
1012	Drug design for neuropathic pain regulation from traditional Chinese medicine. <b>2013</b> , 3, 844	55
1011	Understanding the -C-X1-X2-C- motif in the active site of the thioredoxin superfamily: E. coli DsbA and its mutants as a model system. <b>2013</b> , 52, 5730-45	6
1010	Structural and diffusion properties of formamide/water mixture interacting with TiO2 surface. <b>2013</b> , 50, 11-6	2
1009	Bending free energy from simulation: correspondence of planar and inverse hexagonal lipid phases. <b>2013</b> , 104, 2202-11	55
1008	NMR-based simulation studies of Pf1 coat protein in explicit membranes. <b>2013</b> , 105, 691-8	18
1007	Novel compstatin family peptides inhibit complement activation by drusen-like deposits in human retinal pigmented epithelial cell cultures. <b>2013</b> , 116, 96-108	23
1006	The Interaction of Sorbitol with Caffeine in Aqueous Solution. <b>2013</b> , 8, 216-222	8
1005	Inclusion of multiple fragment types in the site identification by ligand competitive saturation (SILCS) approach. <b>2013</b> , 53, 3384-98	79
1004	Small molecule antivirulents targeting the iron-regulated heme oxygenase (HemO) of P. aeruginosa. <b>2013</b> , 56, 2097-109	23
1003	Development and pharmacological characterization of conformationally constrained urotensin II-related peptide agonists. <b>2013</b> , 56, 9612-22	12
1002	Volarea - a bioinformatics tool to calculate the surface area and the volume of molecular systems. <b>2013</b> , 82, 743-55	24
1001	Molecular Force Field Development for Aqueous Electrolytes: 1. Incorporating Appropriate Experimental Data and the Inadequacy of Simple Electrolyte Force Fields Based on Lennard-Jones and Point Charge Interactions with Lorentz-Berthelot Rules. <b>2013</b> , 9, 5076-85	41
1001	Experimental Data and the Inadequacy of Simple Electrolyte Force Fields Based on Lennard-Jones and Point Charge Interactions with Lorentz-Berthelot Rules. <b>2013</b> , 9, 5076-85	41

998	P450cin active site water: implications for substrate binding and solvent accessibility. <b>2013</b> , 52, 5039-50	14
997	Self-assembly and bilayer-micelle transition of fatty acids studied by replica-exchange constant pH molecular dynamics. <b>2013</b> , 29, 14823-30	34
996	Epitope fluctuations in the human papillomavirus are under dynamic allosteric control: a computational evaluation of a new vaccine design strategy. <b>2013</b> , 135, 18458-68	16
995	Structural refinement from restrained-ensemble simulations based on EPR/DEER data: application to T4 lysozyme. <b>2013</b> , 117, 4740-54	67
994	Impact of substrate protonation and tautomerization states on interactions with the active site of arginase I. <b>2013</b> , 53, 452-60	7
993	How Does the Environment Affect the Absorption Spectrum of the Fluorescent Protein mKeima?. <b>2013</b> , 9, 1731-42	19
992	pH-dependent dynamics of complex RNA macromolecules. <b>2013</b> , 9, 935-943	47
991	Efficient Computation of Small-Molecule Configurational Binding Entropy and Free Energy Changes by Ensemble Enumeration. <b>2013</b> , 9, 5098-5115	24
990	QM/MM molecular dynamics simulations of the hydration of Mg(II) and Zn(II) ions. 2013, 91, 552-558	29
989	Effects of flanking loops on membrane insertion of transmembrane helices: a role for peptide conformational equilibrium. <b>2013</b> , 117, 8330-9	4
988	Changes in protein architecture and subpicosecond protein dynamics impact the reaction catalyzed by lactate dehydrogenase. <b>2013</b> , 117, 7107-13	34
987	Small pH and salt variations radically alter the thermal stability of metal-binding domains in the copper transporter, Wilson disease protein. <b>2013</b> , 117, 13038-50	14
986	Implicit Solvent Models and Stabilizing Effects of Mutations and Ligands on the Unfolding of the Amyloid IPPeptide Central Helix. <b>2013</b> , 9, 834-46	16
985	Thumb inhibitor binding eliminates functionally important dynamics in the hepatitis C virus RNA polymerase. <b>2013</b> , 81, 40-52	35
984	Conformational analysis of furanoside-containing mono- and oligosaccharides. 2013, 113, 1851-76	95
983	14 Description of excited states in photocatalysis with theoretical methods.	2
982	Contactin 4, -5 and -6 differentially regulate neuritogenesis while they display identical PTPRG binding sites. <b>2013</b> , 2, 324-34	31
981	On the origin of the stereoselective affinity of Nutlin-3 geometrical isomers for the MDM2 protein. <b>2013</b> , 12, 3727-35	14

980	Improved constrained optimization method for reaction-path determination in the generalized hybrid orbital quantum mechanical/molecular mechanical calculations. <b>2013</b> , 138, 044106	8
979	Ultrafast 2DIR probe of a host-guest inclusion complex: structural and dynamical constraints of nanoconfinement. <b>2013</b> , 138, 144501	10
978	Electrostatically accelerated encounter and folding for facile recognition of intrinsically disordered proteins. <b>2013</b> , 9, e1003363	67
977	Automatically mining program build information via signature matching. 2013,	2
976	The effect of Thole functions on the simulation of ionic liquids with point induced dipoles at various densities. <b>2013</b> , 138, 204119	12
975	Chemistry Nobel honors computer simulation of biomolecules. <b>2013</b> , 66, 13-16	2
974	Frequency response of a protein to local conformational perturbations. <b>2013</b> , 9, e1003238	5
973	Effects of ligand binding on the mechanical properties of ankyrin repeat protein gankyrin. <b>2013</b> , 9, e1002864	13
972	Assembly of the transmembrane domain of E. coli PhoQ histidine kinase: implications for signal transduction from molecular simulations. <b>2013</b> , 9, e1002878	34
971	Characterizing changes in the rate of protein-protein dissociation upon interface mutation using hotspot energy and organization. <b>2013</b> , 9, e1003216	24
970	Glycan synthesis, structure, and dynamics: A selection. <b>2013</b> , 85, 1759-1770	10
969	Ebola virus RNA editing depends on the primary editing site sequence and an upstream secondary structure. <b>2013</b> , 9, e1003677	40
968	Structure-Based, Rational Design of T Cell Receptors. <b>2013</b> , 4, 268	42
967	Enhancing human spermine synthase activity by engineered mutations. <b>2013</b> , 9, e1002924	17
966	The molecular mechanism of ion-dependent gating in secondary transporters. 2013, 9, e1003296	44
965	Impact of ribosomal modification on the binding of the antibiotic telithromycin using a combined grand canonical monte carlo/molecular dynamics simulation approach. <b>2013</b> , 9, e1003113	15
964	Turning defense into offense: defensin mimetics as novel antibiotics targeting lipid II. 2013, 9, e1003732	41
963	Combining coarse-grained protein models with replica-exchange all-atom molecular dynamics. <b>2013</b> , 14, 9893-905	20

## (2013-2013)

962	Restricted N-glycan conformational space in the PDB and its implication in glycan structure modeling. <b>2013</b> , 9, e1002946	22
961	A molecular dynamics study of the structural and dynamical properties of putative arsenic substituted lipid bilayers. <b>2013</b> , 14, 7702-15	9
960	Phosphorylation of the retinoic acid receptor alpha induces a mechanical allosteric regulation and changes in internal dynamics. <b>2013</b> , 9, e1003012	21
959	Structure-based function prediction of uncharacterized protein using binding sites comparison. <b>2013</b> , 9, e1003341	27
958	Cysteine scanning mutagenesis of transmembrane helix 3 of a brain glutamate transporter reveals two conformationally sensitive positions. <b>2013</b> , 288, 964-73	9
957	A computational study of barium blockades in the KcsA potassium channel based on multi-ion potential of mean force calculations and free energy perturbation. <b>2013</b> , 142, 451-63	13
956	Crenarchaeal chromatin proteins Cren7 and Sul7 compact DNA by inducing rigid bends. <b>2013</b> , 41, 196-205	31
955	Molecular paleontology: a biochemical model of the ancestral ribosome. <b>2013</b> , 41, 3373-85	41
954	Both genome segments contribute to the pathogenicity of very virulent infectious bursal disease virus. <b>2013</b> , 87, 2767-80	60
953	Structure-based discovery of the novel antiviral properties of naproxen against the nucleoprotein of influenza A virus. <b>2013</b> , 57, 2231-42	92
952	Two-state dynamics of the SH3-SH2 tandem of Abl kinase and the allosteric role of the N-cap. <b>2013</b> , 110, E3372-80	26
951	Calcineurin A versus NS5A-TP2/HD domain containing 2: a case study of site-directed low-frequency random mutagenesis for dissecting target specificity of peptide aptamers. <b>2013</b> , 12, 1939-52	1
950	Unusual sequence effects on nucleotide excision repair of arylamine lesions: DNA bending/distortion as a primary recognition factor. <b>2013</b> , 41, 869-80	38
949	FPGA-Accelerated Molecular Dynamics. <b>2013</b> , 105-135	7
948	Exploring the sequence-structure relationship for amyloid peptides. <b>2013</b> , 450, 275-83	38
947	Molecular modeling of nucleic acid structure: energy and sampling. <b>2013</b> , 54, 7.8.1-7.8.21	2
946	Understanding and Exploiting Protein Interactions as Drug Targets. 2013,	2
945	Modifying the catalytic preference of tributyrin in Bacillus thermocatenulatus lipase through in-silico modeling of enzyme-substrate complex. <b>2013</b> , 26, 325-33	23

944	Loop motions important to product expulsion in the Thermobifida fusca glycoside hydrolase family 6 cellobiohydrolase from structural and computational studies. <b>2013</b> , 288, 33107-17		23
943	Structural constraints on the three-dimensional geometry of simple viruses: case studies of a new predictive tool. <b>2013</b> , 69, 140-50		21
942	Cloud infrastructures for in silico drug discovery: economic and practical aspects. <b>2013</b> , 2013, 138012		18
941	Dietary phytochemicals as potent chemotherapeutic agents against breast cancer: Inhibition of NF-B pathway via molecular interactions in rel homology domain of its precursor protein p105. <b>2013</b> , 9, 51-7		38
940	Half a century of Ramachandran plots. <b>2013</b> , 69, 1333-41		50
939	Cholesterol sensitivity of KIR2.1 depends on functional inter-links between the N and C termini. <b>2013</b> , 7, 303-12		18
938	Molecular insight into conformational transmission of human P-glycoprotein. <b>2013</b> , 139, 225102		18
937	Free energy simulation of helical transitions. <i>Journal of Computational Chemistry</i> , <b>2013</b> , 34, 640-5	3.5	4
936	Further refinements of next-generation force fields [Nonempirical localization of off-centered points in molecules. <b>2013</b> , 91, 804-810		10
935	Asymmetric processing of a substrate protein in sequential allosteric cycles of AAA+ nanomachines. <b>2013</b> , 139, 121921		13
934	Dual effect of crowders on fibrillation kinetics of polypeptide chains revealed by lattice models. <b>2013</b> , 138, 185101		20
933	Cross-talk between the ligand- and DNA-binding domains of estrogen receptor. <b>2013</b> , 81, 1900-9		12
932	High-quality protein backbone reconstruction from alpha carbons using Gaussian mixture models. Journal of Computational Chemistry, <b>2013</b> , 34, 1881-9	3.5	39
931	(Ala)(4)-X-(Ala)4 as a model system for the optimization of the 11 and 12 amino acid side-chain dihedral empirical force field parameters. <i>Journal of Computational Chemistry</i> , <b>2013</b> , 34, 593-603	3.5	4
930	Improved flexible refinement of protein docking in CAPRI rounds 22-27. <b>2013</b> , 81, 2129-36		14
929	Molecular electrostatic potentials by systematic molecular fragmentation. 2013, 139, 184117		12
928	pH-sensitive residues in the p19 RNA silencing suppressor protein from carnation Italian ringspot virus affect siRNA binding stability. <b>2013</b> , 22, 595-604		13
927	Molecular force fields for aqueous electrolytes: SPC/E-compatible charged LJ sphere models and their limitations. <b>2013</b> , 138, 154102		67

## (2013-2013)

926	Comparison of the capillary wave method and pressure tensor route for calculation of interfacial tension in molecular dynamics simulations. <i>Journal of Computational Chemistry</i> , <b>2013</b> , 34, 2707-15	3.5	5	
925	Performance of ZDOCK in CAPRI rounds 20-26. <b>2013</b> , 81, 2175-82		18	
924	Graph representation of protein free energy landscape. <b>2013</b> , 139, 185101		8	
923	Efficient lookup table using a linear function of inverse distance squared. <i>Journal of Computational Chemistry</i> , <b>2013</b> , 34, 2412-20	3.5	20	
922	Energy landscapes and global thermodynamics for alanine peptides. <b>2013</b> , 139, 121909		19	
921	Terahertz time-domain spectroscopy of lysozyme and mouse urinary protein single crystals. 2013,			
920	Rational modification of protein stability by targeting surface sites leads to complicated results. <b>2013</b> , 110, 11337-42		35	
919	Loop-loop interaction in an adenine-sensing riboswitch: a molecular dynamics study. <b>2013</b> , 19, 916-26		39	
918	Structure of the biliverdin cofactor in the Pfr state of bathy and prototypical phytochromes. <b>2013</b> , 288, 16800-16814		48	
917	Transmembrane domain II of the human bile acid transporter SLC10A2 coordinates sodium translocation. <b>2013</b> , 288, 32394-32404		7	
916	Allosteric coupling in the bacterial adhesive protein FimH. 2013, 288, 24128-39		25	
915	Physostigmine and galanthamine bind in the presence of agonist at the canonical and noncanonical subunit interfaces of a nicotinic acetylcholine receptor. <b>2013</b> , 33, 485-94		44	
914	Dynamics of the antigen-binding grooves in CD1 proteins: reversible hydrophobic collapse in the lipid-free state. <b>2013</b> , 288, 19528-36		16	
913	Identification of novel cholesterol-binding regions in Kir2 channels. <b>2013</b> , 288, 31154-64		77	
912	Stabilization of the ADP/metaphosphate intermediate during ATP hydrolysis in pre-power stroke myosin: quantitative anatomy of an enzyme. <b>2013</b> , 288, 35569-80		18	
911	Tight conformational coupling between the domains of the enterotoxigenic Escherichia coli fimbrial adhesin CfaE regulates binding state transition. <b>2013</b> , 288, 9993-10001		7	
910	Computational investigation of the pH dependence of loop flexibility and catalytic function in glycoside hydrolases. <b>2013</b> , 288, 12175-86		27	
909	Quantum mechanical modeling: a tool for the understanding of enzyme reactions. <b>2013</b> , 3, 662-702		20	

908	Single transcriptional and translational preQ1 riboswitches adopt similar pre-folded ensembles that follow distinct folding pathways into the same ligand-bound structure. <b>2013</b> , 41, 10462-75	64
907	Molecular determinants of desensitization in an ENaC/degenerin channel. <b>2013</b> , 27, 5034-45	31
906	SUSCEPTIBILITY OF COMMERCIAL NEURAMINIDASE INHIBITORS AGAINST 2013 A/H7N9 INFLUENZA VIRUS: A DOCKING AND MOLECULAR DYNAMICS STUDY. <b>2013</b> , 12, 1350069	2
905	OPTIMIZATION BIAS IN ENERGY-BASED STRUCTURE PREDICTION. <b>2013</b> , 12,	1
904	Supramolecular organization of functional organic materials in the bulk and at organic/organic interfaces: a modeling and computer simulation approach. <b>2014</b> , 352, 39-101	15
903	Thermal denaturation and renaturation of Eglutamyltranspeptidase of Escherichia coli. 2013, 77, 409-12	6
902	Glycosylated linkers in multimodular lignocellulose-degrading enzymes dynamically bind to cellulose. <b>2013</b> , 110, 14646-51	131
901	RNA pentaloop structures as effective targets of regulators belonging to the RsmA/CsrA protein family. <b>2013</b> , 10, 1031-41	32
900	Divide-and-Conquer Electronic-Structure Study on the Mechanism of the West Nile Virus NS3 Protease Inhibitor. <b>2013</b> , 86, 67-74	4
899	Assessment of homology templates and an anesthetic binding site within the Eminobutyric acid receptor. <b>2013</b> , 119, 1087-95	28
898	Comprehensive and accurate Ab initio energy surface of simple alanine peptides. 2013, 14, 3284-93	8
897	UV-radiation induced disruption of dry-cavities in human <b>D</b> -crystallin results in decreased stability and faster unfolding. <b>2013</b> , 3, 1560	33
896	Improving aqueous solubility and antitumor effects by nanosized gambogic acid-mPEGImicelles. <b>2014</b> , 9, 243-55	28
895	Activation Energy Calculations for Formamide-TiO2 and Formamide-Pt Interactions in the Presence of Water. <b>2013</b> , 7, 33-43	2
894	A Stochastic Solver of the Generalized Born Model. <b>2013</b> , 1, 63-74	6
893	Large domain motions in Ago protein controlled by the guide DNA-strand seed region determine the Ago-DNA-mRNA complex recognition process. <b>2013</b> , 8, e54620	12
892	Mapping enzymatic catalysis using the effective fragment molecular orbital method: towards all ab initio biochemistry. <b>2013</b> , 8, e60602	27
891	Diversity of T cell epitopes in Plasmodium falciparum circumsporozoite protein likely due to protein-protein interactions. <b>2013</b> , 8, e62427	16

890	Activity determinants of helical antimicrobial peptides: a large-scale computational study. <b>2013</b> , 8, e66440	24
889	Adding diverse noncanonical backbones to rosetta: enabling peptidomimetic design. <b>2013</b> , 8, e67051	47
888	Monoubiquitination and activity of the paracaspase MALT1 requires glutamate 549 in the dimerization interface. <b>2013</b> , 8, e72051	21
887	OptZyme: computational enzyme redesign using transition state analogues. <b>2013</b> , 8, e75358	18
886	Discovery of dihydrochalcone as potential lead for Alzheimer's disease: in silico and in vitro study. <b>2013</b> , 8, e79151	26
885	Molecular dynamics simulations reveal the HIV-1 Vpu transmembrane protein to form stable pentamers. <b>2013</b> , 8, e79779	16
884	Identifying cytochrome p450 functional networks and their allosteric regulatory elements. <b>2013</b> , 8, e81980	23
883	Dynamics of Bcl-xL in water and membrane: molecular simulations. <b>2013</b> , 8, e76837	11
882	Overcoming mutation-based resistance to antiandrogens with rational drug design. <b>2013</b> , 2, e00499	289
881	Common force field thermodynamics of cholesterol. <b>2013</b> , 2013, 207287	1
880	DelPhi Web Server: A comprehensive online suite for electrostatic calculations of biological macromolecules and their complexes. <b>2013</b> , 13, 269-284	39
879	Computational approaches for the design of proteinprotein interaction inhibitors. <b>2013</b> , 90-102	3
878	Evaluation of unrestrained replica-exchange simulations using dynamic walkers in temperature space for protein structure refinement. <b>2014</b> , 9, e96638	11
877	Differential effects of CSF-1R D802V and KIT D816V homologous mutations on receptor tertiary structure and allosteric communication. <b>2014</b> , 9, e97519	10
876	Rational modification of estrogen receptor by combination of computational and experimental analysis. <b>2014</b> , 9, e102658	8
875	Deciphering the glycolipid code of Alzheimer's and Parkinson's amyloid proteins allowed the creation of a universal ganglioside-binding peptide. <b>2014</b> , 9, e104751	34
874	Energetic changes caused by antigenic module insertion in a virus-like particle revealed by experiment and molecular dynamics simulations. <b>2014</b> , 9, e107313	6
873	Protein NMR structures refined without NOE data. <b>2014</b> , 9, e108888	2

872	Mg2+ effect on argonaute and RNA duplex by molecular dynamics and bioinformatics implications. <b>2014</b> , 9, e109745	9
871	Rational design of small-molecule stabilizers of spermine synthase dimer by virtual screening and free energy-based approach. <b>2014</b> , 9, e110884	19
870	Atomistic detailed mechanism and weak cation-conducting activity of HIV-1 Vpu revealed by free energy calculations. <b>2014</b> , 9, e112983	7
869	Structure-affinity properties of a high-affinity ligand of FKBP12 studied by molecular simulations of a binding intermediate. <b>2014</b> , 9, e114610	5
868	Effects of water models on binding affinity: evidence from all-atom simulation of binding of tamiflu to A/H5N1 neuraminidase. <b>2014</b> , 2014, 536084	29
867	In silico design for adenosine monophosphate-activated protein kinase agonist from traditional chinese medicine for treatment of metabolic syndromes. <b>2014</b> , 2014, 928589	6
866	In Silico Insight into Potent of Anthocyanin Regulation of FKBP52 to Prevent Alzheimer's Disease. <b>2014</b> , 2014, 450592	5
865	Coupling of remote alternating-access transport mechanisms for protons and substrates in the multidrug efflux pump AcrB. <b>2014</b> , 3,	111
864	Molecular docking studies of anti-cancerous candidates in Hippophae rhamnoides and Hippophae salicifolia. <b>2014</b> , 28, 406-15	22
863	. 2014,	55
86 <sub>3</sub>	. 2014,  Structural insights into the substrate specificity and transglycosylation activity of a fungal glycoside hydrolase family 5 \( \text{D-mannosidase}. \) 2014, 70, 2970-82	55 22
	Structural insights into the substrate specificity and transglycosylation activity of a fungal glycoside	
862	Structural insights into the substrate specificity and transglycosylation activity of a fungal glycoside hydrolase family 5 I-mannosidase. <b>2014</b> , 70, 2970-82  Novel LRRK2 GTP-binding inhibitors reduced degeneration in Parkinson's disease cell and mouse	22
862	Structural insights into the substrate specificity and transglycosylation activity of a fungal glycoside hydrolase family 5 \( \text{I-mannosidase}. \) 2014, 70, 2970-82  Novel LRRK2 GTP-binding inhibitors reduced degeneration in Parkinson's disease cell and mouse models. 2014, 23, 6212-22  Computational antigenic epitope prediction by calculating electrostatic desolvation penalties of	22 57
862 861 860	Structural insights into the substrate specificity and transglycosylation activity of a fungal glycoside hydrolase family 5 IJ mannosidase. 2014, 70, 2970-82  Novel LRRK2 GTP-binding inhibitors reduced degeneration in Parkinson's disease cell and mouse models. 2014, 23, 6212-22  Computational antigenic epitope prediction by calculating electrostatic desolvation penalties of protein surfaces. 2014, 1184, 365-74  Effect of moisture on the traction-separation behavior of cellulose nanocrystal interfaces. 2014,	<ul><li>22</li><li>57</li><li>2</li></ul>
862 861 860 859	Structural insights into the substrate specificity and transglycosylation activity of a fungal glycoside hydrolase family 5 \( \text{I-mannosidase.} \) 2014, 70, 2970-82  Novel LRRK2 GTP-binding inhibitors reduced degeneration in Parkinson's disease cell and mouse models. 2014, 23, 6212-22  Computational antigenic epitope prediction by calculating electrostatic desolvation penalties of protein surfaces. 2014, 1184, 365-74  Effect of moisture on the traction-separation behavior of cellulose nanocrystal interfaces. 2014, 105, 243702  Electrostatics, hydration, and proton transfer dynamics in the membrane domain of respiratory	22 57 2 22
862 861 860 859 858	Structural insights into the substrate specificity and transglycosylation activity of a fungal glycoside hydrolase family 5 II-mannosidase. 2014, 70, 2970-82  Novel LRRK2 GTP-binding inhibitors reduced degeneration in Parkinson's disease cell and mouse models. 2014, 23, 6212-22  Computational antigenic epitope prediction by calculating electrostatic desolvation penalties of protein surfaces. 2014, 1184, 365-74  Effect of moisture on the traction-separation behavior of cellulose nanocrystal interfaces. 2014, 105, 243702  Electrostatics, hydration, and proton transfer dynamics in the membrane domain of respiratory complex I. 2014, 111, 6988-93  The molecular charge distribution, the hydration shell, and the unique properties of liquid water.	22 57 2 22 76

854	Hydrophobic plug functions as a gate in voltage-gated proton channels. <b>2014</b> , 111, E273-82	59
853	Molecular dynamics simulations: from structure function relationships to drug discovery. <b>2014</b> , 2, 4	45
852	Langevin dynamics simulations of charged model phosphatidylinositol lipids in the presence of diffusion barriers: toward an atomic level understanding of corralling of PIP2 by protein fences in biological membranes. <b>2014</b> , 7, 13	6
851	Bacterial peptide deformylase inhibitor PMT analogs inhibit cancer cell growth by interacting with human peptide deformylase. <b>2014</b> , 59, 4274-4282	1
850	The X-ray structure of NccX from Cupriavidus metallidurans 31A illustrates potential dangers of detergent solubilization when generating and interpreting crystal structures of membrane proteins. <b>2014</b> , 289, 31160-72	9
849	Computational modeling of RNA 3D structures, with the aid of experimental restraints. <b>2014</b> , 11, 522-36	33
848	Distinct phenotype of a Wilson disease mutation reveals a novel trafficking determinant in the copper transporter ATP7B. <b>2014</b> , 111, E1364-73	33
847	Conformational dynamics of ligand-dependent alternating access in LeuT. <b>2014</b> , 21, 472-9	102
846	Protein structure modeling with MODELLER. <b>2014</b> , 1137, 1-15	406
845	MOLECULAR DYNAMICS STUDY OF PTX ADSORPTION ONTO N-DOPED GRAPHENE IN VACUUM AND AQUEOUS ENVIRONMENTS. <b>2014</b> , 09, 1450088	4
844	Immune responses of linear and cyclic PLP139-151 mutant peptides in SJL/J mice: peptides in their free state versus mannan conjugation. <b>2014</b> , 6, 709-24	7
843	Web-based computational chemistry education with CHARMMing I: Lessons and tutorial. <b>2014</b> , 10, e1003719	10
842	In silico design of BACE1 inhibitor for Alzheimer's disease by traditional Chinese medicine. <b>2014</b> , 2014, 741703	7
841	A kinetic mechanism for in vivo protein folding. <b>2014</b> , 10,	2
840	MDGRAPE-4: a special-purpose computer system for molecular dynamics simulations. <b>2014</b> , 372,	45
839	Web-based computational chemistry education with CHARMMing II: Coarse-grained protein folding. <b>2014</b> , 10, e1003738	5
838	Structure of the trehalose-6-phosphate phosphatase from Brugia malayi reveals key design principles for anthelmintic drugs. <b>2014</b> , 10, e1004245	29
837	Structural basis of G protein-coupled receptor-Gi protein interaction: formation of the cannabinoid CB2 receptor-Gi protein complex. <b>2014</b> , 289, 20259-72	27

836	Investigation of the novel lead of melanocortin 1 receptor for pigmentary disorders. 2014, 2014, 254678	10
835	Lead screening for CXCR4 of the human HIV infection receptor inhibited by traditional Chinese medicine. <b>2014</b> , 2014, 809816	2
834	Intrinsically Disordered Proteins: Where Computation Meets Experiment. <b>2014</b> , 6, 2684-2719	37
833	Lead Screening for HIV of C-C Chemokine Receptor Type 5 Receptor Inhibited by Traditional Chinese Medicine. <b>2014</b> , 2014, 313094	2
832	Lead screening for HIV-1 integrase (IN) inhibited by traditional Chinese medicine. <b>2014</b> , 2014, 479367	4
831	Treatment of rheumatoid arthritis with traditional chinese medicine. <b>2014</b> , 2014, 528018	18
830	The inhibition of folylpolyglutamate synthetase (folC) in the prevention of drug resistance in Mycobacterium tuberculosis by traditional Chinese medicine. <b>2014</b> , 2014, 635152	2
829	In silico investigation of traditional Chinese medicine compounds to inhibit human histone deacetylase 2 for patients with Alzheimer's disease. <b>2014</b> , 2014, 769867	9
828	Drug design of cyclin-dependent kinase 2 inhibitor for melanoma from traditional Chinese medicine. <b>2014</b> , 2014, 798742	8
827	Investigating the structure and dynamics of the PIK3CA wild-type and H1047R oncogenic mutant. <b>2014</b> , 10, e1003895	45
826	Investigation of estrogen receptor (ESR1) for breast cancer from traditional Chinese medicine. <b>2014</b> , 2014, 321486	5
825	In Silico Investigation of Cytochrome P450 2C9 in relation to Aging Using Traditional Chinese Medicine. <b>2014</b> , 2014, 404505	1
824	An arginine-aspartate network in the active site of bacterial TruB is critical for catalyzing pseudouridine formation. <b>2014</b> , 42, 3857-70	14
823	NbITa new information theory-based analysis of allosteric mechanisms reveals residues that underlie function in the leucine transporter LeuT. <b>2014</b> , 10, e1003603	68
822	Correlated inter-domain motions in adenylate kinase. <b>2014</b> , 10, e1003721	17
821	Web-based computational chemistry education with CHARMMing III: Reduction potentials of electron transfer proteins. <b>2014</b> , 10, e1003739	5
820	An investigation of small GTPases in relation to liver tumorigenesis using traditional Chinese medicine. <b>2014</b> , 2014, 428210	1
819	Efficient in silico exploration of RNA interhelical conformations using Euler angles and WExplore. <b>2014</b> , 42, 12126-37	20

818	Investigation of potent lead for acquired immunodeficiency syndrome from traditional Chinese medicine. <b>2014</b> , 2014, 205890	3
817	Insight into HIV of IFN-induced myxovirus resistance 2 (MX2) expressed by traditional Chinese medicine. <b>2014</b> , 2014, 871576	
816	Enhanced sampling simulations of DNA step parameters. <i>Journal of Computational Chemistry</i> , <b>2014</b> , 35, 2297-304	11
815	p34 is a novel regulator of the oncogenic behavior of NEDD4-1 and PTEN. <b>2014</b> , 21, 146-60	37
814	Novel hypoxanthine guanine phosphoribosyltransferase gene mutations in Saudi Arabian hyperuricemia patients. <b>2014</b> , 2014, 290325	2
813	Functional cross-talk between ras and rho pathways: a Ras-specific GTPase-activating protein (p120RasGAP) competitively inhibits the RhoGAP activity of deleted in liver cancer (DLC) tumor suppressor by masking the catalytic arginine finger. <b>2014</b> , 289, 6839-6849	22
812	Molecular dispersion energy parameters for alkali and halide ions in aqueous solution. <b>2014</b> , 140, 044504	32
811	Applications of quantum mechanical/molecular mechanical methods to the chemical insertion step of DNA and RNA polymerization. <b>2014</b> , 97, 83-113	5
810	Fast and efficient optimization of Molecular Dynamics force fields for microporous materials: Bonded interactions via force matching. <b>2014</b> , 197, 339-347	9
809	Trapping the ATP binding state leads to a detailed understanding of the F1-ATPase mechanism. <b>2014</b> , 111, 17851-6	38
808	Physical mechanism for gating and mechanosensitivity of the human TRAAK K+ channel. <b>2014</b> , 516, 126-30	190
807	Potent anti-angiogenesis and anti-tumor activity of a novel human anti-VEGF antibody, MIL60. <b>2014</b> , 11, 285-93	11
806	Modeling Non-Native Interactions in Designed Proteins. <b>2014</b> , 54, 1230-1240	16
805	Sodium recognition by the Na+/Ca2+ exchanger in the outward-facing conformation. <b>2014</b> , 111, E5354-62	51
804	De novo design of a transmembrane ZnÜ+-transporting four-helix bundle. <b>2014</b> , 346, 1520-4	220
803	The effect of classical and quantum dynamics on vibrational frequency shifts of H2 in clathrate hydrates. <b>2014</b> , 140, 024311	9
802	Electrostatic contribution from solvent in modulating single-walled carbon nanotube association. <b>2014</b> , 141, 114906	2
801	Nanobiosensor for Diclofop Detection Based on Chemically Modified AFM Probes. <b>2014</b> , 14, 1467-1475	17

800	FOHI-D: an iterative Hirshfeld procedure including atomic dipoles. <b>2014</b> , 140, 144104		13
799	Using multiscale preconditioning to accelerate the convergence of iterative molecular calculations. <b>2014</b> , 140, 184114		11
798	Stability of amyloid oligomers. <b>2014</b> , 96, 113-41		17
797	Binding site multiplicity with fatty acid ligands: implications for the regulation of PKR kinase autophosphorylation with palmitate. <b>2014</b> , 82, 2429-42		3
796	X-ray structure of a Hg2+ complex of mercuric reductase (MerA) and quantum mechanical/molecular mechanical study of Hg2+ transfer between the C-terminal and buried catalytic site cysteine pairs. <b>2014</b> , 53, 7211-22		39
795	Spatial Averaging: Sampling Enhancement for Exploring Configurational Space of Atomic Clusters and Biomolecules. <b>2014</b> , 10, 4284-96		1
794	Efficient hybrid non-equilibrium molecular dynamicsMonte Carlo simulations with symmetric momentum reversal. <b>2014</b> , 141, 114107		18
793	Molecular structures and solvation of free monomeric and dimeric ferriheme in aqueous solution: insights from molecular dynamics simulations and extended X-ray absorption fine structure spectroscopy. <b>2014</b> , 53, 10811-24		11
792	An efficient and extensible format, library, and API for binary trajectory data from molecular simulations. <i>Journal of Computational Chemistry</i> , <b>2014</b> , 35, 260-9	3.5	9
791	Rebuilding a macromolecular membrane complex at the atomic scale: case of the Kir6.2 potassium channel coupled to the muscarinic acetylcholine receptor M2. <b>2014</b> , 82, 1694-707		2
790	Bridging between normal mode analysis and elastic network models. <b>2014</b> , 82, 2157-68		28
789	iLOGP: a simple, robust, and efficient description of n-octanol/water partition coefficient for drug design using the GB/SA approach. <b>2014</b> , 54, 3284-301		294
788	Calibrated Langevin-dynamics simulations of intrinsically disordered proteins. 2014, 90, 042709		15
787	Dynamic mesoscale model of dipolar fluids via fluctuating hydrodynamics. <b>2014</b> , 141, 174105		1
786	Identification of 5' AMP-activated kinase as a target of reactive aldehydes during chronic ingestion of high concentrations of ethanol. <b>2014</b> , 289, 15449-62		43
785	Structural insight into the unique binding properties of pyridylethanol(phenylethyl)amine inhibitor in human CYP51. <b>2014</b> , 54, 3384-95		7
7 <sup>8</sup> 4	A review of metabolic and enzymatic engineering strategies for designing and optimizing performance of microbial cell factories. <b>2014</b> , 11, 91-9		42
783	A QM/MM study on the reaction pathway leading to 2-aceto-2-hydroxybutyrate in the catalytic cycle of AHAS. <i>Journal of Computational Chemistry</i> , <b>2014</b> , 35, 488-94	3.5	6

782	Toward on-the-fly quantum mechanical/molecular mechanical (QM/MM) docking: development and benchmark of a scoring function. <b>2014</b> , 54, 3137-52	51
781	Water-induced correlation between single ions imaged at the solid-liquid interface. <b>2014</b> , 5, 4400	125
780	New faster CHARMM molecular dynamics engine. <i>Journal of Computational Chemistry</i> , <b>2014</b> , 35, 406-13 3.5	84
779	Euclidean sections of protein conformation space and their implications in dimensionality reduction. <b>2014</b> , 82, 2585-96	4
778	Enzymatic desymmetrising redox reactions for the asymmetric synthesis of biaryl atropisomers. <b>2014</b> , 20, 13084-8	21
777	Recent advances in transferable coarse-grained modeling of proteins. <b>2014</b> , 96, 143-80	33
776	Investigations of ⊞-helix<->⊡sheet transition pathways in a miniprotein using the finite-temperature string method. <b>2014</b> , 140, 175103	13
775	Exploring binding stability of hydroxy-3-(4-hydroxy-benyl)-5,5a,7,8,9,9a-hexahydrothiazolo[2,3-b] quinazolin-6-one with T790M/L858R EGFR-TKD <b>2022</b> , 1-15	1
774	mPPases create a conserved anionic membrane fingerprint as identified via multi-scale simulations.	
773	Adding hydrogen atoms to molecular models via fragment superimposition 2022, 17, 7	
772	Theoretical Study of Dissociation Process of Plastocyanins by PaCS-MD Simulation. 2022, 2207, 012021	1
771	Stretching of long double-stranded DNA and RNA described by the same model.	
770	Second-Generation JK-206 Targets the Oncogenic Signal Mediator RHOA in Gastric Cancer <b>2022</b> , 14,	0
769	Structural basis of Omicron immune evasion: A comparative computational study of Spike protein-Antibody interaction.	
768	Ligand and Structure-Based In Silico Determination of the Most Promising SARS-CoV-2 nsp16-nsp10 2'Methyltransferase Complex Inhibitors among 3009 FDA Approved Drugs <b>2022</b> , 27,	4
767	Supramolecular Engineering of Alkylated, Fluorinated, and Mixed Amphiphiles 2022, e2100914	1
766	Biological Membrane-Penetrating Peptides: Computational Prediction and Applications <b>2022</b> , 12, 838259	1
765	PharmRF: A machine-learning scoring function to identify the best protein-ligand complexes for structure-based pharmacophore screening with high enrichments <i>Journal of Computational</i> 3.5 <i>Chemistry</i> , <b>2022</b> ,	

764	A simple geometrical model of the electrostatic environment around the catalytic center of the ribosome.	
763	From Data to Knowledge: Systematic Review of Tools for Automatic Analysis of Molecular Dynamics Output <b>2022</b> , 13, 844293	
762	Origin of thiocyanate spectral shifts in water and organic solvents <b>2022</b> , 156, 104106	2
761	The assessment of boron nitride nanotubes and functionalized carbon nanotubes as containers for anticancer drug delivery of dacarbazine and effect of urea on adsorption process by molecular dynamics. 1	О
760	Site-selective dynamics of ligand-free and ligand-bound azidolysozyme 2022, 156, 105105	
759	CD33 rs2455069 SNP: Correlation with Alzheimer's Disease and Hypothesis of Functional Role <b>2022</b> , 23,	О
758	Classical and Machine Learning Methods for Protein - Ligand Binding Free Energy Estimation 2022,	
757	Regulation of GTPase function by autophosphorylation <b>2022</b> , 82, 950-968.e14	2
756	Modeling the Membrane Binding Mechanism of a Lipid Transport Protein Osh4 to Single Membranes <b>2022</b> ,	O
755	Zafirlukast inhibits the growth of lung adenocarcinoma via inhibiting TMEM16A channel activity <b>2022</b> , 101731	o
754	The permeation of potassium ions through the lipid scrambling path of the membrane protein nhTMEM16.	
753	Versatile Encapsulation and Synthesis of Potent Liposomes by Thermal Equilibration <b>2022</b> , 12,	o
75 <sup>2</sup>	Molecular Modeling is an Enabling Approach to Complement and Enhance Channelopathy Research <b>2022</b> , 12, 3141-3166	
751	Isolation and In Silico SARS-CoV-2 Main Protease Inhibition Potential of Jusan Coumarin, a New Dicoumarin from <b>2022</b> , 27,	2
750	Aberrant hippocampal transmission and behavior in mice with a stargazin mutation linked to intellectual disability <b>2022</b> ,	
749	Jusanin, a New Flavonoid from with an In Silico Inhibitory Potential against the SARS-CoV-2 Main Protease <b>2022</b> , 27,	3
748	A molecular switch controls the impact of cholesterol on a Kir channel 2022, 119, e2109431119	3
747	Unraveling the Origins of Changing Product Specificity Properties of Arginine Methyltransferase PRMT7 by the E181D and E181D/Q329A Mutations through QM/MM MD and Free-Energy Simulations <b>2022</b> ,	

746	DLPGEN: Preparing Molecular Dynamics Simulations with Support for Polarizable Force Fields <b>2022</b> ,	1
745	Coarse-Grained Molecular Dynamics Simulations of Paclitaxel-Loaded Polymeric Micelles <b>2022</b> ,	Ο
744	Addressing Intersite Coupling Unlocks Large Combinatorial Chemical Spaces for Alchemical Free Energy Methods <b>2022</b> ,	2
743	Variational formulation of the bond capacity charge polarization model <b>2022</b> , 156, 104101	
742	Computational design of a 🛘 wrapin's N-terminal domain with canonical and non-canonical amino acid modifications mimicking curcumin's proposed inhibitory function <b>2022</b> , 286, 106805	0
741	Optimizing Multisite EDynamics Throughput with Charge Renormalization <b>2022</b> , 62, 1479-1488	1
740	Excitatory and inhibitory D-serine binding to the NMDA receptor.	
739	Inhibition of calcium-triggered secretion by hydrocarbon-stapled peptides <b>2022</b> , 603, 949-956	3
738	Multi-Phase In Silico Discovery of Potential SARS-CoV-2 RNA-Dependent RNA Polymerase Inhibitors among 3009 Clinical and FDA-Approved Related Drugs. <b>2022</b> , 10, 530	3
737	Alchemical Free Energy Methods Applied to Complexes of the First Bromodomain of BRD4 2022,	2
736	Pfprex from Plasmodium falciparum can bypass oxidative stress-induced DNA lesions 2022,	1
735	AutoSolvate: A toolkit for automating quantum chemistry design and discovery of solvated molecules <b>2022</b> , 156, 124801	3
734	Computational vaccinology guided design of multi-epitope subunit vaccine against a neglected arbovirus of the Americas <b>2022</b> , 1-18	1
733	Calcium-induced environmental adaptability of the blood protein vitronectin.	
732	Synergistic effect of compounds directed to triosephosphate isomerase, a combination to develop drug against trichomoniasis <b>2022</b> , e2200046	
731	Computational Modeling of T Cell Hypersensitivity during Coronavirus Infections Leading to Autoimmunity and Lethality <b>2022</b> , 2022, 9444502	O
730	Exploring the effect of mechanical anisotropy of protein structures in the unfoldase mechanism of AAA+ molecular machines.	0
729	Enhancement of Methane Catalysis Rates in OB3b <b>2022</b> , 12,	1

 $\,$  Kinetic and Redox Characterization of KRAS G12C Inhibition.

727	Multivalent DNA and nucleosome acidic patch interactions specify VRK1 mitotic localization and activity <b>2022</b> ,	O
726	Concentration Dependence of Dynamics and Hydrogen Bonding in Aqueous Solutions of Urea, Methyl-substituted Ureas, and Trimethylamine N-Oxide. <b>2022</b> , 119120	
725	Influence of oil-phase alkane additives on the evaporation rate of double emulsion curing process. <b>2022</b> , 253, 117561	
724	Secondary structure of peptides mimicking the Gly-rich regions of major ampullate spidroin protein 1 and 2 <b>2022</b> , 284, 106783	
723	New N-aryl-N'-aryl-/(thio)ureido-/sulfamoylamino-derivatives of alkyl/alkylcarbamoyl piperazines: Effect of structural modifications on selectivity over 5-HT receptor <b>2022</b> , 235, 114319	1
722	Intrinsically Disordered N-terminal Domain (NTD) of p53 Interacts with Mitochondrial PTP Regulator Cyclophilin D <b>2022</b> , 434, 167552	1
721	Design, synthesis, evaluation of new 3-acetylisoxazolines and their hybrid analogous as anticancer agents: In vitro and in silico analysis <b>2022</b> , 98, 107666	3
720	Correlated dipolar and dihedral fluctuations in a protein. <b>2022</b> , 797, 139574	1
719	Conserved hydrogen-bond motifs of membrane transporters and receptors <b>2022</b> , 1864, 183896	O
718	Development of immunoassay based on rational hapten design for sensitive detection of pendimethalin in environment <b>2022</b> , 830, 154690	1
717	Implementations of replica-permutation and replica sub-permutation methods into LAMMPS. <b>2022</b> , 276, 108362	O
716	Molecular Simulation of Stapled Peptides <b>2022</b> , 2405, 283-301	
715	Revealing the Mechanism of Isethionate Sulfite-Lyase by QM/MM Calculations. <b>2021</b> ,	O
714	Atomistic Model of Solute Transport across the Blood-Brain Barrier <b>2022</b> , 7, 1100-1112	1
713	CHARMM-GUI Nanomaterial Modeler for Modeling and Simulation of Nanomaterial Systems. <b>2021</b> ,	7
712	Exploring the pH- and Ligand-Dependent Flap Dynamics of Malarial Plasmepsin II 2021,	2
711	Design, synthesis, and biological evaluation of new thieno[2,3-] pyrimidine derivatives as targeted therapy for PI3K with molecular modelling study <b>2022</b> , 37, 315-332	1

710	Connexons Coupling to Gap Junction Channel: Potential Role for Extracellular Protein Stabilization Centers <b>2021</b> , 12,		2
709	Phase Transition toward a Thermodynamically Less Stable Phase: Cross-Nucleation due to Thin Film Growth of a Benzothieno-benzothiophene Derivative <b>2021</b> , 125, 28039-28047		2
708	Modeling the Structure-Activity Relationship of Arbidol Derivatives and Other SARS-CoV-2 Fusion Inhibitors Targeting the S2 Segment of the Spike Protein <b>2021</b> , 61, 5906-5922		О
707	Binding Energy and Free Energy of Calcium Ion to Calmodulin EF-Hands with the Drude Polarizable Force Field. <b>2022</b> , 2, 143-155		1
706	pH-dependent behavior of ionizable cationic lipids in mRNA-carrying lipoplexes investigated by molecular dynamics simulations. <b>2021</b> , e2100683		1
705	A Benchmark Study of Quantum Mechanics and Quantum Mechanics-Molecular Mechanics Methods for Carbocation Chemistry <b>2021</b> ,		2
704	Polyphenols as Potential Inhibitors of SARS-CoV-2 RNA Dependent RNA Polymerase (RdRp) <b>2021</b> , 26,		2
703	Ion Permeation, Selectivity, and Electronic Polarization in Fluoride Channels.		
702	CHARMM-GUI Drude prepper for molecular dynamics simulation using the classical Drude polarizable force field. <i>Journal of Computational Chemistry</i> , <b>2021</b> ,	3.5	4
701	Aray□ ☑ Mutasyonlar̃ñn Protein Etkile□ ímlerine Tesirini Tahmin Eden Algoritmalarla HADDOCKŪn Performans̃ñnn Kar□ ∄la□ ੴr̃lmas̃.		
700	A Computational Approach to Investigate TDP-43 RNA-Recognition Motif 2 C-Terminal Fragments Aggregation in Amyotrophic Lateral Sclerosis <b>2021</b> , 11,		0
699	Reversion mutations in phosphoprotein P of a codon-pair-deoptimized human respiratory syncytial virus confer increased transcription, immunogenicity, and genetic stability without loss of attenuation <b>2021</b> , 17, e1010191		Ο
698	In Silico-Based Experiments on Mechanistic Interactions between Several Intestinal Permeation Enhancers with a Lipid Bilayer Model <b>2022</b> , 19, 124-137		2
697	N-glycosylation modulates enzymatic activity of Trypanosoma congolense trans-sialidase.		1
696	Retinal Vibrations in Bacteriorhodopsin are Mechanically Harmonic but Electrically Anharmonic: Evidence From Overtone and Combination Bands <b>2021</b> , 8, 749261		Ο
695	Deuterium Isotope Effects on Acid-Base Equilibrium of Organic Compounds <b>2021</b> , 26,		
694	Towards Computationally Guided Design and Engineering of a Neisseria meningitidis Serogroup W Capsule Polymerase with Altered Substrate Specificity. <b>2021</b> , 9, 2192		
693	Protein p Prediction with Machine Learning <b>2021</b> , 6, 34823-34831		1

692	All-Atom Modeling of Complex Cellular Membranes 2021,	2
691	Site-Specific Stabilization and Destabilization of ${\mathbb B}$ Helical Peptides upon Phosphorylation and O-GlcNAcylation. <b>2021</b> ,	O
690	Pyranose Ring Puckering Thermodynamics for Glycan Monosaccharides Associated with Vertebrate Proteins <b>2021</b> , 23,	2
689	Recent Developments in Data-Assisted Modeling of Flexible Proteins <b>2021</b> , 8, 765562	1
688	Altering the Double-Stranded DNA Specificity of the bZIP Domain of Zta with Site-Directed Mutagenesis at N182 <b>2022</b> , 7, 129-139	
687	Deep Mutational Engineering of broadly-neutralizing and picomolar affinity nanobodies to accommodate SARS-CoV-1 & amp; 2 antigenic polymorphism.	
686	Engineered Tryptophan Synthase Balances Equilibrium Effects and Fast Dynamic Effects. <b>2022</b> , 12, 913-922	O
685	Leaflet Asymmetry Modeling in the Lipid Composition of Cytoplasmic Membranes 2021,	O
684	Electronic polarization effects on membrane translocation of anti-cancer drugs 2022,	O
683	Some Applications of Electromagnetic Theory. <b>2022</b> , 283-317	
68 <sub>3</sub>	Some Applications of Electromagnetic Theory. 2022, 283-317  Production of Eketoadipic acid from glucose in Pseudomonas putida KT2440 for use in performance-advantaged nylons. 2022, 3, 100840	1
	Production of 🛮 ketoadipic acid from glucose in Pseudomonas putida KT2440 for use in	3
682	Production of ⊡ketoadipic acid from glucose in Pseudomonas putida KT2440 for use in performance-advantaged nylons. <b>2022</b> , 3, 100840	
682	Production of Eketoadipic acid from glucose in Pseudomonas putida KT2440 for use in performance-advantaged nylons. <b>2022</b> , 3, 100840  Machine Learning Approaches and their Applications in Drug Discovery and Design <b>2022</b> ,	
682 681 680	Production of Eketoadipic acid from glucose in Pseudomonas putida KT2440 for use in performance-advantaged nylons. 2022, 3, 100840  Machine Learning Approaches and their Applications in Drug Discovery and Design 2022,  Two physics-based models for pH-dependent calculations of protein solubility 2022, 31, e4299  Novel Imidazole Phenoxyacetic Acids as Inhibitors of USP30 for Neuroprotection Implication via the Ubiquitin-Rho-110 Fluorometric Assay: Design, Synthesis, and In Silico and Biochemical Assays	3
682 681 680	Production of Eketoadipic acid from glucose in Pseudomonas putida KT2440 for use in performance-advantaged nylons. 2022, 3, 100840  Machine Learning Approaches and their Applications in Drug Discovery and Design 2022,  Two physics-based models for pH-dependent calculations of protein solubility 2022, 31, e4299  Novel Imidazole Phenoxyacetic Acids as Inhibitors of USP30 for Neuroprotection Implication via the Ubiquitin-Rho-110 Fluorometric Assay: Design, Synthesis, and In Silico and Biochemical Assays 2022,  Current Trends in Computational Quantum Chemistry Studies on Antioxidant Radical Scavenging	1
682 681 680 679	Production of Eketoadipic acid from glucose in Pseudomonas putida KT2440 for use in performance-advantaged nylons. 2022, 3, 100840  Machine Learning Approaches and their Applications in Drug Discovery and Design 2022,  Two physics-based models for pH-dependent calculations of protein solubility 2022, 31, e4299  Novel Imidazole Phenoxyacetic Acids as Inhibitors of USP30 for Neuroprotection Implication via the Ubiquitin-Rho-110 Fluorometric Assay: Design, Synthesis, and In Silico and Biochemical Assays 2022,  Current Trends in Computational Quantum Chemistry Studies on Antioxidant Radical Scavenging Activity 2022,	1

## (2018-2022)

674	Structural dynamics shape the fitness window of alanine:glyoxylate aminotransferase 2022, 31, e4303	Ο
673	Optimizing the Calculation of Free Energy Differences in Nonequilibrium Work SQM/MM Switching Simulations <b>2022</b> ,	1
672	Lead generation of cysteine based mesenchymal epithelial transition (c-Met) kinase inhibitors: Using structure-based scaffold hopping, 3D-QSAR pharmacophore modeling, virtual screening, molecular docking, and molecular dynamics simulation <b>2022</b> , 146, 105526	1
671	Molecular insights into the differential dynamics of SARS-CoV-2 variants of concern <b>2022</b> , 114, 108194	2
670	Chapter 11. Application of Molecular Modelling to Speed-up the Lead Discovery Process. 281-316	
669	Data_Sheet_1.docx. <b>2019</b> ,	
668	Data_Sheet_2.docx. <b>2019</b> ,	
667	Data_Sheet_1.pdf. <b>2020</b> ,	
666	lmage_1.TIF. <b>2019</b> ,	
665	Table_1.DOCX. <b>2019</b> ,	
664	Data_Sheet_1.pdf. <b>2019</b> ,	
663	Video_1.MP4. <b>2019</b> ,	
662	Video_2.MP4. <b>2019</b> ,	
661	Video_3.MPG. <b>2019</b> ,	
660	Video_4.MPG. <b>2019</b> ,	
659	Video_5.MPG. <b>2019</b> ,	
658	Data_Sheet_1.zip. <b>2018</b> ,	
657	Data_Sheet_2.zip. <b>2018,</b>	



## (2019-2018)



620	Table_2.docx. <b>2019</b> ,	
619	Table_3.docx. <b>2019</b> ,	
618	Table_4.docx. <b>2019</b> ,	
617	Table_5.xlsx. <b>2019</b> ,	
616	Table_6.docx. <b>2019</b> ,	
615	Table_7.docx. <b>2019</b> ,	
614	TUP DElectric field analyses for molecular simulations Journal of Computational Chemistry, 2022, 3.5	1
613	Computational Analysis on the Allostery of Tryptophan Synthase: Relationship between 日/日Ligand Binding and Distal Domain Closure <b>2022</b> ,	1
612	Binding of polar and hydrophobic molecules at the LiCoO (001)-water interface: force field development and molecular dynamics simulations <b>2022</b> ,	
611	Structure of the Shaker Kv channel and mechanism of slow C-type inactivation <b>2022</b> , 8, eabm7814	7
610	Allostery in the dynamic coactivator domain KIX occurs through minor conformational micro-states <b>2022</b> , 18, e1009977	
609	Antibiotic heliomycin and its water-soluble 4-aminomethylated derivative provoke cell death in T24 bladder cancer cells by targeting sirtuin 1 (SIRT1) <b>2022</b> , 12, 1042-1055	
608	OUP accepted manuscript.	
607	Identification of the probable structure of the sAPP <code>H-GABAR1a</code> complex and theoretical solutions for such cases <b>2022</b> ,	2
606	Extracting the Dynamic Motion of Proteins Using Normal Mode Analysis 2022, 2449, 213-231	
605	Principles of cholesterol regulation of ion channels. <b>2022</b> , 169-204	
604	Recent Advances in Application of Computer-Aided Drug Design in Anti-Influenza A Virus Drug Discovery <b>2022</b> , 23,	1
603	Drugsniffer: An Open Source Workflow for Virtually Screening Billions of Molecules for Binding Affinity to Protein Targets <b>2022</b> , 13, 874746	Ο

602	Alchemical free energy simulations without speed limits. A generic framework to calculate free energy differences independent of the underlying molecular dynamics program <i>Journal of Computational Chemistry</i> , <b>2022</b> ,	3.5	0
601	Design and Development of Novel Nutraceuticals: Current Trends and Methodologies. <b>2022</b> , 2, 71-90		1
600	Modulation of Human Transthyretin Stability by the Mutations at Histidine 88 Studied by Free Energy Simulation <b>2022</b> ,		O
599	Allosteric coupling between transmembrane segment 4 and the selectivity filter of TALK1 potassium channels regulates their gating by extracellular pH <b>2022</b> , 101998		O
598	Comparison of approximate intermolecular potentials for ab initio fragment calculations on medium sized N-heterocycles <i>Journal of Computational Chemistry</i> , <b>2022</b> ,	3.5	1
597	All-Atom Molecular Dynamics Simulations of Polyethylene Glycol (PEG) and LIMP-2 Reveal That PEG Penetrates Deep into the Proposed CD36 Cholesterol-Transport Tunnel <b>2022</b> , 7, 15728-15738		O
596	1-Hydroxy-2(1)-pyridinone-Based Chelators with Potential Catechol -Methyl Transferase Inhibition and Neurorescue Dual Action against Parkinson's Disease <b>2022</b> , 27,		
595	TULP3 NLS inhibition: an study to hamper cargo transport to nucleus <b>2022</b> , 1-9		
594	Methionine-Based Radicals: Time Scales and Species.		
593	Comprehensive Folding Variations for Protein Folding 2022,		О
592	How Does Temperature Affect the Dynamics of SARS-CoV-2 M Proteins? Insights from Molecular Dynamics Simulations <b>2022</b> , 1		1
591	Data mining and structural analysis for multi-tissue regeneration potential of BMP-4 and activator drugs <b>2022</b> , 1-16		
590	The mechanism of activation of MEK1 by B-Raf and KSR1 <b>2022</b> , 79, 281		1
589	The influence of copper substrate temperature on the wettability of graphene coating. 1-13		O
588	Ion Correlation in Choline Chloride-Urea Deep Eutectic Solvent (Reline) from Polarizable Molecular Dynamics Simulations <b>2022</b> ,		1
587	Insights into the behavior of unsaturated diacylglycerols in mixed lipid bilayers in relation to protein kinase C activation-A molecular dynamics simulation study <b>2022</b> , 183961		4
586	3,4,5-Trimethoxybenzoate of Catechin, an Anticarcinogenic Semisynthetic Catechin, Modulates the Physical Properties of Anionic Phospholipid Membranes <b>2022</b> , 27,		О
585	Stretching of Long Double-Stranded DNA and RNA Described by the Same Approach 2022,		O

584	Toward the Discovery of a Novel Class of Leads for High Altitude Disorders by Virtual Screening and Molecular Dynamics Approaches Targeting Carbonic Anhydrase <b>2022</b> , 23,	2
583	: A Program for Electrostatic Parameterizations of Additive and Induced Dipole Polarizable Force Fields <b>2022</b> ,	1
582	Origin of metabolites diversity and selectivity of P450 catalyzed benzo[a]pyrene metabolic activation <b>2022</b> , 435, 129008	O
581	Antimalarial potential of naphthalene-sulfonic acid derivatives: Molecular electronic properties, vibrational assignments, and in-silico molecular docking studies. <b>2022</b> , 133298	17
580	Interaction of Arginine-Rich Cell-Penetrating Peptides with an Artificial Neuronal Membrane. <b>2022</b> , 11, 1638	O
579	Computational studies evidenced the potential of steroidal lactone to disrupt surface interaction of SARS-CoV-2 spike protein and hACE2. <b>2022</b> , 105598	
578	Geometrically Induced Selectivity and Unidirectional Electroosmosis in Uncharged Nanopores <b>2022</b> ,	2
577	Structure-based design of ligands of the m6A-RNA reader YTHDC1. <b>2022</b> , 100057	O
576	Discovery of new nicotinamides as apoptotic VEGFR-2 inhibitors: virtual screening, synthesis, anti-proliferative, immunomodulatory, ADMET, toxicity, and molecular dynamic simulation studies <b>2022</b> , 37, 1389-1403	2
575	In silico exploration of disulfide derivatives of Ferula foetida oleo-gum (Covexir <sup>[]</sup> ) as promising therapeutics against SARS-CoV-2. <b>2022</b> , 105566	
574	Plasticity in structure and assembly of SARS-CoV-2 nucleocapsid protein.	3
573	Deep mutational engineering of broadly-neutralizing nanobodies accommodating SARS-CoV-1 and 2 antigenic drift <b>2022</b> , 14, 2076775	1
572	Bomidin: An Optimized Antimicrobial Peptide With Broad Antiviral Activity Against Enveloped Viruses. <b>2022</b> , 13,	O
571	Design principles of PI(4,5)P 2 clustering under protein-free conditions: Specific cation effects and calcium-potassium synergy. <b>2022</b> , 119,	1
570	Epithelial Sodium Channel Inhibition by Amiloride Addressed with THz Spectroscopy and Molecular Modeling. <b>2022</b> , 27, 3271	O
569	Virtual Quasi-2D Intermediates as Building Blocks for Plausible Structural Models of Amyloid Fibrils from Proteins with Complex Topologies: A Case Study of Insulin.	O
568	py-MCMD: Python Software for Performing Hybrid Monte Carlo/Molecular Dynamics Simulations with GOMC and NAMD.	3
567	Differential ion dehydration energetics explains selectivity in the non-canonical lysosomal K+channel TMEM175. 11,	2

566	Obtaining QM/MM binding free energies in the SAMPL8 drugs of abuse challenge: indirect approaches.	1
565	Molecular dynamic simulation and experimental data on graphene wettability on heated structured surfaces. 1-18	1
564	Self-derived peptides from the SARS-CoV-2 spike glycoprotein disrupting shaping and stability of the homotrimer unit. <b>2022</b> , 151, 113190	
563	Effect of mutations on the hydrophobic interactions of the hierarchical molecular structure and mechanical properties of epithelial keratin 1/10. <b>2022</b> , 212, 442-450	O
562	Exploring the Effect of Mechanical Anisotropy of Protein Structures in the Unfoldase Mechanism of AAA+ Molecular Machines. <b>2022</b> , 12, 1849	3
561	Identification of novel natural inhibitors targeting AKT Serine/Threonine Kinase 1 (AKT1) by computational study. <b>2022</b> , 13, 12003-12020	1
560	Mechanistic Insights into Enzyme Catalysis from Explaining Machine-Learned Quantum Mechanical and Molecular Mechanical Minimum Energy Pathways.	Ο
559	Finite element modeling of $\square$ -helices and tropocollagen molecules referring to spike of SARS-CoV-2. <b>2022</b> ,	Ο
558	A brief introduction to contemporary electrokinetics. 1-13	
557	The structural basis of BCR-ABL recruitment of GRB2 in chronic myelogenous leukemia. 2022,	O
556	Proton coupling and the multiscale kinetic mechanism of a peptide transporter. 2022,	2
555	Structural and biophysical properties of farnesylated KRas interacting with the chaperone SmgGDS-558. <b>2022</b> ,	Ο
554	Omega-3 fatty acid epoxides produced by PAF-AH2 in mast cells regulate pulmonary vascular remodeling. <b>2022</b> , 13,	3
553	Edge Weights in a Protein Elastic Network Reorganize Collective Motions and Render Long-Range Sensitivity Responses.	O
552	GPU-Accelerated All-atom Particle-Mesh Ewald Continuous Constant pH Molecular Dynamics in Amber.	0
551	Combined in Silico Prediction Methods, Molecular Dynamic Simulation, and Molecular Docking of FOXG1 Missense Mutations: Effect on FoxG1 Structure and Its Interactions with DNA and Bmi-1 Protein.	Ο
550	Selective and antagonist-dependent Eppioid receptor activation by the combination of 2-{[2-(6-chloro-3,4-dihydro-1(2H)-quinolinyl)-2-oxoethyl]sulfanyl}-5-phenyl-4,6-(1H,5H)-pyrimidinedione and naloxone/naltrexone. <b>2022</b> , 105905	
549	Bacterial H-NS contacts DNA at the same irregularly spaced sites in both bridged and hemi-sequestered linear filaments. <b>2022</b> , 25, 104429	O

548	Molecular engineering and activity improvement of acetylcholinesterase inhibitors: Insights from 3D-QSAR, docking, and molecular dynamics simulation studies. <b>2022</b> , 108239	1
547	Multi-level analysis of intrinsically disordered protein docking methods. <b>2022</b> , 204, 55-63	O
546	Robust, Efficient and Automated Methods for Accurate Prediction of Protein-Ligand Binding Affinities in AMBER Drug Discovery Boost. 161-204	1
545	Glucosylation mechanism of resveratrol through the mutant Q345F sucrose phosphorylase from the organism Bifidobacterium adolescentis: a computational study.	0
544	Collectivity in ionic liquids: A temperature-dependent, polarizable molecular dynamics study	0
543	Design of peptide-based coronavirus inhibitors that target disruption of 3CLpro protease self-association.	
542	Catalyst-Free Direct Regiospecific Multicomponent Synthesis of C3-Functionalized Pyrroles.	1
541	Polarizable molecular dynamics simulations on the conductivity of pure 1-methylimidazolium acetate systems.	O
540	Engineering of a kinetically driven phase of phenoxazine by surface crystallisation.	2
539	SFLADock: A Memetic Protein-Protein Docking Algorithm. <b>2022</b> ,	
538	New Insights into the Determinants of Specificity in Human Type I Arginase: Generation of a Mutant That Is Only Active with Agmatine as Substrate. <b>2022</b> , 23, 6438	0
537	Structural mechanism of leaflet-specific phospholipid modulation of a pentameric ligand-gated ion channel.	
536	Replica-Exchange Enveloping Distribution Sampling Using Generalized AMBER Force-Field Topologies: Application to Relative Hydration Free-Energy Calculations for Large Sets of Molecules.	1
535	Recent advances in RNA structurome.	1
534	Development and characterization of chlorophyll-amended montmorillonite clays for the adsorption and detoxification of benzene. <b>2022</b> , 118788	1
533	Protein structural bioinformatics: An overview. <b>2022</b> , 105695	O
532	Protein Nucleic Acid Interactions for RNA Polymerase II Elongation Factors by Molecular Dynamics Simulations.	2
531	Effective natural inhibitors targeting IGF-1R by computational study. <b>2022</b> , 14, 4874-4887	

Binding of DEP domain to phospholipid membranes: More than just electrostatics. 2022, 183983 530 Keap1-resistant Ŋ-Nrf2 isoform does not translocate to the nucleus upon electrophilic stress. 529 Rational exploration of fold atlas for human solute carrier proteins. 2022, 528 1 Graph-Learning Guided Mechanistic Insights into Imipenem Hydrolysis in GES Carbapenemases. 527 In silico study to identify novel potential thiadiazole-based molecules as anti-Covid-19 candidates 526 3 by hierarchical virtual screening and molecular dynamics simulations. Molecular Dynamics Simulations Establish the Molecular Basis for the Broad Allostery Hotspot 4 Distributions in the Tetracycline Repressor. 2022, 144, 10870-10887 Oncogenic KRAS G12C: Kinetic and Redox Characterization of Covalent Inhibition. 2022, 102186 524 O Computational Study of Asian Propolis Compounds as Potential Anti-Type 2 Diabetes Mellitus Agents by Using Inverse Virtual Screening with the DIA-DB Web Server, Tanimoto Similarity 523 Analysis, and Molecular Dynamic Simulation. 2022, 27, 3972 RNABPDB: Molecular Modeling of RNA Structure From Base Pair Analysis in Crystals to Structure 522  $\circ$ Prediction. Recent Molecular Insights into Agonist-specific Binding to the Mu-Opioid Receptor. 9, 521 Application of In Silico Filtering and Isothermal Titration Calorimetry for the Discovery of Small 520 Molecule Inhibitors of MDM2. 2022, 15, 752 Midazolam as a Probe for Heterotropic Drug-Drug Interactions Mediated by CYP3A4. 2022, 12, 853 519  $\circ$ 518 Insights into the capsid structure of banana bunchy top virus. 2022, 12, O Discovery of novel gating checkpoints in the Orai1 calcium channel by systematic analysis of 517 constitutively active mutants of its paralogs and orthologs. 2022, 102616 Conformational Dynamics Allows Sampling of an Active-like State by Oncogenic K-Ras-GDP. 2022, 167695 516 Electronic Polarization at the Interface between the p53 Transactivation Domain and Two Binding 515 Partners. Mechanisms of Listeria monocytogenes disinfection with Benzalkonium chloride: from molecular 514 dynamics to kinetics of time-kill curves. Structure of SARS-CoV-2 M protein in lipid nanodiscs. 513

512	Direct Generation of Protein Conformational Ensembles via Machine Learning.	О
511	AlphaFold2 models indicate that protein sequence determines both structure and dynamics. <b>2022</b> , 12,	1
510	Structural basis of Omicron immune evasion: A comparative computational study. <b>2022</b> , 147, 105758	0
509	Endocrine-disrupting metabolic activation of 2-nitrofluorene catalyzed by human cytochrome P450 1A1: A QM/MM approach. <b>2022</b> , 166, 107355	O
508	Molecular dynamic simulation, free binding energy calculation of Thiazolo-[2,3-b]quinazolinone derivatives against EGFR-TKD and their anticancer activity. <b>2022</b> , 4, 100418	1
507	Molecular simulations of the interfacial properties in silk-hydroxyapatite composites.	1
506	Critical Evaluation of Reactive Force Fields for Vibrational Spectra: Case Study of Crystalline Cellulose I $\Box$	0
505	Computational Study of the Allosteric Effects of p5 on CDK5\$\bar{p}\$25 Hyperactivity as Alternative Inhibitory Mechanisms in Neurodegeneration. <b>2022</b> , 126, 5033-5044	
504	Human Growth Hormone Fragment 176¶91 Peptide Enhances the Toxicity of Doxorubicin-Loaded Chitosan Nanoparticles Against MCF-7 Breast Cancer Cells. Volume 16, 1963-1974	1
503	Design, Synthesis, In Silico and In Vitro Studies of New Immunomodulatory Anticancer Nicotinamide Derivatives Targeting VEGFR-2. <b>2022</b> , 27, 4079	2
502	Newly Synthesized Pyrazolinone Chalcones as Anticancer Agents via Inhibiting the PI3K/Akt/ERK1/2 Signaling Pathway.	4
501	Ion-Dependent Conformational Plasticity of Telomeric G-Hairpins and G-Quadruplexes. <b>2022</b> , 7, 23368-23379	1
500	Potential Autoimmunity Resulting from Molecular Mimicry between SARS-CoV-2 Spike and Human Proteins. <b>2022</b> , 14, 1415	2
499	Effect of membrane lipid fluidity, composition, and charge on the ability of the antimicrobial peptide ascaphin-8 to insert into the membrane and form pores. <b>2022</b> ,	
498	Computational study on novel natural compound inhibitor targeting IDH1_R132H.	0
497	A new approach used in docking study for predicting the combination drug efficacy in EML4-ALK target of NSCLC. 1-17	
496	Allostery Inhibition of BACE1 by Psychotic and Meroterpenoid Drugs in Alzheimer Disease Therapy. <b>2022</b> , 27, 4372	1
495	Structure Prediction, Evaluation, and Validation of GPR18 Lipid Receptor Using Free Programs. <b>2022</b> , 23, 7917	

494	Institutional Value of a Nobel Prize. <b>2022</b> ,	О
493	Physical insight into the entropy-driven ion association. <i>Journal of Computational Chemistry</i> , 3.5	O
492	Spatial organization of hydrophobic and charged residues affects protein thermal stability and binding affinity. <b>2022</b> , 12,	0
491	Multifaceted Computational Modeling in Glycoscience.	7
490	Transition Path Sampling Based Calculations of Free Energies for Enzymatic Reactions: The Case of Human Methionine Adenosyl Transferase and Plasmodium vivax Adenosine Deaminase.	1
489	Discovering and targeting dynamic drugging pockets of the oncogene KRAS-G12D.	
488	State-specific morphological deformations of the lipid bilayer explain mechanosensitive gating of MscS ion channels.	
4 <sup>8</sup> 7	Computational Assessment of Protein <b>B</b> rotein Binding Specificity within a Family of Synaptic Surface Receptors.	1
486	Design and synthesis of thiazolidine-2,4-diones hybrids with 1,2-dihydroquinolones and 2-oxindoles as potential VEGFR-2 inhibitors: in-vitro anticancer evaluation and in-silico studies. <b>2022</b> , 37, 1903-1917	10
485	CryoEM Structures of the Human HIV-1 Restriction Factor SERINC3 and Function as a Lipid Transporter.	2
484	Computationally profiling peptide:MHC recognition by T-cell receptors and T-cell receptor-mimetic antibodies.	
483	Molecular Insights into the Regulation of 3-Phosphoinositide-Dependent Protein Kinase 1: Modeling the Interaction between the Kinase and the Pleckstrin Homology Domains.	1
482	Mechanisms of isoform-specific residue influence on GTP-bound HRas, KRas, and NRas. 2022,	O
481	Cryo-EM structure of anchorless RML prion reveals variations in shared motifs between distinct strains. <b>2022</b> , 13,	4
480	Engineering EmbdenMeyerhofParnas Glycolysis to Generate Noncanonical Reducing Power. <b>2022</b> , 12, 8582-8592	1
479	Uncovering the Domain-Specific Interactome of the TAF1 Tandem Reader Using Site-Specific Azide-Acetyllysine Photochemistry.	O
478	CDI Exerts Anti-Tumor Effects by Blocking the FoxM1-DNA Interaction. <b>2022</b> , 10, 1671	
477	WiChR, a highly potassium selective channelrhodopsin for low-light two-photon neuronal inhibition.	1

476	Structural and thermodynamics properties of pure phase alkanes, monoamides and alkane/monoamide mixtures with an ab initio based force-field model. <b>2022</b> , 119797	
475	The Elephant Evolved p53 Isoforms that Escape MDM2-Mediated Repression and Cancer. <b>2022</b> , 39,	2
474	Modeling Gd3+ Complexes for Molecular Dynamics Simulations: Toward a Rational Optimization of MRI Contrast Agents.	
473	10-Alkoxy-anthracenyl-isoxazole analogs have sub-micromolar activity against a Glioblastoma multiforme cell line. <b>2022</b> , 69, 116911	
472	A review on computational approaches that support the researches on traditional Chinese medicines (TCM) against COVID-19. <b>2022</b> , 104, 154324	O
471	Towards Covid-19 TMPRSS2 enzyme inhibitors and antimicrobial agents: Synthesis, antimicrobial potency, molecular docking, and drug-likeness prediction of thiadiazole-triazole hybrids. <b>2022</b> , 1268, 133659	2
470	Molecular dynamics simulations of cRGD-conjugated PEGylated TiO2 nanoparticles for targeted photodynamic therapy. <b>2022</b> , 627, 126-141	1
469	Engineering of enzymes using non-natural amino acids.	
468	Pollution caused by nanoplastics: adverse effects and mechanisms of interaction via molecular simulation. 10, e13618	
467	Exploring the Binding Interaction of Active Compound of Pineapple against Foodborne Bacteria and Novel Coronavirus (SARS-CoV-2) Based on Molecular Docking and Simulation Studies. <b>2022</b> , 14, 3045	1
466	The permeation of potassium ions through the lipid scrambling path of the membrane protein nhTMEM16. 9,	O
465	Structural basis of mammalian complex IV inhibition by steroids. <b>2022</b> , 119,	2
464	Free energy simulations to study mutational effect of a conserved residue, Trp24, on stability of human serum retinol-binding protein. 1-11	
463	Structure, Organization, and Heterogeneity of Water-Containing Deep Eutectic Solvents.	2
462	Comprehensive mapping of mutations in the C9ORF72 that affect folding and binding to SMCR8 protein. <b>2022</b> , 121, 312-321	1
461	Development of Potent SARS-CoV 3CL Protease Inhibitors: In silico Analogues Designing of Darunavir, Molecular Modelling and Molecular Dynamic Simulation. <b>2022</b> , 34, 2343-2350	
460	MDZ: An Efficient Error-bounded Lossy Compressor for Molecular Dynamics. 2022,	1
459	In Silico Study of Selected Natural Products as SARS-CoV-2 MPro Binder: Molecular Docking and Molecular Dynamics Simulation. 1-13	

458	INAQS, a Generic Interface for Nonadiabatic QM/MM Dynamics: Design, Implementation, and Validation for GROMACS/Q-CHEM simulations. <b>2022</b> , 18, 4601-4614	1
457	In silico modelling human VPS13 proteins associated with donor and target membranes suggests lipid transfer mechanisms.	1
456	Computational insights on molecular interactions of acifran with GPR109A and GPR109B. 2022, 28,	O
455	The Computational Preventive Potential of the Rare Flavonoid, Patuletin, Isolated from Tagetes patula, against SARS-CoV-2. <b>2022</b> , 11, 1886	O
454	Molecular mechanism of GTP binding- and dimerization-induced enhancement of Sar1-mediated membrane remodeling.	
453	Thermodynamic Study of Assembling <-> Disassembling of Microtubules via the Monte Carlo Simulation. <b>2022</b> , 96, 1474-1483	
452	Generation and Computational Characterization of a Complex Staphylococcus aureus Lipid Bilayer. <b>2022</b> , 38, 9481-9499	1
451	Evaluation of EDTA Dianhydride Versus Diphenyl Carbonate Nanosponges for Curcumin. <b>2022</b> , 23,	
450	A potent virucidal activity of functionalized TiO2 nanoparticles adsorbed with flavonoids against SARS-CoV-2.	О
449	Computational Modeling of Molecular Mechanics for the Experimentally Inclined.	
448	Targeting SARS-CoV-2 endoribonuclease: a structure-based virtual screening supported by in vitro analysis. <b>2022</b> , 12,	2
447	New quinoline and isatin derivatives as apoptotic VEGFR-2 inhibitors: design, synthesis, anti-proliferative activity, docking, ADMET, toxicity, and MD simulation studies. <b>2022</b> , 37, 2191-2205	2
446	Crystal structure of ChbG from Klebsiella pneumoniae reveals the molecular basis of diacetylchitobiose deacetylation. <b>2022</b> , 5,	
445	On the Rapid Calculation of Binding Affinities for Antigen and Antibody Design and Affinity Maturation Simulations. <b>2022</b> , 11, 51	1
444	A PARP1-related prognostic signature constructing and PARP-1 inhibitors screening for glioma. 10,	
443	Molecular mechanisms from reaction coordinate graph enabled multidimensional free energies illustrated on water dimer hydrogen bonding.	
442	Peroxy Intermediate Drives Carbon Bond Activation in the Dioxygenase AsqJ.	
441	A key residue of plant ABC transporter modulates access path geometry and phenylpropanoid substrate selectivity.	

440	CHARMM-GUI high-throughput simulator for efficient evaluation of protein ligand interactions with different force fields. <b>2022</b> , 31,	2
439	Molecular Insights into the Impacts of Calcite Nanoparticles on Methane Hydrate Formation.	o
438	A Universal Framework for Featurization of Atomistic Systems. 7911-7919	О
437	Isolation and In Silico Inhibitory Potential against SARS-CoV-2 RNA Polymerase of the Rare Kaempferol 3-O-(6?-O-acetyl)-Glucoside from Calligonum tetrapterum. <b>2022</b> , 11, 2072	
436	A self-adaptive evolutionary algorithm using Monte Carlo Fragment insertion and conformation clustering for the protein structure prediction problem.	
435	Searching for new mTOR kinase inhibitors: Analysis of binding sites and validation of docking protocols.	O
434	Phosphorylation at Ser65 modulates ubiquitin conformational dynamics.	
433	Covalent docking in CDOCKER.	
432	Structural insights into ATP-sensitive potassium channel mechanics: a role of intrinsically disordered regions.	
431	A receptor-independent signaling pathway for BDNF.	
430	Unexpected structures formed by the kinase RET C634R mutant extracellular domain suggest	
	potential oncogenic mechanisms in MEN2A. <b>2022</b> , 102380	
429	Multistep orthophosphate release tunes actomyosin energy transduction. <b>2022</b> , 13,	2
429 428		2
	Multistep orthophosphate release tunes actomyosin energy transduction. <b>2022</b> , 13,  Structure-activity relationships of mitochondria-targeted tetrapeptide pharmacological	
428	Multistep orthophosphate release tunes actomyosin energy transduction. <b>2022</b> , 13,  Structure-activity relationships of mitochondria-targeted tetrapeptide pharmacological compounds. 11,  ppdx: Automated modeling of proteinBrotein interaction descriptors for use with machine	
428	Multistep orthophosphate release tunes actomyosin energy transduction. 2022, 13,  Structure-activity relationships of mitochondria-targeted tetrapeptide pharmacological compounds. 11,  ppdx: Automated modeling of proteinBrotein interaction descriptors for use with machine learning. 2022, 43, 1747-1757  Evolution of Stronger SARS-CoV-2 Variants as Revealed Through the Lens of Molecular Dynamics	
428 427 426	Multistep orthophosphate release tunes actomyosin energy transduction. 2022, 13,  Structure-activity relationships of mitochondria-targeted tetrapeptide pharmacological compounds. 11,  ppdx: Automated modeling of proteinBrotein interaction descriptors for use with machine learning. 2022, 43, 1747-1757  Evolution of Stronger SARS-CoV-2 Variants as Revealed Through the Lens of Molecular Dynamics Simulations.	1

2022, 182, 107875

Novel natural inhibitors targeting KRAS G12C by computational study. Publish Ahead of Print, 422 The two enantiomers of 2-hydroxyglutarate differentially regulate cytotoxic T cell function. 421 Capturing Concentration-Induced Aggregation of Nucleobases on a Graphene Surface through 420  $\circ$ Polarizable Force Field Simulations. 2022, 126, 13122-13131 Derivatives of [P4-VP] 2% DVB as corrosion inhibitors for St-37 in 1 M H2SO4: an experimental and 419 theoretical investigations. Recognition in the Domain of Molecular Chirality: From Noncovalent Interactions to Separation of 418 7 Enantiomers. 2022, 122, 13235-13400 Effect of ultrasonication on the protein polysaccharide complexes: a review. 417 416 Newly designed melatonin analogues with potential neuroprotective effects. 2022, 141, O Microsecond MD Simulations of the Plexin-B1 RBD: N⊞ Probability Density as Descriptor of Structural Dynamics, Dimerization-Related Conformational Entropy, and Transient Dimer 415 Asymmetry. N-glycosylation modulates enzymatic activity of Trypanosoma congolense trans-sialidase. 2022, 102403 414 In-silico probing of AML related RUNX1 cancer-associated missense mutations: Predicted 413 relationships to DNA binding and drug interactions. 9, Amino acid deprotonation rates from classical force fields. 2022, 157, 085101 412 Structure-Based Virtual Screening, Docking, ADMET, Molecular Dynamics, and MM-PBSA Calculations for the Discovery of Potential Natural SARS-CoV-2 Helicase Inhibitors from the 411 Traditional Chinese Medicine. 2022, 2022, 1-23 Catalytic Mechanism of ATP Hydrolysis in the ATPase Domain of Human DNA Topoisomerase IIH. 410 1 2022, 62, 3896-3909 Using Selectively Scaled Molecular Dynamics Simulations to Assess Ligand Poses in RNA Aptamers. 409 Discovery of new 1H-pyrazolo[3,4-d]pyrimidine derivatives as anticancer agents targeting EGFRWT 408 3 and EGFRT790M. 2022, 37, 2283-2303 Remote communication between unstructured and structured regions of Bcl-2 tunes its ligand 407 binding capacity: Mechanistic insights. 2022, 100, 107736 A stepwise docking and molecular dynamics approach for enzymatic biolubricant production using 406 4 Lipase Eversa Transform as a biocatalyst. 2022, 187, 115450 Theoretical and experimental model of molecularly imprinted polymer surface microenvironment for selective stationary phase Exemplary of S-pramipexole for potential pharmaceutical analysis. 405

404	Modified pyrido[2,3-d]pyrimidin-4(3H)-one derivatives as EGFRWT and EGFRT790M inhibitors: Design, synthesis, and anti-cancer evaluation. <b>2022</b> , 1270, 133971	О
403	Calcium-induced environmental adaptability of the blood protein vitronectin. 2022,	О
402	Relative binding free energy calculations with transformato: A molecular dynamics engine-independent tool. 9,	О
401	Bioinformatics analysis of Muscovy duck parvovirus REP and VP1 proteins. 1-16	О
400	Molecular Simulations and NMR Reveal How Lipid Fluctuations Affect Membrane Mechanics.	О
399	Structural basis for membrane attack complex inhibition by CD59.	О
398	Anticancer drugs tamoxifen and 4hydroxytamoxifen as effectors of phosphatidylethanolamine lipid polymorphism. <b>2022</b> , 248, 105239	1
397	Biphenyl-based small molecule inhibitors: Novel cancer immunotherapeutic agents targeting PD-1/PD-L1 interaction. <b>2022</b> , 73, 117001	2
396	Integrated network pharmacology and DSS-induced colitis model to determine the anti-colitis effect of Rheum palmatum L. and Coptis chinensis Franch in granules. <b>2023</b> , 300, 115675	0
395	Allosteric regulation of autoinhibition and activation of c-Abl. <b>2022</b> , 20, 4257-4270	O
394	On modeling and utilizing chemical compound information with deep learning technologies: A task-oriented approach. <b>2022</b> , 20, 4288-4304	О
393	Structure-based thermodynamics of ion selectivity (Mg2+versus Ca2+ and K+versus Na+) in the active site of the eukaryotic lariat group II intron from algae Pylaiella littoralis.	O
392	Planning, executing and assessing the validity of SANS contrast variation experiments. 2022,	0
391	A theoretical insight into excited-state decay and proton transfer of p-nitrophenylphenol in the gas phase and methanol solution. <b>2022</b> , 24, 20517-20529	1
390	ABCG2/BCRP transport mechanism revealed through kinetically excited targeted molecular dynamics simulations. <b>2022</b> , 20, 4195-4205	О
389	Deep eutectic solvents as green and efficient media for biocatalytic processes. <b>2022</b> , 161-180	1
388	Crystal structure prediction of hostguest supramolecular systems based on I-cyclodextrin dimers and trimers with luminescent probes. <b>2022</b> , 24, 6654-6661	0
387	Virtual screening techniques in pharmaceutical research. <b>2022</b> , 89-128	О

386	Hydration Dynamics and IR Spectroscopy of 4-Fluorophenol.	О
385	EFFECTS OF TEMPERATURE ON THE INTERACTION OF WATER AND OIL COMPONENTS ON THE CARBONATED PORE WALL: MOLECULAR DYNAMICS SIMULATION STUDY. <b>2022</b> , 25, 83-107	O
384	Interacci∏ in silico de las mol∏ culas Agathisflavona, Amentoflavona y Punicalina con la Importina ⊞1 humana. <b>2022</b> , 23, 15-24	0
383	The Role of Molecular Dynamics Simulations in Multiscale Modeling of Nanocarriers for Cancer Treatment. <b>2022</b> , 209-235	O
382	Quantum Tunneling in Computational Catalysis and Kinetics: Is it Really Important?. 2022,	O
381	From Skeptic to Believer: The Power of Models.	O
380	Probing the Energy Landscapes of Biomolecular Folding and Function. 2022, 61-82	O
379	Modern Methods and Software Systems of Molecular Modeling and Application of Behavior Algebra. <b>2022</b> , 58, 454-464	O
378	Eccrine Sweat Molecular Model for Development of de novo Biosensors. 2022,	0
377	Rational polypharmacological targeting of FLT3, JAK2, ABL, and ERK1 suppresses the adaptive resistance to FLT3 inhibitors in AML.	O
376	Combined Computational and Experimental Studies of Anabasine Encapsulation by Beta-Cyclodextrin. <b>2022</b> , 11, 2283	1
375	In silico identification of potential drug-like molecules against G glycoprotein of Nipah virus by molecular docking, DFT studies, and molecular dynamic simulation. 1-15	O
374	SARS-CoV-2 Delta Variant is Recognized Through GRP78 Host-Cell Surface Receptor, In Silico Perspective. <b>2022</b> , 28,	1
373	Applications of Molecular Dynamics Simulation in Protein Study. <b>2022</b> , 12, 844	1
372	Effects of Presenilin-1 Familial Alzheimer Disease Mutations on Esecretase Activation for Cleavage of Amyloid Precursor Protein.	O
371	Structural basis of substrate recognition by human tRNA splicing endonuclease TSEN.	O
370	Anti-Phytophthora Activity of Halofuginone and the Corresponding Mode of Action. 2022, 70, 12364-12371	O
369	Electric fields control water-gated proton transfer in cytochrome c oxidase. <b>2022</b> , 119,	О

368	Potential Distribution across Model Membranes. 2022, 126, 7664-7675	O
367	Pharmacoinformatic study of inhibitory potentials of selected flavonoids against papain-like protease and 3-chymotrypsin-like protease of SARS-CoV-2. <b>2022</b> , 8,	o
366	Charged Small Molecule Binding to Membranes in MD Simulations Evaluated against NMR Experiments. <b>2022</b> , 126, 6955-6963	0
365	Parametrization of Force Field Bonded Terms under Structural Inconsistency.	o
364	Balanced Force Field ff03CMAP Improving the Dynamics Conformation Sampling of Phosphorylation Site. <b>2022</b> , 23, 11285	1
363	From skeptic to believer: The power of models. <b>2022</b> , 123, 132984	O
362	Committor-Consistent Variational String Method. 9263-9271	0
361	Bottom-up Coarse-Graining: Principles and Perspectives.	6
360	Accurate prediction by AlphaFold2 for ligand binding in a reductive dehalogenase: Implications for PFAS (per- and polyfluoroalkyl substance) biodegradation.	0
359	Hybrid in vitro/in silico analysis of low-affinity proteinprotein interactions that regulate signal transduction by Sema6D.	1
358	Discovery of New VEGFR-2 Inhibitors: Design, Synthesis, Anti-Proliferative Evaluation, Docking, and MD Simulation Studies. <b>2022</b> , 27, 6203	0
357	Inhibitory potentials of phytocompounds from Ocimum gratissimum against anti-apoptotic BCL-2 proteins associated with cancer: an integrated computational study. <b>2022</b> , 9, 588-608	O
356	Oxidative Stress and Mitochondrial Complex I Dysfunction Correlate with Neurodegeneration in an $\Box$ -Synucleinopathy Animal Model. <b>2022</b> , 23, 11394	1
355	On the Tracks of the Aggregation Mechanism of the PHF6 Peptide from Tau Protein: Molecular Dynamics, Energy, and Interaction Network Investigations. <b>2022</b> , 13, 2874-2887	o
354	Potential molecular mechanisms of Ermiao san in the treatment of hyperuricemia and gout based on network pharmacology with molecular docking. <b>2022</b> , 101, e30525	0
353	Modeling peptide-protein complexes: docking, simulations, and machine learning. 1-54	0
352	Identification of promising anti-EBOV inhibitors: de novo drug design, molecular docking and molecular dynamics studies. <b>2022</b> , 9,	O
351	Homology modeling of Forkhead box protein C2: identification of potential inhibitors using ligand and structure-based virtual screening.	O

350	Chemically inducible split protein regulators for mammalian cells.	О
349	Effect of Tacticity and Degree of Sulfonation of Polystyrene Sulfonate on Calcium-Binding Behavior in the Presence of Dodecyl Sulfate. <b>2022</b> , 61, 13442-13452	Ο
348	Galvani Offset Potential and Constant-pH Simulations of Membrane Proteins. 2022, 126, 6868-6877	O
347	A molecular dynamics simulation study to investigate the effect of C60 on thermo- mechanical and elastic properties of DGEBA/DETA nanocomposites. <b>2022</b> , 32, 32-42	O
346	Self-Uptake Mechanism of Polymyxin-Based Lipopeptide against Gram-Negative Bacterial Membrane: Role of the First Adsorbed Lipopeptide.	O
345	Physical Characteristics of von Willebrand Factor Binding with Platelet Glycoprotein Ib∃ Mutants at Residue 233 Causing Various Biological Functions	0
344	MAIA, Fc receptorlike 3, supersedes JUNO as IZUMO1 receptor during human fertilization. <b>2022</b> , 8,	1
343	A filarial parasite-encoded human IL-10 receptor antagonist reveals a novel strategy to modulate host responses.	Ο
342	Targeting of the Mitochondrial TET1 Protein by Pyrrolo[3,2-b]pyrrole Chelators. 2022, 23, 10850	1
341	Toward Accurate Coarse-Grained Simulations of Disordered Proteins and Their Dynamic Interactions. <b>2022</b> , 62, 4523-4536	1
340	Effects of Familial Alzheimer∄ Disease Mutations on the Folding Free Energy and Dipole <b>D</b> ipole Interactions of the Amyloid □Peptide. <b>2022</b> , 126, 7552-7566	О
339	Mechanistic insight into impact of phosphorylation on the enzymatic steps of farnesyltransferase. <b>2022</b> , 31,	O
338	Design, synthesis, anti-proliferative evaluation, docking, and MD simulations studies of new thiazolidine-2,4-diones targeting VEGFR-2 and apoptosis pathway. <b>2022</b> , 17, e0272362	4
337	Accurate Reproduction of Quantum Mechanical Many-Body Interactions in Peptide Main-Chain Hydrogen-Bonding Oligomers by the Polarizable Gaussian Multipole Model.	O
336	CHARMM-GUI Implicit Solvent Modeler for Various Generalized Born Models in Different Simulation Programs. <b>2022</b> , 126, 7354-7364	0
335	A look at the face of the molten globule: structural model of the Helicobacter pylori apoflavodoxin ensemble at acidic pH.	O
334	Recognition of A□oligomer by LilrB2 acceptor: a tetracoordinated zipper mechanism. <b>2022</b> , 28,	О
333	SP-A binding to the SARS-CoV-2 spike protein using hybrid quantum and classical in silico modeling and molecular pruning by Quantum Approximate Optimization Algorithm (QAOA) Based MaxCut with ZDOCK. 13,	O

332	Rutin Potentially Binds the Gamma Secretase Catalytic Site, Down Regulates the Notch Signaling Pathway and Reduces Sphere Formation in Colonospheres. <b>2022</b> , 12, 926	1
331	Allosteric regulation of switch-II controls K-Ras oncogenicity.	О
330	Simulated Docking Predicts Putative Channels for the Transport of Long-Chain Fatty Acids in Vibrio cholerae. <b>2022</b> , 12, 1269	О
329	CHARMM-GUI Enhanced Sampler for Various Collective Variables and Enhanced Sampling Methods.	O
328	C/EBP[]Promotes LPS-Induced IL-1[]Transcription and Secretion in Alveolar Macrophages via NOD2 Signaling. Volume 15, 5247-5263	О
327	Predicting bioactivity of antibiotic metabolites by molecular docking and dynamics.	О
326	Thermodynamic and structural profiles of multi-target binding of vinblastine in solution.	1
325	Atomistic Modeling of Jet Formation in Charged Droplets.	Ο
324	A New Formulation for the Concerted Alchemical Calculation of van der Waals and Coulomb Components of Solvation Free Energies.	О
323	Conjugated Polymer Nanoparticles as a Universal High-Affinity Probe for the Selective Detection of Microplastics.	О
322	M-Chem: a modular software package for molecular simulation that spans scientific domains.	0
321	mPPases create a conserved anionic membrane fingerprint as identified via multi-scale simulations. <b>2022</b> , 18, e1010578	O
320	Comparison of the United- and All-Atom Representations of (Halo)alkanes Based on Two Condensed-Phase Force Fields Optimized against the Same Experimental Data Set.	2
319	Targeting plasma membrane and mitochondrial instability in breast cancer cells and breast epithelial to mesenchymal transition-model cells by adamantyl diaza-crown ether ZG613.	O
318	Constraint Guided Beta-Sheet Refinement for Protein Structure Prediction. 2022, 101, 107773	0
317	Calculation of the permeability coefficients of small molecules through lipid bilayers by free-energy reaction network analysis following the explicit treatment of the internal conformation of the solute. <b>2022</b> , 24, 26070-26082	O
316	Facilitating ab initio QM/MM free energy simulations by Gaussian process regression with derivative observations. <b>2022</b> , 24, 25134-25143	О
315	FPGA-Accelerated Tersoff Multi-body Potential for Molecular Dynamics Simulations. 2022, 17-31	О

314	MoS2 nanosheets effectively binds to the receptor binding domain of SARS-CoV-2 spike protein and destabilizes the spike-human ACE2 receptor interactions.	О
313	In silico study of inhibitory capacity of sacubitril/valsartan toward neprilysin and angiotensin receptor. <b>2022</b> , 12, 29719-29726	О
312	Modeling difference x-ray scattering observations from an integral membrane protein within a detergent micelle. <b>2022</b> , 9, 054102	О
311	The core complex of the Ca2+-triggered presynaptic fusion machinery. <b>2022</b> , 167853	1
310	Biochemical and Structural Characterization of Chi-Class Glutathione Transferases: A Snapshot on the Glutathione Transferase Encoded by sll0067 Gene in the Cyanobacterium Synechocystis sp. Strain PCC 6803. <b>2022</b> , 12, 1466	0
309	Structural and electronic properties of the active site of [ZnFe] SulE. 9,	О
308	2-Hydroxychalconel-Cyclodextrin Conjugate with pH-Modulated Photoresponsive Binding Properties.	О
307	CAT: A Compound Attachment Tool for the Construction of Composite Chemical Compounds.	O
306	Computational study on new natural compound inhibitors of Traf2 and Nck-interacting kinase (TNIK).	0
305	Accurate Quantum-Mechanically Derived Force-Fields through a Fragment-Based Approach: Balancing Specificity and Transferability in the Prediction of Self-Assembly in Soft Matter.	o
304	Lateral fenestrations in the extracellular domain of the glycine receptor contribute to the main chloride permeation pathway. <b>2022</b> , 8,	0
303	Endometriyal h∏ drelerde Spirulina platensis ekstresinin kimyasal bile∏ lminin se∏ l̃ci sitotoksisitesi: d vitro ve in siliko yakla∏ m.	О
302	Modeling the partitioning of amphiphilic molecules and co-solvents in biomembranes. 2022, 55,	0
301	The emergence of protein dynamics simulations: how computational statistical mechanics met biochemistry. <b>2022</b> , 47,	0
300	Binding of piperine to mycobacterial RNA polymerase improves the efficacy of rifampicin activity against Mycobacterium leprae and nontuberculous mycobacteria. 1-11	0
299	Staphylococcus aureusFtsZ and PBP4 bind to the conformationally dynamic N-terminal domain of GpsB.	1
298	A Theoretical and Experimental Study for Enzymatic Biodiesel Production from Babassu Oil (Orbignya sp.) Using Eversa Lipase. <b>2022</b> , 12, 1322	3
297	Copper Coordination States Affect the Flexibility of Copper Metallochaperone Atox1: Insights from Molecular Dynamics Simulations.	О

296	An inducible amphipathic ⊞-helix mediates subcellular targeting and membrane binding of RPE65. <b>2023</b> , 6, e202201546	Ο
295	Improving Condensed-Phase Water Dynamics with Explicit Nuclear Quantum Effects: The Polarizable Q-AMOEBA Force Field. <b>2022</b> , 126, 8813-8826	1
294	Mulberroside A could serve as a pan inhibitor for the tyrosine kinase domains of the HER family. 11, 1201	О
293	Dual-Reporter System for Real-Time Monitoring of SARS-CoV-2 Main Protease Activity in Live Cells Enables Identification of an Allosteric Inhibition Path.	O
292	Mind the Gap <b>D</b> eciphering GPCR Pharmacology Using 3D Pharmacophores and Artificial Intelligence. <b>2022</b> , 15, 1304	О
291	Structural resemblance of the DNAJA-family protein, Tid1, to the DNAJB-family Hsp40. <b>2022</b> , 55, 488-493	O
290	Structural Achievability of an NHIInteraction between Gln and Phe in a Crystal Structure of a Collagen-like Peptide. <b>2022</b> , 12, 1433	0
289	Excitatory and inhibitory D-serine binding to the NMDA receptor. 11,	1
288	Identification of potential antifibrinolytic compounds against kringle-1 and serine protease domain of plasminogen and kringle-2 domain of tissue-type plasminogen activator using combined virtual screening, molecular docking, and molecular dynamics simulation approaches.	0
287	Designing an Epitope-Based Peptide Vaccine Derived from RNA-Dependent RNA Polymerase (RdRp) against Dengue Virus Serotype 2. <b>2022</b> , 10, 1734	O
286	Structure of SARS-CoV-2 M protein in lipid nanodiscs. 11,	1
285	Distinct Antifouling Mechanisms on Different Chain Densities of Zwitterionic Polymers. <b>2022</b> , 27, 7394	О
284	N-Hydroxy-N-Propargylamide Derivatives of Ferulic Acid: Inhibitors of Cholinesterases and Monoamine Oxidases. <b>2022</b> , 27, 7437	1
283	Assessment of two-dimensional materials on the biological membrane permeability of Epirubicin anti-cancer drug. <b>2022</b> , 155557	O
282	A 3D <b>B</b> redicted Structure of the Amine Oxidase Domain of Lysyl Oxidasellike 2. <b>2022</b> , 23, 13385	1
281	Evolution of bioinformatics and its impact on modern bio-science in the twenty-first century: Special attention to pharmacology, plant science and drug discovery. <b>2022</b> , 24, 100248	1
280	Characterization of the interaction of metal-protoporphyrins photosensitizers with $\square$ lactoglobulin. <b>2022</b> , 106918	0
279	How to Stabilize Carbenes in Enzyme Active Sites without Metal Ions.	1

278	An understanding of coronavirus and exploring the molecular dynamics simulations to find promising candidates against the Mpro of nCoV to combat the COVID-19: A systematic review. <b>2022</b> , 15, 1326-1349	О
277	Modeling the vibrational spectroscopy of carbonmonoxymyoglobin using DFT and molecular dynamics. <b>2022</b> , 123, 103455	O
276	Structural insights into conformational stability and binding of thiazolo-[2,3-b] quinazolinone derivatives with EGFR-TKD and in-vitro study. <b>2022</b> , 29, 103478	О
275	Adaptive boost approach for possible leads of triple-negative breast cancer. <b>2022</b> , 231, 104690	1
274	Biophysical interactions of phenolic acids from yerba mate tea with lipid membranes. 2022, 291, 106911	О
273	Free energy reconstruction/decomposition from WHAM, force integration and free energy perturbation for an umbrella sampling simulation. <b>2023</b> , 565, 111736	O
272	Lipid-mediated activation of plasma membrane-localized deubiquitylating enzymes modulate endosomal trafficking. <b>2022</b> , 13,	О
271	Molecular Dynamics Methods for Antibody Design. <b>2023</b> , 109-124	O
270	The Discovery of Potential SARS-CoV-2 Natural Inhibitors among 4924 African Metabolites Targeting the Papain-like Protease: A Multi-Phase In Silico Approach. <b>2022</b> , 12, 1122	O
269	Describing Inhibitor Specificity for the Amino Acid Transporter LAT1 from Metainference Simulations. <b>2022</b> ,	1
268	Pose, duplicate, then elaborate: Steps towards increased affinity for inhibitors targeting the specificity surface of the Pim-1 kinase. <b>2022</b> , 114914	О
267	Malonyl-CoA is an ancient physiological ATP-competitive mTORC1 inhibitor.	O
266	Identification of novel interferon responsive protein partners of human leukocyte antigen A (HLA-A) using cross-linking mass spectrometry (CLMS) approach. <b>2022</b> , 12,	О
265	Allosteric Boost by TAB1 on the TAK1 Kinase Favorably Sculpts the Thermodynamic Landscape of Activation.	O
264	GPU-Accelerated All-Atom Particle-Mesh Ewald Continuous Constant pH Molecular Dynamics in Amber.	1
263	The conformation of the intrinsically disordered N-terminal region of Barrier-to-Autointegration factor (BAF) is regulated by pH and phosphorylation. <b>2022</b> , 167888	1
262	PyMM: An Open-Source Python Program for QM/MM Simulations Based on the Perturbed Matrix Method.	2
261	Insights into DNA Solvation Found in Protein-DNA Structures. 2022,	O

260	Synthesis, Molecular Docking, and Antitumor Evaluation of Some New Pyrazole, Pyridine, and Thiazole Derivatives Incorporating Sulfonamide Residue. 1-14	O
259	Domain-selective disruption and compression of phase-separated lipid vesicles by amphiphilic Janus nanoparticles. <b>2022</b> , 105525	O
258	Discovering and Targeting Dynamic Drugging Pockets of Oncogenic Proteins: The Role of Magnesium in Conformational Changes of the G12D Mutated Kirsten Rat Sarcoma-Guanosine Diphosphate Complex. <b>2022</b> , 23, 13865	1
257	Analyzing the potential of selected plant extracts and their structurally diverse secondary metabolites for ⊞-glucosidase inhibitory activity: in vitro and in silico approach. 1-16	O
256	In Silico Study of the Mechanisms Underlying the Action of the Snake Natriuretic-Like Peptide Lebetin 2 during Cardiac Ischemia. <b>2022</b> , 14, 787	1
255	Open-channel structure of a pentameric ligand-gated ion channel reveals a mechanism of leaflet-specific phospholipid modulation. <b>2022</b> , 13,	2
254	Higher order interactions of Bcr-Abl can broaden chronic myeloid leukemia ( CML ) drug repertoire.	O
253	Hydration Free Energies of Polypeptides from Popular Implicit Solvent Models versus All-Atom Simulation Results Based on Molecular Quasichemical Theory.	1
252	Molecular mechanism of ion channel protein TMEM16A regulated by natural product of narirutin for lung cancer adjuvant treatment. <b>2022</b> , 223, 1145-1157	O
251	Anticarcinogenic trimethoxybenzoate of catechin stabilizes the liquid crystalline bilayer phase in phosphatidylethanolamine membranes. <b>2022</b> , 368, 120774	O
250	Nontoxic Artificial Chloride Channel Formation in Epithelial Cells by Isophthalic Acid-Based Small Molecules.	O
249	Effect of surfactants on SARS-CoV-2: Molecular Dynamics Simulations.	O
248	Molecular origins of asymmetric proton conduction in the influenza M2 channel. 2022,	0
247	How binding to surfaces affects disorder?. <b>2023</b> , 455-489	O
246	In silico modelling human VPS13 proteins associated with donor and target membranes suggests lipid transfer mechanisms.	O
245	Excess-electron capture and energy transfer to bulk water for aqueous DNA nucleotide. <b>2022</b> , 25, 471-477	1
244	Benchmark of a functional-group database for distributed polarizability and dipole moment in biomolecules. <b>2022</b> , 24, 29495-29504	О
243	Brave New Surfactant World Revisited by Thermoalkalophilic Lipases: Computational Insights into the Role of SDS as a Substrate Analog.	1

242	Unveiling the structural features that regulate carbapenem deacylation in KPC-2 through QM/MM and interpretable machine learning.	O
241	A theoretical framework for the design of molecular crystal engines.	О
240	Ginkgolic acids inhibit SARS-CoV-2 and its variants by blocking the spike protein/ACE2 interplay. <b>2023</b> , 226, 780-792	0
239	Design, synthetic approach, in silico molecular docking and antibacterial activity of quinazolin-2,4-dione hybrids bearing bioactive scaffolds. <b>2022</b> , 13, 292-308	O
238	Plasma membrane lipid bilayer is druggable: Selective delivery of gemcitabine-squalene nano-medicine to cancer cells. <b>2023</b> , 1869, 166614	О
237	Identification of a novel adiponectin receptor and opioid receptor dual acting agonist as a potential treatment for diabetic neuropathy. <b>2023</b> , 158, 114141	O
236	Illustrating the atomic structure and formation mechanism of ion tracks in polyethylene terephthalate with molecular dynamics simulations. <b>2023</b> , 535, 102-111	0
235	Computational and experimental studies of magnetic molecularly imprinted sorbent with high specificity towards aceclofenac. <b>2023</b> , 186, 108272	O
234	Oxygen Storage in Stacked Phospholipid Membranes Under an Oxygen Gradient as a Model for Myelin Sheaths. <b>2022</b> , 301-307	0
233	A building-block database of distributed polarizabilities and dipole moments to estimate optical properties of biomacromolecules in isolation or in an explicitly solvated medium.	o
232	Insights into the Mechanism of the Cardiac Drug Omecamtiv Mecarbil-A Computational Study. <b>2022</b> , 126, 10069-10082	0
231	Molecular Dynamics Simulations of Rhodamine B Zwitterion Diffusion in Polyelectrolyte Solutions. <b>2022</b> , 126, 10256-10272	O
230	The Effect of the Ala16Val Mutation on the Secondary Structure of the Manganese Superoxide Dismutase Mitochondrial Targeting Sequence. <b>2022</b> , 11, 2348	0
229	How Accurate Is the Egg-Box Model in Describing the Binding of Calcium to Polygalacturonate? A Molecular Dynamics Simulation Study. <b>2022</b> , 126, 10206-10220	O
228	In silico targeting breast cancer biomarkers by applying rambutan (Nephelium lappaceum) phytocompounds. 1-14	0
227	Computer-Aided Drug Design: An Update. <b>2023</b> , 123-152	1
226	Molecular Dynamics Simulation of the Thermal Behavior of Hydroxyapatite. 2022, 12, 4244	0
225	Protein conformation stabilized by newly formed turns for thermal resilience. 2022,	О

224	Identification of novel natural product inhibitors of BRD4 using high throughput virtual screening and MD simulation.	O
223	Molecular Dynamics Simulation as a Promising Approach for Computational Study of Liquid Crystal-based Aptasensors.	O
222	Exploring GPR109A Receptor Interaction with Hippuric Acid Using MD Simulations and CD Spectroscopy. <b>2022</b> , 23, 14778	0
221	The Binding Specificity of PAB1 with Poly(A) mRNA, Regulated by Its Structural Folding. 2022, 10, 2981	Ο
220	Molecular basis for selective activation of DREADD-based chemogenetics. 2022, 612, 354-362	3
219	Planar aggregation of the influenza viral fusion peptide alters membrane structure and hydration, promoting poration. <b>2022</b> , 13,	Ο
218	Molecular Simulations and NMR Reveal How Lipid Fluctuations Affect Membrane Mechanics. 2022,	О
217	L-Ascorbic acid and Phosphatidylcholine complex vesicles: formation and elucidation of their biological activities, and their molecular interactions. 1-38	O
216	Proteinligand Binding Free-Energy Calculations with ARROW-A Purely First-Principles Parameterized Polarizable Force Field. <b>2022</b> , 18, 7751-7763	Ο
215	Knowledge-driven design and optimization of potent symmetric anticancer molecules: A case study on PKM2 activators. <b>2022</b> , 151, 106313	Ο
214	Effective natural inhibitors targeting granzyme B in rheumatoid arthritis by computational study. 9,	0
213	In vitro and computational studies of the 🕒 lactamase inhibition and 🗗 lactam potentiating properties of plant secondary metabolites. 1-21	Ο
212	Protein binding sites for drug design.	О
211	Mechanism of pH sensing in the human voltage-gated proton channel hHv1.	Ο
210	ATESA: An Automated Aimless Shooting Workflow.	1
209	Quality over quantity: Sampling high probability rare events with the weighted ensemble algorithm.	Ο
208	Varying molecular interactions explain crowder-dependent enzyme function of a viral protease.	0
207	Discovery of small molecule mechanistic target of rapamycin inhibitors as anti-aging and anti-cancer therapeutics. 14,	Ο

206	Artificial intelligence for template-free protein structure prediction: a comprehensive review.	О
205	RNA-guided DNA base damage repair via DNA polymerase-mediated nick translation.	O
204	The development of nucleic acids force fields: From an unchallenged past to a competitive future. <b>2022</b> ,	O
203	QM/MM methods in studies of coinage metals: copper, silver, and gold interacting with biological and organic molecules. <b>2023</b> , 8,	O
202	Analytical Perspectives in the Study of Polyvalent Interactions of Free and Surface-Bound Oligonucleotides and Their Implications in Affinity Biosensing. <b>2023</b> , 24, 175	O
201	Dual Impacts of a Glycan Shield on the Envelope Glycoprotein B of HSV-1: Evasion from Human Antibodies In Vivo and Neurovirulence.	O
200	Screening and Identification of Potential MERS-CoV papain-like protease (PLpro) Inhibitors; Steady-state kinetic and Molecular Dynamic Studies. <b>2022</b> ,	O
199	MoBioTools : A toolkit to setup quantum mechanics/molecular mechanics calculations.	O
198	Elucidation of the Reaction Mechanism of Cavia porcellus l-Asparaginase: A QM/MM Study.	0
197	Pyrido-pyrimido-thiadiazinones: green synthesis, molecular docking studies and biological investigation as obesity inhibitors. <b>2022</b> , 16, 1275-1286	O
196	Structural and Energetic Origin of Different Product Specificities and Activities for SETD3 and Its Mutants on the Methylation of the I-Actin H73K Peptide: Insights from a QM/MM Study.	0
195	Discovery of imidazole-based GSK-3 inhibitors for transdifferentiation of human mesenchymal stem cells to neurons: A potential single-molecule neurotherapeutic foresight. 15,	O
194	WiChR, a highly potassium-selective channelrhodopsin for low-light one- and two-photon inhibition of excitable cells. <b>2022</b> , 8,	1
193	Dendrimer-Peptide Conjugates for Effective Blockade of the Interactions between SARS-CoV-2 Spike Protein and Human ACE2 Receptor.	1
192	Can de-phosphorylation of serine-5 in the C-terminal domain of human polymerase II affect its interaction with the PA C-terminal domain of bat Flu A polymerase?. 1-10	O
191	Identification of novel natural product inhibitors of BRD4 using high throughput virtual screening and MD simulation. 1-13	O
190	Small GTPase Ran: Depicting the nucleotide-specific conformational landscape of the functionally important C-terminus. 10,	0
189	Influence of Electronic Polarization on the Binding of Anions to a Chloride-Pumping Rhodopsin.	O

188	MDexciteR: Enhanced Sampling Molecular Dynamics by Excited Normal Modes or Principal Components Obtained from Experiments.	O
187	SDEGen: Learning to Evolve Molecular Conformations from Thermodynamic Noise for Conformation Generation.	O
186	Identification and characterization of a flexile G-quadruplex in the distal promoter region of stemness gene REX1. <b>2023</b> , 123263	Ο
185	Discovery and Mechanism of Action of a Novel Antimicrobial Peptide from an Earthworm.	O
184	Free energy calculations and solubility in water of organic molecules: a numerical relation through molecular dynamics. 1-10	0
183	Modeling Concentration-dependent Phase Separation Processes Involving Peptides and RNA via Residue-Based Coarse-Graining.	Ο
182	Identification of New N-methyl-piperazine Chalcones as Dual MAO-B/AChE Inhibitors. 2023, 16, 83	Ο
181	Effects of a Semisynthetic Catechin on Phosphatidylglycerol Membranes: A Mixed Experimental and Simulation Study. <b>2023</b> , 28, 422	O
180	Composition, Antibacterial Efficacy, and Anticancer Activity of Essential Oil Extracted from Psidium guajava (L.) Leaves. <b>2023</b> , 12, 246	3
179	The Effect of Arginine on the Phase Stability of Aqueous Hen Egg-White Lysozyme Solutions. <b>2023</b> , 24, 1197	O
178	West Nile virus ssociated HLA-DRB1 alleles in the Greek population: A structural perspective.	О
177	Investigating the Unbinding of Muscarinic Antagonists from the Muscarinic 3 Receptor.	O
176	Effect of alanine versus serine at position 88 of human transthyretin mutants on the protein stability.	Ο
175	The buckling-condensation mechanism driving gas vesicle collapse.	Ο
174	Conformational and mechanical stability of the isolated large subunit of membrane-bound [NiFe]-hydrogenase from Cupriavidus necator. 13,	O
173	Intact Transition Epitope MappingHorce Differences between Original and Unusual Residues (ITEM-FOUR). <b>2023</b> , 13, 187	1
172	Colchicine as potential inhibitor targeting MMP-9, NOX2 and TGF-II in myocardial infarction: a combination of docking and molecular dynamic simulation study. 1-11	0
171	Structural optimization and binding energy prediction for globomycin analogs based on 3D-QSAR and molecular simulations. <b>2023</b> , 134981	Ο

170	Amphiphilic Co-Solvents Modulate the Structure of Membrane Domains.	0
169	Discovery of new quinoline and isatine derivatives as potential VEGFR-2 inhibitors: design, synthesis, antiproliferative, docking and MD simulation studies. 1-16	O
168	Critical Assessment of Methods for Predicting the 3D Structure of Proteins and Protein Complexes. <b>2023</b> , 52,	О
167	Proteogenomic Approaches to Understand Gene Mutations and Protein Structural Alterations in Colon Cancer. <b>2023</b> , 3, 11-29	O
166	New amidine-benzenesulfonamides as iNOS inhibitors for the therapy of the triple negative breast cancer. <b>2023</b> , 248, 115112	1
165	Theoretical investigations of TTR derived aggregation-prone peptides potential to biochemically attenuate the amyloidogenic propensities of V30 M TTR amyloid fibrils. <b>2023</b> , 100, 100892	O
164	In silico identification of potential Becretase inhibitor of marine-algal origin: an anticancer intervention. 1-10	O
163	Free energy and kinetic rate calculation via non-equilibrium molecular simulation: application to biomolecules. <b>2022</b> , 14, 1303-1314	O
162	The Formation of RNA Pre-Polymers in the Presence of Different Prebiotic Mineral Surfaces Studied by Molecular Dynamics Simulations. <b>2023</b> , 13, 112	O
161	CLIP-Seq Analysis Enables the Design of Ribosomal RNA Bait Oligonucleotides That Protect AgainstC9ORF72ALS/FTD-Associated Poly-GR Pathophysiology.	O
160	Origin of Catalysis by Nitroalkane Oxidase. <b>2023</b> , 127, 151-162	0
159	A Guide to In Silico Drug Design. <b>2023</b> , 15, 49	O
158	Regulation of Ion Permeation of the KcsA Channel by Applied Midinfrared Field. 2023, 24, 556	О
157	Ultrasound-assisted green synthesis of triazole-based azomethine/thiazolidin-4-one hybrid inhibitors for cancer therapy through targeting dysregulation signatures of some Rab proteins. <b>2023</b> , 16,	O
156	Molecular Orientation of <b>B</b> O3H2 and <b>C</b> OOH Functionalized Dyes on TiO2, Al2O3, ZrO2, and ITO: A Comparative Study. <b>2023</b> , 127, 2705-2715	O
155	Identification of potent EGFR-TKD inhibitors from NPACT database through combined computational approaches. 1-14	O
154	State-specific morphological deformations of the lipid bilayer explain mechanosensitive gating of MscS ion channels. 12,	О
153	The application of QM/MM simulations in heterogeneous catalysis.	O

152	Response of Sulfonated Polystyrene Melts to Nonlinear Elongation Flows.	Ο
151	Translocation of a single Arg\$\$_9\$\$ peptide across a DOPC/DOPG(4:1) model membrane using the weighted ensemble method. <b>2023</b> , 13,	O
150	Molecular Modeling Study of a Receptor Drthosteric Ligand Allosteric Modulator Signaling Complex. <b>2023</b> , 14, 418-434	0
149	How PTEN mutations degrade function at the membrane and life expectancy of carriers of mutations in the human brain.	O
148	Reparameterization of the Chemical-Potential Equalization Model with DFTB3: A Practical Balance Between Accuracy and Transferability.	О
147	Dual Anta-Inhibitors of the A2A Adenosine Receptor and Casein Kinase CK1delta: Synthesis, Biological Evaluation, and Molecular Modeling Studies. <b>2023</b> , 16, 167	O
146	Physical properties of phospholipids at low temperatures through Slipid force field. <b>2023</b> , 2436, 012025	1
145	Discovery of differentially expressed novel miRNAs in breast normal cells and their putative targets.	O
144	Interaction of Tryptophan- and Arginine-Rich Antimicrobial Peptide with E. coli Outer Membrane Molecular Simulation Approach. <b>2023</b> , 24, 2005	1
143	Solvation Structure and Dynamics of Aqueous Solutions of Au+ Ions: A Molecular Dynamics Simulation Study.	О
142	In silico Identification of Potential Human Acetylcholinesterase Inhibitors from the Nigella sativa Phytochemicals. <b>2023</b> , 13, 112-117	О
141	Plant Terpenoid Permeability through Biological Membranes Explored via Molecular Simulations. <b>2023</b> , 127, 1144-1157	O
140	How a single mutation alters the protein structure: a simulation investigation on protein tyrosine phosphatase SHP2. <b>2023</b> , 13, 4263-4274	0
139	TIES 2.0: A Dual-Topology Open Source Relative Binding Free Energy Builder with Web Portal.	O
138	Anillin Related Mid1 as an Adaptive and Multimodal Contractile Ring Anchoring Protein: A Simulation Study.	0
137	Molecular interaction modeling of carbon nanotubes and fullerene toward prioritized targets of SARS-CoV-2 by computer-aided screening and docking studies. <b>2023</b> , 157-179	O
136	Mechanisms of Sugar Aminotransferase-like Enzymes to Synthesize Stereoisomers of Non-proteinogenic Amino Acids in Natural Product Biosynthesis.	О
135	Wordom update 2: A user-friendly program for the analysis of molecular structures and conformational ensembles. <b>2023</b> , 21, 1390-1402	0

134	QM/MM study of the [4Fe-4S]-dependent (R)-2-hydroxyisocaproyl-CoA dehydratase: Dehydration via a redox pathway with an $\oplus$ -carbonyl radical intermediate. <b>2023</b> ,	0
133	LAVA 1.0: A general-purpose python toolkit for calculation of material properties with LAMMPS and VASP. <b>2023</b> , 286, 108667	Ο
132	Assessment of alteration in antiviral plasma concentration across dialysis days: computational and analytical study. <b>2022</b> , 14, 1563-1581	Ο
131	State-of-the-art experimental and computational approaches to investigate structure, substrate recognition, and catalytic mechanism of enzymes. <b>2023</b> , 75-107	O
130	The Effect of Cholesterol in SOPC Lipid Bilayers at Low Temperatures. 2023, 13, 275	О
129	Identification and Molecular Mechanism of Novel Immunomodulatory Peptides from Gelatin Hydrolysates: Molecular Docking, Dynamic Simulation, and Cell Experiments. <b>2023</b> , 71, 2924-2934	Ο
128	Insertion Depth Modulates Protein Kinase C-EC1b Domain Interactions with Membrane Cholesterol as Revealed by MD Simulations. <b>2023</b> , 24, 4598	Ο
127	Effect of Newly Synthesized Structures of Peptides on the Stability of the Monolayers Formed. <b>2023</b> , 24, 4318	O
126	Direct generation of protein conformational ensembles via machine learning. 2023, 14,	Ο
125	Characterisation of a cyclic peptide that binds to the RAS binding domain of phosphoinositide 3-kinase p110 $\mathbb B$ . <b>2023</b> , 13,	O
124	Validation of an MD simulation approach for electrical field responsive micelles and their application in drug delivery. <b>2023</b> , 13,	О
123	Toward overcoming pyrethroid resistance in mosquito control: the role of sodium channel blocker insecticides.	O
122	Improving Properties of Podophyllic Aldehyde-Derived Cyclolignans: Design, Synthesis and Evaluation of Novel Lignohydroquinones, Dual-Selective Hybrids against Colorectal Cancer Cells. <b>2023</b> , 15, 886	Ο
121	Molecular-level understanding of the rovibrational spectra of N2O in gaseous, supercritical, and liquid SF6 and Xe. <b>2023</b> , 158, 144302	O
120	Genetically engineered PD-1 displaying nanovesicles for synergistic checkpoint blockades and chemo-metabolic therapy against non-small cell lung cancer. <b>2023</b> , 161, 184-200	О
119	In silico targeting of SARS-CoV-2 spike receptor-binding domain from different variants with chaga mushroom terpenoids. 1-9	O
118	Phosphatidylcholine in the tear film of the eye: Enhanced topical delivery of fluorometholone to the eye. <b>2023</b> , 150, 110506	Ο
117	Galaxolide and Irgacure 369 are novel environmental androgens. <b>2023</b> , 324, 138329	Ο

116	Revealing intrinsic changes of DNA induced by spore photoproduct lesion through computer simulation. <b>2023</b> , 296, 106992	0
115	Water-Mediated attraction between Like-charged species involved in calcium phosphate nucleation. <b>2023</b> , 378, 121585	O
114	Unveiling mutation effects on the structural dynamics of the main protease from SARS-CoV-2 with hybrid simulation methods. <b>2023</b> , 121, 108443	0
113	Functionalized silica nanoparticles within a multicomponent oil emulsion by molecular dynamic study. <b>2023</b> , 732, 122283	O
112	Influence of electronic polarization on the binding of anions to a chloride-pumping rhodopsin. <b>2023</b> , 122, 1548-1556	O
111	Modelling the enantiorecognition of structurally diverse pharmaceuticals on O-substituted polysaccharide-based stationary phases. <b>2023</b> , 259, 124497	O
110	Potential of mean force conformational energy maps for disaccharide linkages of the Burkholderia multivorans exopolysaccharide C1576 in aqueous solution. <b>2023</b> , 524, 108741	0
109	Structure restoration and aggregate inhibition of V30M mutant transthyretin protein by potential quinoline molecules. <b>2023</b> , 231, 123318	2
108	P450-catalyzed polyethylene oligomer degradation: A quantum mechanics/molecular mechanics study. <b>2023</b> , 389, 136130	O
107	The role of conformational change and key glutamic acid residues in the ClC-ec1 antiporter. <b>2023</b> , 122, 1068-1085	O
106	In Silico Drug Design and Analysis of Dual Amyloid-Beta and Tau Protein-Aggregation Inhibitors for Alzheimer Disease Treatment. <b>2023</b> , 28, 1388	O
105	Molecular and kinetic properties of copper nitrite reductase from Sinorhizobium meliloti 2011 upon substituting the interfacial histidine ligand coordinated to the type 2 copper active site for glycine. <b>2023</b> , 241, 112155	O
104	CHARMM-GUI PDB Manipulator: Various PDB Structural Modifications for Biomolecular Modeling and Simulation. <b>2023</b> , 167995	O
103	Solvent Dynamics of Aqueous Halides before and after Photoionization. <b>2023</b> , 127, 1399-1413	O
102	Towards Probing Conformational States of Y2 Receptor Using Hyperpolarized 129Xe NMR. <b>2023</b> , 28, 1424	0
101	Computer-Aided Screening and Revealing Action Mechanism of Green Tea Polyphenols Intervention in Alzheimer Disease. <b>2023</b> , 12, 635	O
100	Statistical Mechanical Design Principles for Coarse-Grained Interactions across Different Conformational Free Energy Surfaces. <b>2023</b> , 14, 1354-1362	0
99	The effect of temperature on the contact angle of a water drop on graphene and graphene synthesized on copper. <b>2023</b> , 290, 116341	O

98	Sphingoid Bases Regulate the Sigma-1 Receptor Sphingosine and N,ND imethylsphingosine Are Endogenous Agonists. <b>2023</b> , 24, 3103	О
97	Deciphering the therapeutic role of Kigelia africana fruit in erectile dysfunction through metabolite profiling and molecular modelling. <b>2023</b> , 37, 101190	O
96	Quality assessment of VHH models. 1-15	0
95	Identification of AHL Synthase in Desulfovibrio vulgaris Hildenborough Using an In-Silico Methodology. <b>2023,</b> 13, 364	O
94	Bioinformatics and Cheminformatics Tools in Early Drug Discovery. 2023, 147-181	O
93	Coupled binding and folding of disordered SPIN N-terminal region in myeloperoxidase inhibition. 10,	O
92	Insight into the Role of Active Site Protonation States and Water Molecules in the Catalytic Inhibition of DPP4 by Vildagliptin. <b>2023</b> , 63, 1338-1350	O
91	Local Hydration Control and Functional Implications Through S-Nitrosylation of Proteins: Kirsten Rat Sarcoma Virus (K-RAS) and Hemoglobin (Hb). <b>2023</b> , 127, 1526-1539	O
90	Identification of binding sites in nicastrin and binding modes of its inhibitors. 12, 150	0
89	Structure-Based Optimization of ProteaseIhhibitor Interactions to Enhance Specificity of Human Stefin-A against Falcipain-2 from the Plasmodium falciparum 3D7 Strain. <b>2023</b> , 62, 1053-1069	O
88	Neutron Reflectometry and Molecular Simulations Demonstrate HIV-1 Nef Homodimer Formation on Model Lipid Bilayers. <b>2023</b> , 435, 168009	O
87	Ferroptosis in Rat Lung Tissue during Severe Acute Pancreatitis-Associated Acute Lung Injury: Protection of Qingyi Decoction. <b>2023</b> , 2023, 1-22	O
86	Crystal structures reveal the framework ofcis-acyltransferase modular polyketide synthases.	O
85	Revealing Structural and Physical Properties of Polylactide: What Simulation Can Do beyond the Experimental Methods. 1-39	O
84	Energy decomposition and waterswapping analysis to investigate the SNP associated DPD mediated 5-FU resistance. <b>2023</b> , 34, 39-64	O
83	The combination of polyphenols and phospholipids as an efficient platform for delivery of natural products. <b>2023</b> , 13,	O
82	Effects of presenilin-1 familial Alzheimer disease mutations on Elecretase activation for cleavage of amyloid precursor protein. <b>2023</b> , 6,	О
81	MDBuilder: a PyMOL plugin for the preparation of molecular dynamics simulations. <b>2023</b> , 24,	O

80	MoSDeF-GOMC: Python Software for the Creation of Scientific Workflows for the Monte Carlo Simulation Engine GOMC. <b>2023</b> , 63, 1218-1228	1
79	Re-Balancing Replica Exchange with Solute Tempering for Sampling Dynamic Protein Conformations. <b>2023</b> , 19, 1602-1614	O
78	Assessments of Variational Autoencoder in Protein Conformation Exploration. 1-13	О
77	Structural basis for membrane attack complex inhibition by CD59. <b>2023</b> , 14,	O
76	Metallodrugs against Breast Cancer: Combining the Tamoxifen Vector with Platinum(II) and Palladium(II) Complexes. <b>2023</b> , 15, 682	0
75	Cholesterol esters form supercooled lipid droplets whose nucleation is facilitated by triacylglycerols. <b>2023</b> , 14,	Ο
74	ProtexA Python utility for proton exchange in molecular dynamics simulations. 11,	0
73	SOURSOP: A Python package for the analysis of simulations of intrinsically disordered proteins.	Ο
7 <sup>2</sup>	A review on shale oil and gas characteristics and molecular dynamics simulation for the fluid behavior in shale pore. <b>2023</b> , 376, 121507	Ο
71	Anti-Diabetic Activity of Flavonol Glucosides From Fumana montana Pomel: In vitro Analysis, In Silico Docking, ADMET Prediction, and Molecular Dynamics Simulations. <b>2023</b> , 8,	0
7°	Mechanistic Basis for a Connection between the Catalytic Step and Slow Opening Dynamics of Adenylate Kinase. <b>2023</b> , 63, 1556-1569	Ο
69	Conformational Control of Fast Asparagine Deamidation in a Norovirus Capsid Protein. <b>2023</b> , 62, 1032-1043	O
68	Atomistic molecular insight on Angiotensin-(1-7) interpeptide interactions.	Ο
67	Bacterial origins of thymidylate metabolism in Asgard archaea and Eukarya. 2023, 14,	Ο
66	Intrinsically disordered region of talin FERM domain functions as an initial PIP2 recognition site. <b>2023</b> , 122, 1277-1286	О
65	Investigating the competition between ACE2 natural molecular interactors and SARS-CoV-2 candidate inhibitors. <b>2023</b> , 374, 110380	Ο
64	Allosteric regulation of ⊡reaction stage I in tryptophan synthase upon the ⊞-ligand binding. <b>2023</b> , 158, 115101	0
63	MiMiCPy: An Efficient Toolkit for MiMiC-Based QM/MM Simulations. <b>2023</b> , 63, 1406-1412	O

62	Human Glucosylceramide Synthase at Work as Provided by Ih Silico Molecular Docking, Molecular Dynamics, and Metadynamics. <b>2023</b> , 8, 8755-8765	0
61	Concentration-Dependent Inhibition of Mesophilic PETases on Poly(ethylene terephthalate) Can Be Eliminated by Enzyme Engineering. <b>2023</b> , 16,	O
60	Heterogeneous and Allosteric Role of Surface Hydration for Proteinligand Binding. 2023, 19, 1875-1887	О
59	In silico prediction of potential inhibitors for SARS-CoV-2 Omicron variant using molecular docking and dynamics simulation-based drug repurposing. <b>2023</b> , 29,	O
58	Nanoscale crack propagation in clay with water adsorption through reactive MD modeling. <b>2023</b> , 47, 1103-1133	O
57	Drug repurposing and molecular mechanisms of the antihypertensive drug candesartan as a TMEM16A channel inhibitor. <b>2023</b> , 235, 123839	O
56	Recent Advances in Molecular Dynamics Simulations of Tau Fibrils and Oligomers. 2023, 13, 277	О
55	Response and Resistance to Trametinib in MAP2K1-Mutant Triple-Negative Melanoma. <b>2023</b> , 24, 4520	O
54	Structural and biochemical insight into a modular 🖟 1,4-galactan synthase in plants. 2023, 9, 486-500	0
53	Routine Molecular Dynamics Simulations Including Nuclear Quantum Effects: From Force Fields to Machine Learning Potentials. <b>2023</b> , 19, 1432-1445	O
52	On the Mechanism of Membrane Permeabilization by Tamoxifen and 4-Hydroxytamoxifen. <b>2023</b> , 13, 292	O
51	Mechanistic Insight into the Amyloid Fibrillation Inhibition of Hen Egg White Lysozyme by Three Different Bile Acids. <b>2023</b> , 127, 2198-2213	O
50	Extension of the TraPPE Force Field for Battery Electrolyte Solvents. 2023, 127, 2224-2236	О
49	A novel strategy for producing low-sugar pomegranate jam with better anthocyanin stability: Combination of high-pressure processing and low methoxyl & mp; amidated pectin. <b>2023</b> , 179, 114625	O
48	Insights at the atomistic resolution of lantibiotics using multiscale simulations. 2023, 241-253	0
47	Are computational approaches critically important for solving real-world problems?. 2023, 567-583	O
46	Exploring the potential use of natural polymers to enhance the performance of MXene/MOF-5 nanocarrier in loading and co-loading of doxorubicin and curcumin.	O
45	In silico approaches for xenobiotic polymers and their degradation mechanism. 2023, 479-501	O

44	Effective natural inhibitors targeting LSD1 by computational study.	0
43	Fluids and Electrolytes under Confinement in Single-Digit Nanopores. <b>2023</b> , 123, 2737-2831	О
42	QSAR via multisite Edynamics in the orphaned TSSK1B kinase. <b>2023</b> , 32,	0
41	Accurate prediction by AlphaFold2 for ligand binding in a reductive dehalogenase and implications for PFAS (per- and polyfluoroalkyl substance) biodegradation. <b>2023</b> , 13,	O
40	Beta-KTx14.3, a scorpion toxin, blocks the human potassium channel KCNQ1. 2023, 1871, 140906	0
39	Atomistic MD Simulations of n -Alkanes in a Phospholipid Bilayer: CHARMM36 versus Slipids. 2200078	O
38	Structural basis of GAIN domain autoproteolysis and cleavage-resistance in the adhesion G-protein coupled receptors.	0
37	Predicting residue cooperativity during protein folding: A combined, molecular dynamics and unsupervised learning approach. <b>2023</b> , 158, 134108	O
36	Molecular analyses of the C-terminal CRAF variants associated with cardiomyopathy reveal their opposing impacts on the active conformation of the kinase domain. 1-11	O
35	Molecular basis of polyspecific drug binding and transport by OCT1 and OCT2.	O
34	Forced Interactions: Ionic Polymers at Charged Surfactant Interfaces. 2023, 127, 2829-2836	0
33	MM/GBSA prediction of relative binding affinities of carbonic anhydrase inhibitors: effect of atomic charges and comparison with Autodock4Zn. <b>2023</b> , 37, 167-182	O
32	Cooperative mechanics of PR65 scaffold underlies the allosteric regulation of the phosphatase PP2A. <b>2023</b> ,	0
31	Hyperthermal Dynamics and Kinetics of the C(3P) + N2(X1 $\frac{1}{9}$ +) -> CN(X2 $\frac{1}{9}$ +) + N(4S) Reaction. <b>2023</b> , 127, 2839-2845	1
30	The intramembrane COOH-terminal domain of PRRT2 regulates voltage-dependent Na+ channels. <b>2023</b> , 104632	0
29	Restriction of access to the central cavity is a major contributor to substrate selectivity in plant ABCG transporters. <b>2023</b> , 80,	O
28	New experimental evidence for pervasive dynamics in proteins. <b>2023</b> , 32,	0
27	Molecular modeling and simulations of some antiviral drugs, benzylisoquinoline alkaloid, and coumarin molecules to investigate the effects on Mpro main viral protease inhibition. <b>2023</b> , 34, 101459	О

26	Soft Matter under Pressure: Pushing Particle <b>l</b> ield Molecular Dynamics to the Isobaric Ensemble. <b>2023</b> , 63, 2207-2217	О
25	Structures and Dynamics of DNA Mini-Dumbbells Are Force Field Dependent.	Ο
24	Fast prediction of antibiotic permeability through membrane channels using Brownian dynamics. <b>2023</b> ,	О
23	Cheminformatics-Based Study Identifies Potential Ebola VP40 Inhibitors. <b>2023</b> , 24, 6298	1
22	Water-soluble 4-(dimethylaminomethyl)heliomycin exerts greater antitumor effects than parental heliomycin by targeting the tNOX-SIRT1 axis and apoptosis in oral cancer cells.	0
21	Benchmarking the Drude Polarizable Force Field Using the r(GACC) Tetranucleotide.	Ο
20	Targeting Olokizumab-Interleukin 6 interaction interface to discover novel IL-6 inhibitors. 1-13	О
19	All -atom simulations of the trimeric spike protein of SARS-CoV -2 in aqueous medium: Nature of interactions, conformational stability and free energy diagrams for conformational transition of the protein.	O
18	In silico and in vitro Identification of Compounds with Dual Pharmacological Activity against Metionyl-tRNA Synthetase and Isoleucyl-tRNA Synthetase of Staphylococcus aureus. <b>2023</b> , 8,	0
17	Expanding the Paradigm of Structure-Based Drug Design: Molecular Dynamics Simulations Support the Development of New Pyridine-Based Protein Kinase C-Targeted Agonists. <b>2023</b> , 66, 4588-4602	Ο
16	Analysis of the ERK Pathway Cysteinome for Targeted Covalent Inhibition of RAF and MEK Kinases.	O
15	A Benzohydrazide-Based Artificial Ion Channel that Modulates Chloride Ion Concentration in Cancer Cells and Induces Apoptosis by Disruption of Autophagy.	Ο
14	Polyethylene Glycol 20k. Does It Fluoresce?. <b>2023</b> , 8, 14208-14218	О
13	Computer-aided drug design in seeking viral capsid modulators. <b>2023</b> , 28, 103581	O
12	Inhibitory Potential of the Ocimum sanctum Phytochemicals on Bruton Tyrosine Kinase, a Well-Known Drug Target for Treatment of Chronic Lymphocytic Leukemia: An In Silico Investigation. <b>2023</b> , 28, 3287	0
11	Ion Conduction Mechanisms in Potassium Channels Revealed by Permeation Cycles.	O
10	Tool and Techniques on Computer-Aided Drug Design for Targeted Cancer Therapy. <b>2023</b> , 781-829	О
9	Computational Insights on the Impact of Allotypic Variation and Dimerization on Erap1 and Erap2 Structures Running Title: Structural Analysis of Erap1 and Erap2 Allotype Dimers.	Ο

8	Efficient production of hydroxytyrosol by directed evolution of HpaB in Escherichia coli. 2023,	O
7	Drude Polarizable Lipid Force Field with Explicit Treatment of Long-Range Dispersion: Parametrization and Validation for Saturated and Monounsaturated Zwitterionic Lipids.	O
6	Cryo-EM structure of the folded-back state of human □cardiac myosin*.	О
5	A Retrospective on the Development of Methods for the Analysis of Protein Conformational Ensembles.	O
4	Dynamical changes of SARS-CoV -2 spike variants in the highly immunogenic regions impact the viral antibodies escaping.	О
3	Compounds Interacting with Cholecystokinin as Potential Drugs Against Excessive Weight Gain and Obesity. <b>2023</b> , 8,	O
2	An unexpected hydratase synthesizes the green light-absorbing pigment fucoxanthin.	О
1	Evolutionary adaptation from hydrolytic to oxygenolytic catalysis.	O